Space Sci Rev
DOI 10.1007/s11214-014-0108-9

Review of Solar Wind Entry into and Transport Within the Plasma Sheet

S. Wing · J.R. Johnson · C.C. Chaston · M. Echim · C.P. Escoubet · B. Lavraud · C. Lemon · K. Nykyri · A. Otto · J. Raeder · C.-P. Wang

Received: 8 May 2014 / Accepted: 29 September 2014

Abstract The plasma sheet is populated in part by the solar wind plasma. Four solar entry mechanisms are examined: (1) double cusp or double lobe reconnection, (2) Kelvin-Helmholtz Instability (KHI), (3) Kinetic Alfvén waves (KAW), and (4) Impulsive Penetra-

S. Wing (✉)
The Johns Hopkins University Applied Physics Laboratory, Laurel, MD, USA
e-mail: simon.wing@jhuapl.edu

J.R. Johnson
Princeton Plasma Physics Laboratory, Princeton, NJ, USA

C.C. Chaston
University of California Berkeley, Berkeley, CA, USA

C.C. Chaston
School of Physics, The University of Sydney, Sydney, Australia

M. Echim
Institute for Space Aeronomy, Brussels, Belgium

M. Echim
Institute for Space Sciences, Magurele, Romania

C.P. Escoubet
ESA/ESTEC (SCI-RSSD), Noordwijk, The Netherlands

B. Lavraud
Institut de Recherche en Astrophysique et Planétologie, Université de Toulouse, Toulouse, France

B. Lavraud
Centre National de la Recherche Scientifique, Toulouse, France

C. Lemon
The Aerospace Corporation, El Segundo, CA, USA

K. Nykyri
Embry-Riddle Aeronautical University, Daytona Beach, FL, USA

Published online: 04 November 2014

tion. These mechanisms can efficiently fill the plasma sheet with cold dense ions during northward interplanetary magnetic field (IMF). The solar wind ions appear to have been heated upon entry along the plasma sheet dawn flank. The cold-component (solar wind origin) ion density is higher on the dawn flank than the dusk flank. The asymmetric evolution of the KAW and magnetic reconnection in association with the KHI at the dawn and dusk flank magnetopause may partly produce the dawn-dusk temperature and density asymmetries. Solar wind that crosses the magnetopause lowers the specific entropy ($s = p/\rho^{\gamma}$) of the plasma sheet along the flanks. Subsequent transport of the cold ions from the flanks to the midnight meridian increases s by a factor of 5. T_i, T_e, s_i, and s_e increase when the solar wind particles are transported across the magnetopause, but T_i/T_e is roughly conserved. Within the magnetotail, $\mathbf{E} \times \mathbf{B}$ and curvature and gradient drifts play important roles in the plasma transport and can explain the large features seen in the plasma sheet. Turbulence can also play a significant role, particularly in the cold plasma transport from the flanks to the midnight meridian. Total entropy ($S = pV^{\gamma}$) conservation provides important constraints on the plasma sheet transport, e.g., fast flows.

Keywords Solar wind entry · Particle transport · Double cusp (lobe) reconnection · Kelvin-Helmholtz · Kinetic Alfvén wave (KAW) · Entropy · Fast flow · Turbulence · Ion to electron temperature ratio · Ion outflow

Key Points (1) Double cusp reconnection, KHI, KAW, and impulsive penetration can play significant roles in filling the plasma sheet. (2) Observations of dawn-dusk density and temperature asymmetries suggest that KAW may play a role in particle heating during solar wind entry at the dawn flank. (3) T_i/T_e is roughly conserved during solar wind entry, even though specific entropy ($s = p/\rho^{\gamma}$) is not conserved. (4) $\mathbf{E} \times \mathbf{B}$, curvature and gradient drifts can explain large scale features in the plasma sheet. (5) Turbulence can play a significant role in cold plasma transport from the flanks to the center of the plasma sheet. (6) Total entropy ($S = pV^{\gamma}$) can provide constraints on the plasma transport within the plasma sheet.

1 Introduction

The Earth's magnetosphere forms by the interaction of the solar wind and the interplanetary magnetic field (IMF) with Earth's intrinsic magnetic field. On the sunward side, the Earth's field, which is mainly dipolar, is compressed, whereas on the nightside, the field is stretched out in an elongated fashion that resembles a tail like configuration that is referred to as the magnetotail. The magnetotail consists mainly of the northern and southern lobes, which are separated by the plasma sheet. The lobes typically have lower densities and temperatures than the plasma sheet. Because the lobes bulge out into the solar wind flow, a force is imparted on the magnetotail towards its center. The lobes transmit

A. Otto
University of Alaska, Fairbanks, AL, USA

J. Raeder
University of New Hampshire, Durham, NH, USA

C.-P. Wang
University of California Los Angeles, Los Angeles, CA, USA

this force, which is balanced by the plasma pressure in the plasma sheet (Coroniti and Kennel 1972). While this pressure equilibrium exists most of the time, the plasma sheet can also be highly dynamic. In particular, the lobes and the plasma sheet can store energy, which is often released in explosive fashion, such as during substorms and storms (McPherron 1991). The plasma sheet continuously looses plasma. Part of the losses comes through precipitation into the ionosphere; however, the majority of the losses occur by plasma flowing out through the back of the tail. For the latter loss process to be effective, closed field lines of the plasma sheet need to reconnect and form plasmoids that are ejected from the tail together with the plasma they carry. This process is highly dynamic and correlates with geomagnetic activity and IMF direction. The total losses during quiet times have been estimated to be of the order of 10^{25} to 10^{26} particles per second (Hill 1974; Nishida and Hones 1974), whereas loss rates during active times can be 1–2 orders of magnitude larger.

Determining the sources of the plasma sheet has thus been a fundamental problem of magnetospheric physics for a long time. Although it is known that the only substantive sources for magnetotail plasma are the solar wind and the ionosphere, their relative importance, the particle paths, and their energization, are still poorly known (e.g., Williams 1997). Early investigations focused on the solar wind source, after it was established that the magnetosphere is open by way of magnetic reconnection most of the time (Paschmann et al. 1979; Sonnerup et al. 1981), which had previously been predicted by Dungey (1961). With the discovery of the plasma mantle (Hones et al. 1973; Rosenbauer et al. 1975) solar wind plasma was seen streaming along open lobe field lines into the tail. The mantle could also be explained in terms of MHD (Siscoe and Sanchez 1987; Sanchez et al. 1990) as an expansion fan that emanates from the tailward edge of the cusp and propagates towards the tail center. In terms of particle drift, the particles of the mantle $\mathbf{E} \times \mathbf{B}$ drift towards the distant tail plasma sheet. Once those particles reach the plasma sheet they would interact with the current sheet and follow Speiser type orbits (Speiser 1965, 1967) that would energize and thermalize the particles. Provided there is an x-line tailward of the locations where the mantle particles enter the tail, the plasma would be trapped on closed field lines and thus provide a source of the plasma sheet (Cowley and Southwood 1980; Cowley 1980). Pilipp and Morfill (1978) constructed quantitative models of this entry mechanism. They used empirical magnetic and electric field models to calculate the entry rates and came to the conclusion that the mantle could supply enough plasma to the plasma sheet to compensate for the losses, which were estimated to be of the order of 10^{25} to 10^{26} particles per second during quiet times (Hill 1974; Nishida and Hones 1974). Later, it was shown that the ionosphere as well could provide the same flux of particles to the plasma sheet (Chappell et al. 1987).

However, each of these models has issues. The presence of significant amounts of ionospheric plasma, i.e., oxygen ions, is mostly restricted to the storm-time plasma sheet. It is also difficult to explain how ionospheric protons would be heated, because when they escape the ionosphere they have very low energies, typically 10–100 times less than plasma sheet ions. Ionospheric outflow is also strongly modulated by the solar EUV flux and the amount of the ionospheric origin plasma population in the plasma sheet was found to be modulated by the geomagnetic and solar activity (e.g., Maggiolo and Kistler 2014; Mouikis et al. 2010). While ionospheric plasma plays a role in the plasma sheet, and at times may even dominate the plasma pressure there, we will leave the discussion of its properties to other papers (e.g., Kistler et al. 2010, 2006).

The mantle model also has several issues. First, it assumes that the IMF is southward and dayside reconnection provides a steady supply of open field lines convecting into the tail

carrying magnetosheath plasma. In reality, the typical IMF orientation is Parker spiral like, with a small IMF Bz component, either southward or northward. Under such conditions, the symmetries assumed in the entry models do not exist and thus the models might require serious modification. Indeed, these asymmetries are observed (Gosling et al. 1985) and call into question the validity of these models. Second, Erickson and Wolf (1980) showed that steady convection from the distant neutral line to the near-Earth plasma sheet is impossible, because it would lead to a near-Earth pressure buildup that would choke convection. Since mantle plasma reaches the plasma sheet far down the tail, around 100 R_E, even if that plasma were captured somehow in the plasma sheet, it would never make it close to the Earth. There is also not much evidence that a steady x-line exists beyond lunar distance, thus most of the mantle plasma likely keeps moving anti-sunward once it reaches the current sheet. Third, modern observations of the near-Earth, midtail, and lunar-distance plasma sheet by the THEMIS, ARTEMIS, and other probes, have now created a picture that is significantly different from the cartoons of the 70s and 80s. Laminar flows and well-ordered fields rarely exist in the plasma sheet. Instead, transport primarily occurs in spatially and temporally bursts, called Bursty Bulk Flows (BBFs) and dipolarization fronts (DFs) that transport plasma and field both earthward (Angelopoulos et al. 1992, 1994; Nakamura et al. 2005; Runov et al. 2009, 2011a, 2011b) and tailward (Kiehas et al. 2012). Since it is well established that plasma sheet properties such as density, pressure, and temperature are correlated with solar wind conditions (e.g., Borovsky et al. 1998a; Terasawa et al. 1997; Wing and Newell 2002; Lavraud et al. 2006a; Nagata et al. 2008), the solar wind is likely to provide the bulk of the plasma sheet plasma; however, the path the solar wind takes to reach the plasma sheet and the subsequent plasma transport within the plasma sheet is not always clear.

While during southward IMF conditions, reconnection occurs at the magnetopause on the dayside at low-latitude as depicted in Fig. 1a, during northward IMF conditions reconnection occurs at high-latitude poleward of the cusp as depicted in Fig. 1b. It was long believed that the magnetosphere–solar wind coupling is stronger and reconnection rate is higher during southward than northward IMF (e.g., Perreault and Akasofu 1978; Newell et al. 2007). However, over the past 15 years evidence mounted that compared to southward IMF conditions, more solar wind particles enter the magnetotail during northward IMF conditions. In particular, an extended period of northward IMF generally leads to the formation of a cold and dense plasma sheet (CDPS) (e.g., Terasawa et al. 1997; Fujimoto et al. 1998; Wing and Newell 2002; Stenuit et al. 2002) compared to the more common hot and tenuous plasma sheet. CDPS is characterized by low temperature (<1 keV) and high density (>1 cm^{-3}), whereas the more typical hot and tenuous plasma sheet has a temperature of several keV and a density less than 0.1 cm^{-3}.

Reconnection may also play an important role in transporting solar wind plasma into the magnetotail during periods of northward IMF. High latitude reconnection, where the Earth's field lines are reconnected behind the cusps with IMF field lines in both hemispheres, forms new closed field lines filled with magnetosheath plasma ("double cusp or double lobe reconnection") (Crooker 1992; Song and Russell 1992; Le et al. 1996; Sandholt et al. 1999; Fuselier et al. 2002a, 2002b; Øieroset et al. 2005; Lavraud et al. 2005a, 2006d; Imber et al. 2006; Pitout et al. 2012), which then become part of the magnetosphere. Magnetohydrodynamic (MHD) simulations have been performed to show that this process can effectively bring magnetosheath plasma into plasma sheet (Raeder et al. 1995, 1997). This process is depicted in Fig. 2, which can be contrasted with Fig. 1a. Figure 2, from an MHD simulation (Li et al. 2005), shows the time sequence of a field line as it convects with the solar wind, crosses the bow shock, and then reconnects sequentially in short order with lobe field lines

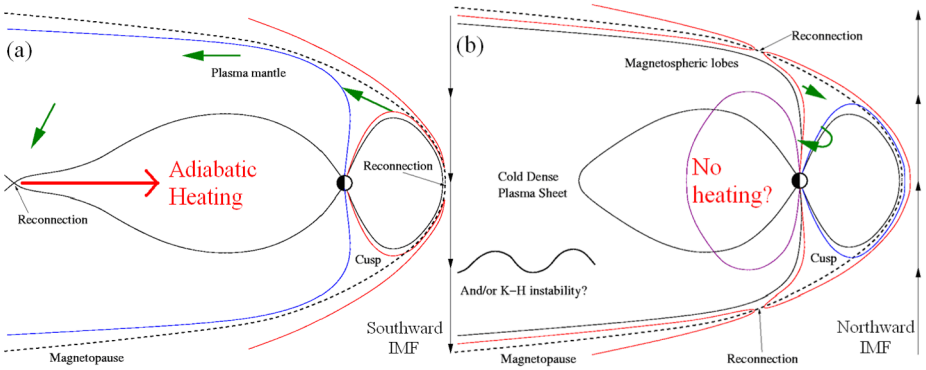

Fig. 1 Schematic of solar wind plasma circulation and magnetic topology of the magnetosphere in the context of magnetic reconnection for (**a**) southward and (**b**) northward IMF directions. (Adapted from Lavraud et al. 2006c)

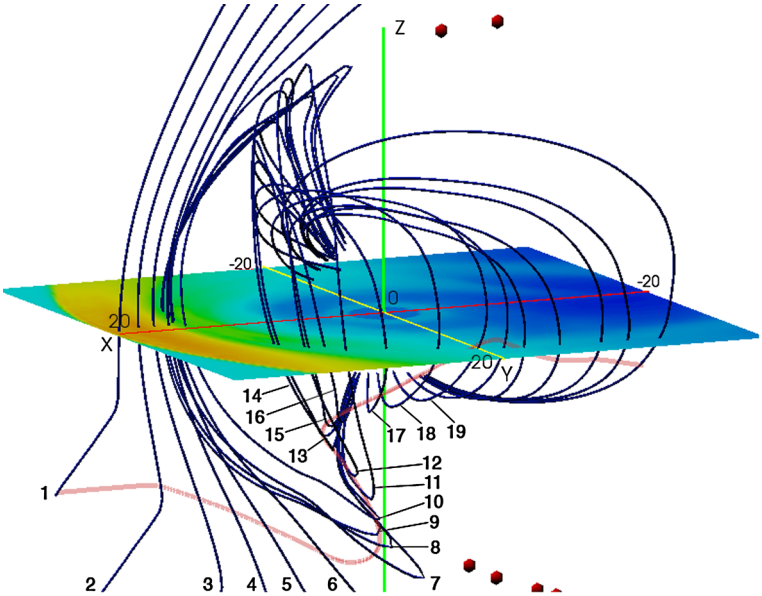

Fig. 2 OpenGGCM simulation (Raeder 2003) of the October 23, 2003 CDPS event. The *color-coded equatorial plane* shows the plasma density. The *pink line* traces a fluid element from the solar wind into the plasma sheet, where the CDPS is observed. The *dark blue line* shows the frozen-in magnetic field lines. The *red dots* are the magnetic nulls. The *red*, *yellow*, and *green axes* are Geocentric Solar Ecliptic (GSE) X, Y, and Z axes, respectively. The numbers 1–19 indicate the progression of the field line in time. A sequence of field lines attached to that fluid element are drawn *in blue*. The sequence shows how the field line that convects with the fluid element changes its topology from solar wind (unconnected) to closed, i.e., the transition from 6 to 7, thereby capturing the fluid element. (From Li et al. 2005)

in each hemisphere. After that, the field line, along with the captured magnetosheath plasma, slowly (on a time scale of 1–3 h) convects into the tail. Initially, the newly closed dayside field line would move sunward and then it would move tailward to the flanks.

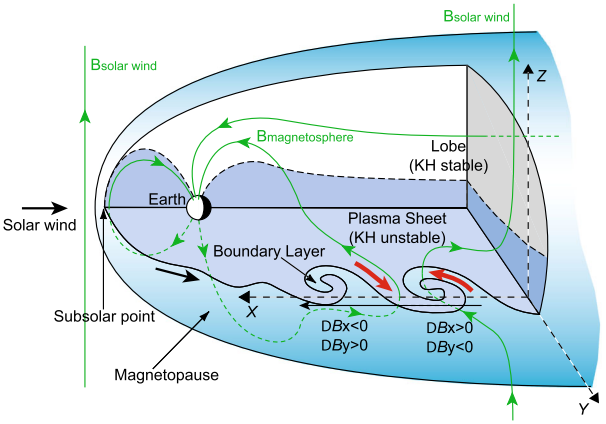

Fig. 3 Three dimensional view of the magnetosphere showing the KH vortices at the duskside magnetopause. (From Hasegawa et al. 2004b)

Another possible solar wind entry mechanism is Kelvin-Helmholtz Instability (KHI). Kelvin-Helmholtz waves grow along an inhomogeneous velocity shear layer (as found on the flank magnetopause) and eventually develop a rolled up vortex pattern in density and magnetic field, as illustrated in Fig. 3. KHI has been successfully simulated with local MHD simulations (e.g., Otto and Fairfield 2000; Nakamura and Fujimoto 2005; Nykyri and Otto 2001; Nykyri et al. 2006; Matsumoto and Hoshino 2004, 2006; Matsumoto and Seki 2010), global MHD (e.g. Guo et al. 2010; Merkin et al. 2013), Hall-MHD (e.g., Nykyri and Otto 2004; Faganello et al. 2012), two fluid with electron inertia (e.g., Nakamura et al. 2005, 2006; Nakamura and Fujimoto 2008), hybrid (e.g., Thomas and Winske 1991, 1993; Fujimoto and Terasawa 1994, 1995; Cowee et al. 2009, 2010; Delamere 2009; Delamere et al. 2011, 2013; Paral and Rankin 2013) and full particle simulations (e.g., Nakamura et al. 2011, 2013). Observational signatures of these vortices have been found on the dusk and dawn flanks of the magnetosphere (e.g., Fairfield et al. 2000; Fujimoto et al. 2003; Hasegawa et al. 2006). Moreover, reconnection in the nonlinear stage of the KHI could lead to the detachment of plasma from the vortex structures, leading to significant transport across the magnetopause (e.g., Otto and Fairfield 2000; Nykyri et al. 2006). Hybrid simulations have indicated that ion blobs could become detached from the vortex structure of the KHI and could provide filaments, producing a mixing of plasma in the shear layer (Thomas and Winske 1991, 1993; Fujimoto and Terasawa 1994, 1995). Hasegawa et al. (2006) noted that there is an inverse relationship between the magnetospheric plasma density and tailward flow speed in KH vortices, leading to the development of an algorithm for detecting rolled up KH vortices with a single spacecraft.

In addition to KH waves, large-amplitude Alfvén waves have also been observed on the magnetospheric boundary (e.g., Tsurutani et al. 1982; LaBelle and Treumann 1988; Anderson and Fuselier 1994). There is evidence that the waves could be the result of mode conversion of magnetosheath compressions in the sharp magnetopause gradients at the magnetopause (Lee et al. 1994; Johnson and Cheng 1997; Johnson et al. 2001). Because the wavelength of the mode converted waves is on the order of the ion gyroradius, they can lead to efficient convective and diffusive transport of ions across the magnetopause, as illustrated in Fig. 4 (Johnson and Cheng 1997; Chen 1999; Chaston et al. 2008). The mode conversion process has been simulated with 2D hybrid simulations (Lin et al. 2010) showing linear mode conversion, and 3D simulations (Lin et al. 2012) showing nonlinear decay of the mode converted waves such that transport is

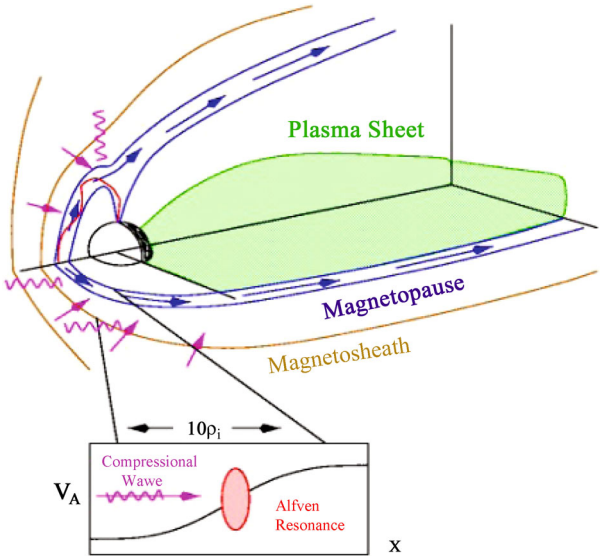

Fig. 4 Three dimensional view of the magnetosphere showing kinetic Alfvén waves in the magnetosheath leading to magnetosheath plasma entry into the magnetosphere

greatly enhanced because of the development of modes with large azimuthal wave number. Kinetic Alfvén waves (KAWs) also lead to nonlinear transverse plasma heating because of the large amplitudes observed at the magnetopause (Johnson and Cheng 2001; Chaston et al. 2008).

Direct or impulsive entry of magnetosheath plasma jets/blobs as those observed in situ by Cluster and/or THEMIS (Karlsson et al. 2012; Archer and Horbury 2013; Plaschke et al. 2013; Lundin and Aparicio 1982; Gunell et al. 2012) can occur at all latitudes and magnetic local times provided the magnetosheath irregularities have enough momentum to cross the magnetopause (Lemaire 1977; Lemaire and Roth 1978). This is illustrated in Fig. 5. The penetration of the magnetopause is possible due to kinetic effects at the edges of the 3D plasma jets/blobs that create space charge layers that sustain an electric field, $\mathbf{E_P}$, enabling the forward motion of the core of the blob with the bulk velocity, $\mathbf{E_P} \times \mathbf{B_0}$, where $\mathbf{B_0}$ is the background magnetic field (Schmidt 1960). Once inside the magnetosphere the jets/blobs are slowed down by two competing processes: (i) the adiabatic breaking and transformation of the motional energy into gyration energy (Lemaire 1985; Demidenko et al. 1969) and (ii) short circuiting of the polarization electric field by the conducting ionosphere connected to the blob by the "closed" geomagnetic field lines (Lemaire and Roth 1991; Baker and Hammel 1965).

These four processes are not necessarily mutually exclusive and have all been demonstrated to be capable to transport plasma across magnetic boundaries. For example, KH waves can excite KAW (Sibeck et al. 1999). KAWs have been observed in conjunction with reconnection and Kelvin-Helmholtz structures (Chaston et al. 2005, 2007, 2009). Nishino et al. (2007) also observed bidirectional electrons and cold protons inside a KH vortical structure, which they interpreted as a signature of reconnection. Additionally, they observed electron and ion heating, which they attributed to wave-particle interactions such as KAW heating (Johnson and Cheng 1997, 2001). Taylor and Lavraud (2008) found that there exist at least at times two distinct ion populations of solar wind origin in the downtail magnetopause boundary layers, which may be interpreted as evidence for combined occurrence of a few entry processes. KHI and KAW can also play significant roles in the plasma entry during southward IMF.

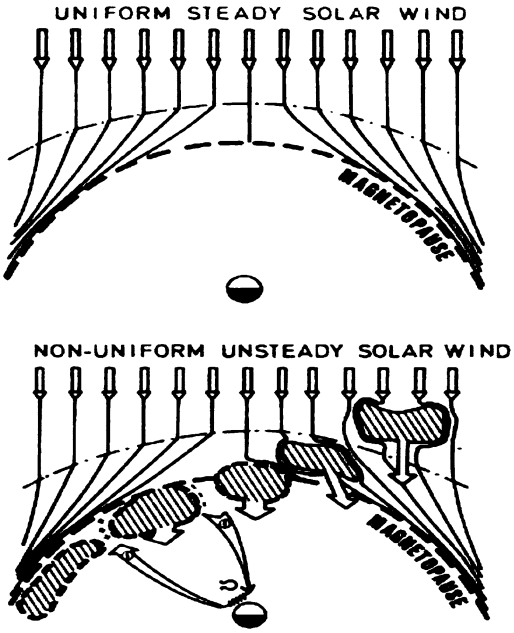

Fig. 5 Illustration of steady state models (*upper diagram*) and non-steady and non-uniform interaction model (*bottom diagram*) of the shocked solar wind at the front-side magnetosphere. Equatorial cross sections of the magnetopause interaction regions are shown. Plasma elements with excess dynamic pressure (larger density, and/or bulk velocity) move across the magnetopause and penetrate inside the magnetosphere. The entry site is determined by the kinetic and dynamic properties of the blobs. (From Lemaire and Roth 1978)

It has been a challenge to distinguish which of these mechanisms play a more significant role than the others and under what conditions. Recent observations have attempted to identify several potential discriminators based on both *in situ* and remote sensing methods. One potential discriminator is the filling rate. Each entry mechanism might lead to a different entry or filling rate and different dependencies on parameters. For example, Taylor et al. (2008) studied the role of both high-latitude reconnection and KHI for the generation of the Low Latitude Boundary Layer (LLBL) and CDPS. They concluded that the electron phase space densities measured by Polar satellite at the dayside LLBL were not sufficient to explain the measured phase space densities at the tail LLBL observed at TC-1 spacecraft, indicating that the KH instability also contributes to the formation of the boundary layers and CDPS on that day. Another potential discriminator is the dawn-dusk asymmetries. Dawn-dusk asymmetries are particularly interesting because they may be related to how upstream boundary conditions (e.g. Parker spiral magnetic field orientation) affect the various entry mechanisms, which can be tested by observations and theories. Another potential discriminator is the specific entropy or entropy per unit volume ($s = p/\rho^{\gamma}$ where γ is polytropic index). Changes in the entropy profiles may be indicators that nonadiabatic processes are operating in conjunction with plasma transport, and how the entropy changes are related to the entry mechanism.

While cold plasma is preferentially observed in the plasma sheet during periods of northward IMF, hot plasma is preferentially observed during periods of southward IMF. However, both hot and cold plasma have been observed to co-exist in the same region/field-line under all IMF conditions (e.g., Wing et al. 2005; Wang et al. 2012). The mechanisms for heating cold plasma, either solar wind or ionospheric origin, to hot plasma population has not been firmly established, but it does appear that the ion to electron temperature ratio (T_i/T_e) is roughly conserved by the entry, energization, heating, and transport processes. This quasi "conserved" property deserves close and careful examination, because it puts stringent con-

straints on the entry and heating mechanisms. Unlike entropy, there has not been a physical argument for the conservation of T_i/T_e ratio.

Once the solar wind plasma enters the magnetotail, it will be distributed throughout the plasma sheet by the transport processes within the magnetotail or plasma sheet. The plasma gets heated and accelerated during these processes. Some of the transport processes such as curvature and gradient drifts introduce dawn-dusk asymmetries in the particles, especially for the hot component. Transport within the plasma sheet has been described with MHD models, which conserve total entropy ($S = pV^{\gamma}$). Total entropy conservation provides important constraints on the accessibility of plasma to the plasma sheet and governs the redistribution of plasma when flux tubes are depleted of total entropy due to nonadiabatic processes such as reconnection, plasma diffusion, and wave-particle interactions.

In the following sections, we will discuss and review solar wind entry mechanisms, constraints to solar wind entry, and plasma transport within the plasma sheet. We will end with a summary and conclusion.

2 Solar Wind Entry Mechanisms

2.1 Double Cusp (Double Lobe) Reconnection

During southward IMF, reconnection occurs at the low latitude magnetopause on the dayside where the IMF and the Earth's magnetic field line are nearly anti-parallel (Crooker 1979). Following reconnection, the open field lines convect to the nightside toward the lobe region, forming the plasma mantle (Rosenbauer et al. 1975; Cowley 1981; Siscoe and Sanchez 1987; Sanchez et al. 1990). Because of the solar wind duskward electric field, these open field lines $\mathbf{E} \times \mathbf{B}$ drift to the nightside equatorial region where they can once again reconnect (e.g., Hones 1979; Onsager et al. 1993; Keiling et al. 2004). This process is depicted in Fig. 1a. Subsequently, because the magnetic flux must be conserved, $\nabla \cdot B = 0$, these closed field lines $\mathbf{E} \times \mathbf{B}$ convect sunward to the dayside, returning the magnetic flux back to the dayside into the magnetic reconnection line. This process is known as the Dungey cycle (Dungey 1961). The solar wind entry into the plasma sheet during southward IMF, however, can involve other processes and be more complicated than this simple picture.

Dungey (1963) also realized that during northward IMF, IMF field lines should reconnect behind the cusps. In the simple cartoon depicted in Fig. 1b, for almost due northward IMF reconnection occurs simultaneously in both hemispheres, thereby attaching a new flux tube filled with magnetosheath plasma to the dayside magnetosphere. This would indeed be an efficient entry mechanism for solar wind plasma. In reality, however, the IMF orientation is rarely purely northward, so this process may be of much less significance if the field lines only reconnect in one hemisphere and remain open. Most of the time the IMF is oriented in a Parker-spiral configuration with only a small Bz component that varies between southward and northward.

In the anti-parallel merging model (Crooker 1986, 1979), reconnection would still be possible at the flanks and at high-latitudes poleward of the cusp even when there is a significant By component to the IMF. Such reconnection is indeed observed, both *in-situ* (Gosling et al. 1991; Kessel et al. 1996; Safrankova et al. 1998; Lavraud et al. 2002, 2005b; Phan et al. 2003), and remotely (Burch et al. 1980; Reiff et al. 1980; Escoubet et al. 2008). Using Doppler-shifted Lyman-alpha observations from the IMAGE spacecraft, Frey et al. (2003) showed that such reconnection is persistent and occurs uninterrupted over periods of hours for northward IMF. A finite IMF By component changes

the magnetic local time (MLT) of the reconnection footpoint, but does not interrupt the reconnection process, although it may be time dependent. Ionosphere convection maps also provide evidence for this process. After the reconnection, the footpoints of the newly reconnected field lines move initially sunward (Crooker 1992) before being swept sideways into the nightside, which is indicated by the green arrows in Fig. 1b. This gives rise to a four-cell convection pattern, where the flows over the poles are sunward and form a pair of reverse convection cells, with normal polarity cells confined at lower latitudes (Maezawa 1976; Burke et al. 1979). Such a configuration is frequently observed during periods of northward IMF (Reiff 1982; Lu et al. 1989, 2011). However, such observations are not sufficient to show that dual lobe reconnection occurs simultaneously (or simultaneously enough to capture entire magnetosheath flux tubes). A process by which IMF flux tubes would only reconnect in one hemisphere but not in the other would still be consistent with these observations. For that reason, the dual-lobe reconnection mechanism was dismissed as a viable entry mechanism for a long time, although it had been proposed as a possible mechanism for the generation of the LLBL during northward IMF (Song and Russell 1992).

Over the past decade, however, new observations and simulations have given much support to the dual lobe reconnection mechanism as a viable plasma entry process (Le et al. 1996; Sandholt et al. 1999; Onsager et al. 2001; Fuselier et al. 2002b; Lavraud et al. 2005a, 2006d; Cattaneo et al. 2006; Taylor et al. 2008; Pitout et al. 2012). Lavraud et al. (2005a) established that freshly reconnected flux tubes just outside the dayside magnetopause were often populated with bidirectional heated electrons, which is only consistent with closed field lines. Statistical analyses (Lavraud et al. 2006d) confirmed that such bidirectional heated electrons were observed outside the magnetopause only during strong northward IMF, as expected from this process. These newly closed field lines must have reconnected in both hemispheres within a short amount of time, and captured magnetosheath plasma. The dual lobe reconnection is also clearly seen in the polar cusp ion populations. Pitout et al. (2012) showed that two ion populations could be distinguished in the mid-altitude cusp and suggested that one was coming from the northern lobe reconnection and one from the southern lobe reconnection.

The THEMIS mission, while the 5 spacecraft were still in a string-of-pearls configuration, provided more strong evidence for the dual lobe reconnection entry mechanism. On Jun 3, 2007 the five THEMIS spacecraft consecutively traversed the dayside magnetopause while the IMF turned northward (Øieroset et al. 2008). Because the 5 spacecraft sequentially observed the plasma entry, possible spatio-temporal ambiguity was largely removed. This event was characterized by the gradual thickening of the LLBL as observed sequentially at each spacecraft, therefore showing unambiguously the ongoing capture of magnetosheath plasma at the dayside magnetopause under northward IMF. MHD simulations for the event replicate the development of a LLBL detected by the five THEMIS spacecraft as they encountered the magnetopause (Li et al. 2009). The simulations furthermore showed that the entry process operated across the entire dayside magnetopause. This event was also remarkable because the IMF was only moderately northward with a 40° clock angle, consistent with previous observations and simulations suggesting that the process may occur for large clock angles (Lavraud et al. 2006d; Li et al. 2008).

While the dayside observations show clear evidence for direct plasma entry associated with dual lobe reconnection, it is less clear how it leads to the population of the tail plasma sheet. Magnetohydrodynamic (MHD) simulations have been performed to show that this process can effectively bring magnetosheath plasma into the plasma sheet (Ogino et al. 1994; Fedder and Lyon 1995; Raeder et al. 1995, 1997). While the early simulations were not

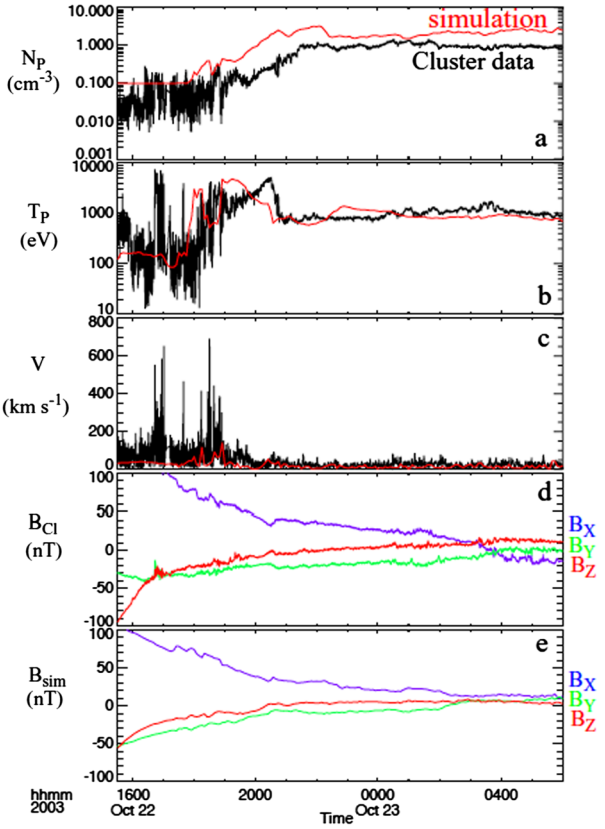

Fig. 6 The October 22–23, 2003 CDPS event. Comparison between Cluster observations (*black*) and OpenGGCM MHD (Raeder 2003) simulated data along the Cluster path (*red*) (**a**) density; (**b**) temperature; (**c**) flow speed; (**d**) magnetic field components observed by Cluster (GSM); (**e**) simulated magnetic field components (GSM). (From Øieroset et al. 2005)

corroborated by observations, Øieroset et al. (2005) reported a case study (October 22–24, 2003) that showed a fairly good agreement in the plasma sheet temperature and density between an OpenGGCM MHD simulation (Raeder 2003) and Cluster satellite observations. In this event, the IMF stayed strongly northward for more than 30 hours. Figure 6 shows how the CDPS developed within 3 h of the northward turning and remained until the IMF turned southward again.

The CDPS formation process is depicted in Fig. 2, which comes from an MHD simulation (Li et al. 2005). The paper shows that the plasma sheet filling time scale of the simulation agrees very well with the observed time scale. Thus, at least for the case simulated here, the simulation suggests that dual lobe reconnection is sufficient to form the CDPS.

Li et al. (2008) later used OpenGGCM simulations (Raeder 2003) to investigate the dual lobe reconnection entry rates as a function of clock angle and other parameters. They found that there exists an entry window, whose shape and area depends primarily on the IMF clock angle. The entry window still exists for clock angles as large as 90°, but its area diminishes as the clock angle increases and as the solar wind density or the IMF magnitude increases. The entry rates maximize for zero clock angle at $\sim 1.2 \times 10^{27}\ s^{-1}$ and decrease as the IMF clock angle or the dipole tilt increases. On the other hand, the entry rates depend only weakly on the solar wind speed and density, but maximize as a function of the IMF magnitude at 10 nT.

2.2 Kelvin-Helmholtz Instability (KHI)

Another possible solar wind entry mechanism is the KHI, which is reviewed in a companion review paper (Johnson et al. 2014). KH waves grow along an inhomogeneous velocity shear layer (Chandrasekhar 1961) (as found on the flank magnetopause) and eventually develop nonlinear rolled up vortices, as illustrated in Fig. 3.

Satellites crossing the magnetopause boundary often encounter boundary waves that exhibit typical signatures of KH instability. The instability is most easily detected when it forms vortex structures, and satellites passing through the structures exhibit characteristic fluctuations in pressure, velocity and magnetic field. Fairfield et al. (2000) reported observations of multiple crossing of the magnetopause boundary and argued that Geotail detected vortices moving past the spacecraft, and boundary normals showed nonlinear steepening of the waves on the leading edge of the wave rather than on the trailing edge consistent with MHD simulations of magnetic field fluctuations and plasma properties of KH vortices (Otto and Fairfield 2000).

The multisatellite Cluster mission made it possible to examine the two-dimensional structure of the vortices. Hasegawa et al. (2004b) presented observations from the four spacecraft that showed vortex structure in the velocity field and the presence of high density magnetosheath plasma on the magnetospheric side of the magnetopause consistent with simulations of KH instability, and the interchange of plasma suggests an important mechanism of plasma entry.

In the nonlinear development of the KHI, vortices form as the penetrating plasma is carried by the flow in the shear layer. Such vortices are commonly seen in MHD and Hall-MHD (Miura 1987; Otto and Fairfield 2000; Hasegawa et al. 2004b; Nykyri and Otto 2004) and particle simulations (Thomas and Winske 1993; Fujimoto and Terasawa 1994; Wilber and Winglee 1995; Matsumoto and Hoshino 2004; Nakamura et al. 2011; Cowee et al. 2009; Delamere et al. 2011) of KH growth. The interchange motion inherent to the KHI leads to transport of momentum through Reynolds and Maxwell stresses (Miura 1987). Transport of mass, momentum, and energy also occurs through plasma mixing, when kinetic effects, such as ion inertia and ion Larmor radius allow ions to move across magnetic field lines. The development of vortices that entwine magnetosheath field lines with magnetospheric field lines ultimately leads to the development of strong shear and thin current layers that allow reconnection and the interchange of plasma from open to closed field lines (Otto and Fairfield 2000; Nykyri and Otto 2001; Otto 2006; Nakamura and Fujimoto 2008; Nakamura et al. 2011, 2013; Ma et al. 2014a, 2014b). Such transport typically pinches off blobs of magnetic flux from the vortex structures (Otto 2006; Ma et al. 2014a, 2014b). Plasma entry rates inferred from simulations are generally adequate to provide a flank source for the CDPS material (Nykyri and Otto 2001; Otto 2006); however, it is of particular interest to understand the nature of the transport and conditions where it is dominated by mixing or blobs.

The nonlinear development of the vortices also involves the process of coalescence where smaller vortices coalesce into larger and larger vortices with a characteristic inverse cascade of energy from small to large scale (Winant and Browand 1974). Because the saturation amplitude of the vortex is expected to determine the width of the boundary layer, it is important to understand how saturation occurs and how nonlinear development of the instability compares with the wave phase speed along the boundary. Initially, waves with short wavelength grow faster. Waves with longer wavelength are "subharmonics" in that the frequency and growth rate are smaller. So, at longer times, the fundamental may saturate and the longer wavelength waves will eventually grow, but more slowly until they become the same size as

the fundamental. The 2D nonlinear ideal MHD study of Miura (1997) showed that growth of the subharmonics tends to occur on a timescale comparable to their linear growth rate, suggestive that the emergence of larger scale vortices is due to the linear growth of the subharmonic modes. However, the 2D MHD and PIC simulations of Matsumoto and Seki (2010) suggested that a substantially larger growth of subharmonics occurs when a broad spectrum of subharmonics is included. These processes rapidly broaden the boundary layer and transfer mass, momentum, and energy across the boundary.

A number of studies have emerged from recent satellite missions to confirm the importance of these transport processes at the magnetopause. Eriksson et al. (2009) used 2D MHD and Grad-Shavranov reconstructions (Hasegawa et al. 2004a, 2005) of THEMIS observations to examine KH waves with magnetic islands that appear between two large-scale vortices, and suggested that the observed islands may be generated by a time-varying reconnection process induced by the flow of observed KH vortices as seen in two-fluid simulations (Nakamura et al. 2006). THEMIS observations of a KH event also showed reasonable consistencies with size and structure to 3D full particle simulations (Nakamura et al. 2013), which showed that compressed current sheets give rise to magnetic flux ropes over a range of oblique angles and along the entire extent of the compressed current layer around the periphery of the vortex.

Taylor et al. (2008) noted, based on a multisatellite comparison of phase space density of electrons by Polar (from high-latitude reconnection) and Double Star (down the flanks), that additional entry must occur resulting from either KH or turbulent entry. Hasegawa et al. (2009) used multisatellite observations to examine the breakup and coalescence of vortices as they developed along the dusk flank. Similar to Taylor et al. (2008) they concluded that KH wave excitation can be facilitated by formation of the LLBL through high latitude reconnection and compressional magnetosheath fluctuations. Although high latitude reconnection on the dayside facilitates the development of KH waves on the flanks, multipoint density measurements along the flank suggest that the flank LLBL is not simply formed by this process alone. Local transport processes associated with KH vortices or kinetic Alfvén waves are also required.

Based on MHD simulations of KH instability, Hasegawa et al. (2006) determined that when vortices form it is likely that the tailward speed of a fraction of low-density magnetospheric plasma exceeds the magnetosheath flow leading to an inverse relationship between plasma density and flow speed. These conditions are quite different from the typical magnetopause where the higher density magnetosheath flow is large in contrast with the stagnant low density magnetospheric population. Hence, this inverse relationship can be particularly useful to identify KH structures with a single satellite and performing large data surveys. The technique was used to identify KH vortices and perform a survey of events leading to the conclusion that both dawn and dusk events occur regularly for northward IMF conditions. However, a follow-up study (Taylor et al. 2012) using Double Star 1 magnetopause crossings using the density-velocity relationship based on 623 orbits suggests a clear dawn-dusk asymmetry in vortex events with preferential occurrence at the dusk flank. These observational results contrast with the simulation results of Nykyri (2013), which show that Parker spiral configuration would favor faster growth of KH on the dawn flank. However, Taylor et al. (2012) found all the events on the dayside magnetopause, whereas the Nykyri (2013) analysis chose the simulation initial conditions from the dawn-dusk terminator, where the ratio between the shear flow and the Alfvén speed along the k-vector is higher at the dawn flank for the Parker Spiral IMF. Therefore, the non-linear waves originating from the terminator would be observed about 9–15 R_E downstream assuming KH wave speed of 150–250 km/s and a growth time of 400 s.

The global development of KH waves at the magnetopause has been studied using a number of global MHD models (Claudepierre et al. 2008; Guo et al. 2010; Li et al. 2013). In these simulations, KH surface waves develop at both the magnetopause boundary and the inner edge of the boundary layer with formation of large vortices at the inner boundary. Wave energy penetrates into the inner magnetosphere where the waves can energize and transport radiation belt electrons (Claudepierre et al. 2008). More recent LFM (Lyon-Fedder-Mombarry) simulations demonstrate that KH instability has a global three-dimensional character, whereby the surface-modes are coupled to body modes and drive global fluctuations of the plasma sheet (Merkin et al. 2013). Such coupling along with interchange motion could serve as the source of turbulence seen in the plasma sheet (Borovsky and Funsten 2003), which may dominate plasma transport within the distant plasma sheet (Wang et al. 2010).

Dawn-dusk asymmetries provide a significant observational constraint on plasma transport at Earth (Wing et al. 2005). Dawn-dusk asymmetries can result from: (a) differences in the shear velocity or magnetic field configuration on the two flanks (which relates to whether the instability is considered as an initial value problem or boundary value problem), (b) kinetic effects when the gyroradius is the order of the shear layer, (c) diamagnetic drifts, (d) the presence of heavy ions on one of the flanks, and (e) differences in fluid mass density on the flanks. The dawn-dusk asymmetries are discussed further in Sect. 3.2.

Some key questions for future research are: (1) What is the role of reconnection vs. the role of mixing for plasma transport?; (2) Can shocks that form at the edge of vortex structures heat plasma and increase the entropy?; (3) How are KH structures coupled with the ionosphere?; (4) How are KH structures coupled with kinetic Alfvén waves; (5) How do the local coupling between the KH instability and reconnection and between the KH instability and the secondary instability affect the global structure of the magnetospheres? It would also be particularly useful if there were more large-scale systematic observational studies of KH signatures and properties for various boundary layer conditions (e.g., large magnetic shear).

2.3 Kinetic Alfvén Waves (KAW)

Low frequency electromagnetic fluctuations are regularly observed in the vicinity of the magnetospheric boundary layer (e.g. Tsurutani et al. 1982; LaBelle and Treumann 1988; Rezeau et al. 1989, 2001; Anderson and Fuselier 1994; Stasiewicz et al. 2001; Johnson et al. 2001; Lucek et al. 2005; Yao et al. 2011; Chaston et al. 2005, 2013). It has long been speculated that diffusion-like processes in these waves could allow leakage of magnetosheath plasma across the magnetopause into the magnetosphere and even account for the formation of the boundary layer under conditions of northward IMF (Hasegawa and Mima 1978; Lee et al. 1994; Treumann et al. 1995). Kinetic Alfvén waves have been a prime candidate to drive this transport phenomenon because of the fact that they carry a parallel electric field and occur at the magnetopause with large amplitude. Nonetheless, observational confirmation of the action of these waves remains somewhat ambiguous because with present day instrumentation it is not possible to measure the diffusion drift speeds ($\sim$1 km/s) normal to the magnetopause associated with this process. Consequently, the case for kinetic Alfvén wave driven transport is somewhat indirect and based on estimates of diffusion coefficients for observed wave properties (Hasegawa and Mima 1978; Lee et al. 1994; Johnson and Cheng 1997; Chaston et al. 2007, 2008; Izutsu et al. 2012), correlation between the distribution of these waves along the magnetopause and that of magnetosheath plasma in the magnetosphere (Wing et al. 2005; Yao et al. 2011) and specific features of the velocity space distributions of the transported ions (Izutsu et al. 2012; Chaston et al. 2013).

Cross field ion drift occurs in kinetic Alfvén waves due to the combined operation of guiding center drifts and wave-particle resonant interactions that transfer energy from the waves to particles. These drifts allow motion of plasma across the magnetic field, which in the case of a density gradient allows the transport of plasma from high density regions (magnetosheath) to low density regions (magnetosphere). From a quasi-linear treatment of the gyrokinetic equation, Johnson and Cheng (1997) have provided a generalized cross-field diffusion coefficient for Landau damping associated with the parallel electric field, transit time damping associated with the perturbed mirror force, and the coupling between ion motion in the wave field and grad ∇B drift on the magnetopause through the $\mathbf{v}_{\mathrm{d}} \times \delta\mathbf{B}_{\perp}$ force. Very simply, when particles are in resonance with the wave the parallel forces mentioned above accelerate/decelerate particles along the perturbed magnetic field, which causes cross-field transport across the background magnetic field (Lee et al. 1994; Johnson and Cheng 1997; Chen 1999; Izutsu et al. 2012). In order for the transport to be effective across the boundary, the magnetic field perturbation of the wave must be in the direction across the boundary, which means that the wavevector ($\boldsymbol{k}$) that contributes to diffusion is along the boundary in the azimuthal direction (k_y). Moreover, as expected from quasi-linear theory, the diffusion coefficients are proportional to the wave power. Transport coefficients have been derived for the kinetic Alfvén wave based on quasi-linear theory including Landau damping (Hasegawa and Mima 1978; Lee et al. 1994), transit time damping and grad-B drift (Johnson and Cheng 1997; Chen and Wolf 1999). Typically, the grad-B drift contribution is largest at the magnetopause.

Recent observations from multi-spacecraft missions to the magnetosphere have made it possible to unambiguously identify the broadband wave activity across the magnetopause as KAW and from measurements of wave scale have facilitated robust estimates of the transport rates that these waves can drive. Using observations from the THEMIS mission, Chaston et al. (2008) considered 10 spacecraft traversals across or near the magnetopause where KAW were observed. At these times at least two of the THEMIS spacecraft were sufficiently close together that comparisons of the magnetopause transition between spacecraft could be used to estimate the density gradient scales and estimate the wavelength along the vector between the spacecraft. To then derive the ratio $k_{\perp}/k_{\parallel}$ from these single baseline measurements, fits of the observed $E_{\perp}/B_{\perp}$ as a function of k as shown in Fig. 7b were used to demonstrate that $k_{\perp}/k_{\parallel} \geq 40$. The significance of the ratio $k_{\perp}/k_{\parallel}$ is that it demonstrates that the waves are KAW and that this parameter can be used to compute the transport and heating coefficients. Transport across the boundary is generally proportional to the azimuthal wavenumber and so it will increase with the ratio $k_{\perp}/k_{\parallel}$. More recent work has shown that this ratio increases with k (Chaston et al. 2013). However, for the purpose of estimating the diffusion coefficient, which primarily arises from contributions near $k_{\perp}\rho_i = 1$, we consider here two cases within the range of observations; namely $k_{\perp}/k_{\parallel} = 40$ and 100. Figures 7c and 7d show the diffusion coefficients for these two cases for Landau damping, transit time damping and ∇B contributions as a function of $k_{\perp}$ according to the model of Johnson and Cheng (1997). The largest contribution arises from the ∇B contribution. To determine the net diffusion coefficient across the magnetopause we integrate these results over the range $k_{\perp} > 2\pi/L_B$ where L_B is gradient scale length of the magnetopause as estimated in Chaston et al. (2008) to be $\sim$1000 km. These parameters provide cross field diffusion coefficients of 1 and 5×10^9 m^2 s^{-1} for $k_{\perp}/k_{\parallel} = 40$ and 100 respectively. To account for the width of the boundary layer, it was shown by Sonnerup (1980) that the required diffusion coefficient is 10^9 m^2 s^{-1}, which is roughly equivalent to the Bohm diffusion coefficient across the layer. Therefore, subject to the condition that $k_{\perp}$ has a significant component along the magnetopause, the diffusion coefficients obtained from the observed kinetic Alfvén wave properties are sufficient for boundary layer formation.

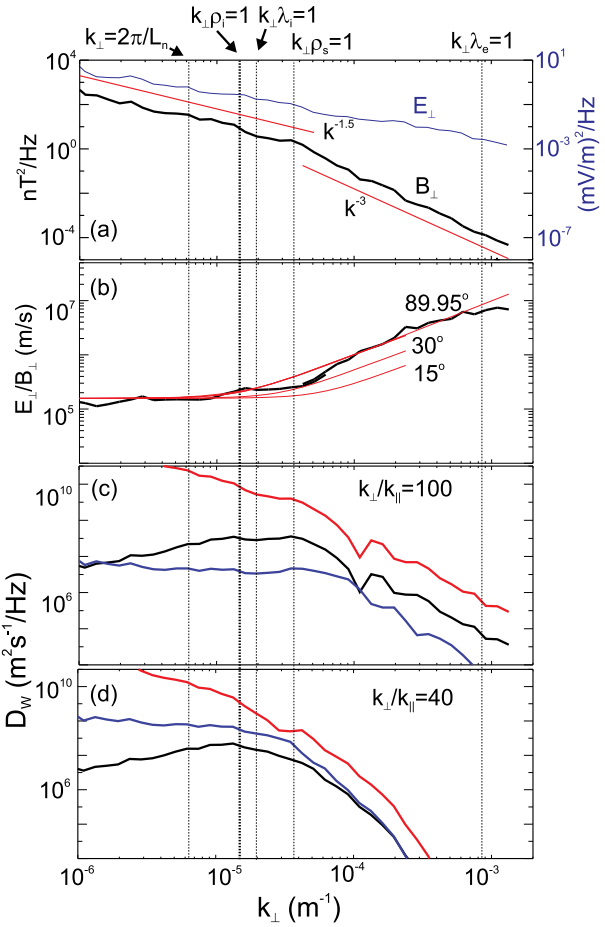

Fig. 7 (**a**) Average spectral results for perpendicular electric ($E_\perp$) and magnetic fields ($B_\perp$) from 10 traversals across or near the magnetopause. (**b**) Average $E_\perp/B_\perp$ ratio and model results (*red*). (**c**) and (**d**) diffusion coefficients for Landau damping (*black*), transit time damping (*blue*) and coupling to gradient drift along the magnetopause (*red*) for different $k_\perp/k_\parallel$ ratios. (From Chaston et al. 2008)

Another observable supporting diffusive entry of plasmas into the magnetosphere is the correlated distribution of KAWs at the magnetopause and the distribution of magnetosheath plasma inside the magnetosphere. Figure 8 shows results from a statistical study of KAW wave events observed within ten ion gyro radii of the magnetopause (outer circle) (cf., Berchem and Russell 1982), across the magnetopause itself (middle circle) and in the boundary layer (inner circle) as functions of magnetic local time (Yao et al. 2011). The largest spectral energy densities are found just outside the magnetopause at noon and under conditions of southward directed IMF. However, for both the northward and southward IMF cases there exists an enhancement on the dawn side relative to the dusk side—particularly at the magnetopause itself. Locally, this distribution can be qualitatively understood as a consequence of magnetosheath flow around the magnetopause, where slowly propagating waves 'pile-up' in the depletion layer and progressively propagate inwards across field lines as they advect tailward with the flow. The asymmetry, which favors the dawnside, is presumably a consequence of the preferred location for quasi-parallel shocks on the dawnside (Luhmann et al. 1986) due to Parker spiral configuration.

The significance of the spectral energy distribution shown Fig. 8 for transport across the magnetopause is that the cross-field diffusion coefficients in kinetic Alfvén waves are

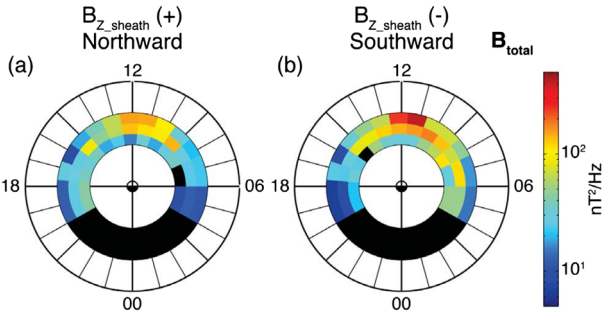

Fig. 8 Statistical distribution of wave spectral energy density as a function of magnetic local time at $k_\perp \rho_i \approx 1$. The *outer circle*, *middle* and *inner circle* correspond to observations just outside the magnetopause, on the magnetopause and in the boundary respectively. (From Yao et al. 2011)

proportional to spectral energy density (Johnson and Cheng 1997). Consequently, the distribution shown in Fig. 8 is a proxy for the relative efficacy of the cross-field transport in kinetic Alfvén waves as a function of location time on the magnetopause. If kinetic Alfvén waves are an important driver of cross-field transport, the spatial distribution of magnetosheath ions within the magnetosphere should be consistent with the distribution of these waves at the magnetopause. Studies have indeed found that magnetosheath ions have higher densities when observed in the dawnside magnetosphere than the duskside under conditions of northward IMF (Hasegawa et al. 2003; Wing et al. 2005). The distribution of these ions inside the magnetosphere as reported by Wing et al. (2005) is shown in Fig. 9c. This distribution is perhaps representative of what one would expect from diffusion for the wave distribution shown in Fig. 8. Additionally, enhanced wave amplitudes at pre-noon will drive enhanced inward fluxes of magnetosheath ions across the magnetopause on the dawnside. The tangential flow of these ions as they diffuse across the magnetopause will then carry these ions tailward to form the boundary layer and account for the distribution of these ions as shown in Fig. 9c. Moreover, the smaller spectral energy densities observed post-noon on the dusk-side, as shown in Fig. 8, would presumably drive the same process, albeit weaker, resulting in the observed dawn-dusk asymmetry apparent in Fig. 9c.

In addition to estimates of the diffusion coefficients and the spatial distribution of KAWs on the magnetopause, there are specific features of the ion distribution which are suggestive of the action of KAWs in cross magnetopause transport. Izutsu et al. (2012) noted that because transport in KAWs is energy dependent, it should be possible to see energy dependence in the transport of plasma across the magnetopause by comparing distribution functions. Essentially, to interact with the waves, the particles must be in resonance with the KAW, which in a high-beta plasma, is faster than the Alfvén velocity meaning that KAWs selectively transport more energetic particles. One feature of the observations of cold dense plasma (Wing et al. 2005; Johnson and Wing 2009) is that the temperature of the cold dense plasma sheet material increases across the flanks, which could be the result of such a filtering effect. On the other hand, within the plasma sheet, where the Alfvén velocity is large enough, the nominal CDPS material (1 keV) may not have sufficient energy to resonant with Alfvén waves and KAW transport may have a more limited role.

Another expected characteristic of ion distributions transported across the magnetopause through the action of KAWs is a temperature anisotropy of the magnetosheath ion component where $T_\perp / T_\parallel > 1$. This is a consequence of the heating that these ions undergo if the guiding center drifts in the wave field over a gyro-orbit are comparable to the wave scale. Under these conditions the normal adiabatic motion of the ions can be disrupted and energy may be gained in a stochastic manner leading to an effective heating of the ion plasma in the direction transverse to B_o. This mechanism was first suggested by Johnson and Cheng (2001) at the magnetopause. Through this process, heating generally occurs when the wave

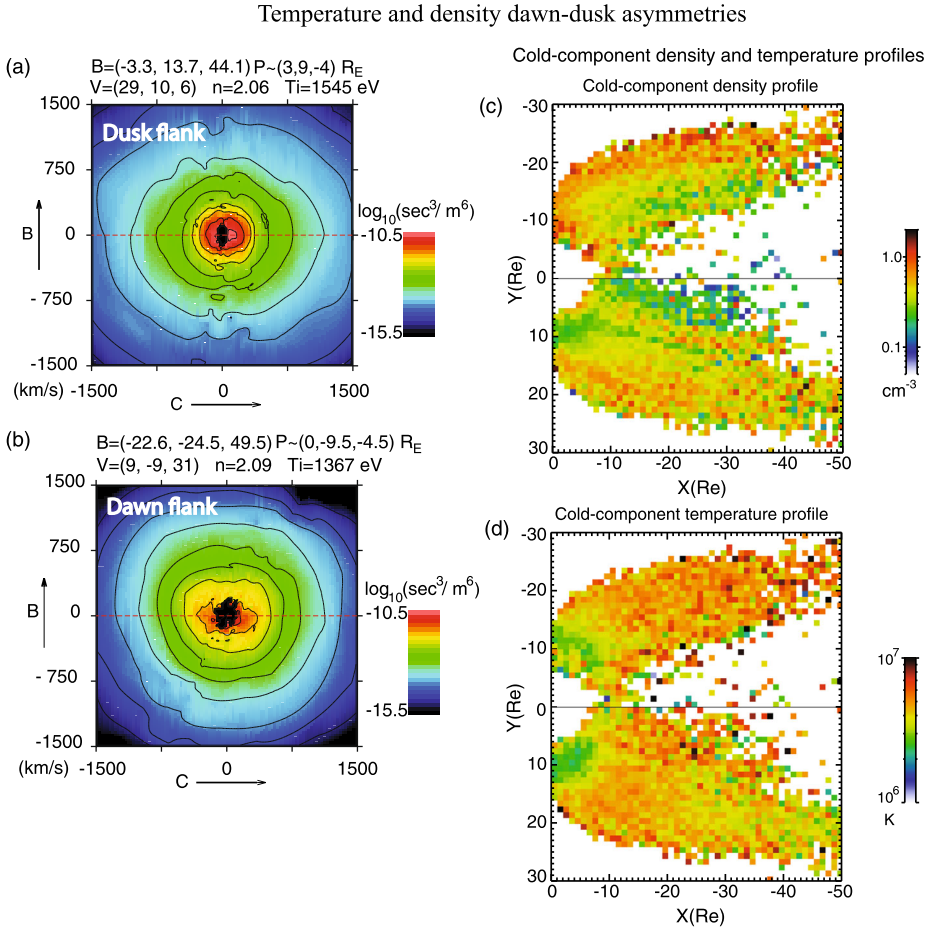

Fig. 9 Ion distribution functions in the mixed region where cold magnetosheath-like and hot magnetospheric ions are simultaneously observed in (**a**) the dusk flank and (**b**) the dawn flank during northward IMF. Shown are the slices of the flow in the BC planes, where the Y-axis $= B =$ aligned with the magnetic field and the X-axis $= C =$ perpendicular to the magnetic field. The cold and hot components in the dusk flank (**a**) are fairly isotropic. However, in the dawn flank (**b**), while the hot component is fairly isotropic, the cold component shows evidence of heating in the direction perpendicular to the magnetic field. $B =$ magnetic field (nT), $P =$ satellite coordinate (R_E), $V =$ ion velocity (km/s), $n =$ ion density (cm^{-3}), $T_i =$ ion temperature (eV) (from Hasegawa et al. 2003). (**c**) Density and (**d**) temperature profiles of the cold component of the two-component Maxwellian distribution of the plasma sheet ions during northward IMF. Note that the dawn-dusk asymmetry in the temperature profile, with the dawn flank ions having higher temperatures than the dusk flank ions. (From Wing et al. 2005)

amplitude exceeds a threshold condition, but particles are only heated to a maximum energy dictated by the amplitude of the wave (Johnson and Cheng 2001; Chen et al. 2001). Figure 10a shows an example ion distribution function in the low latitude boundary layer observed in KAWs for which $T_\perp / T_\parallel > 1$ and Fig. 10b shows the statistical relationship between the perpendicular adiabatic invariant (Chew et al. 1956) and the wave spectral energy density taken from a study by Chaston et al. (2013). The latter provides evidence for the widespread heating of the ion plasma by an amount proportional to the wave spectral energy

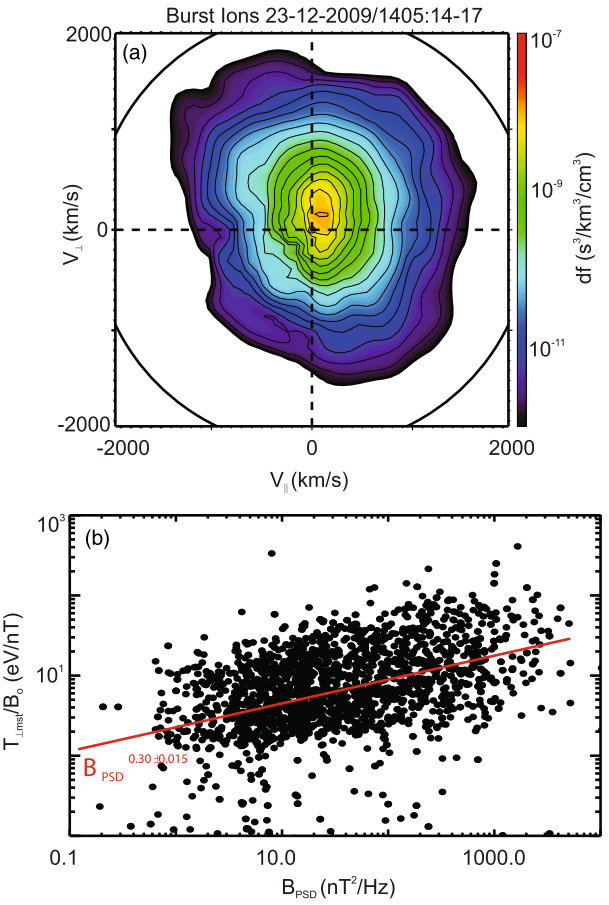

Fig. 10 (**a**) Ion phase space density snapshot taken during a KAW wave event and projected onto a plane defined by the magnetic field and the ion flow velocity vector. (**b**) Variation of the perpendicular CGL adiabatic invariant plotted against total magnetic spectral energy density at spacecraft frame frequencies where $k_\perp \rho_i \approx 1$. *Red line* shows a power-law fit. (From Chaston et al. 2013)

density. In the study by Chaston et al. (2013) the heating rates for the stochastic process based on the formalism of Chandran et al. (2010) were used to demonstrate that the amount of heating was commensurate with the wave amplitudes observed. Significantly, since this heating process effectively demagnetizes the ion plasma it will also contribute to cross-field transport in addition to the resonant mechanisms described earlier, consistent with the result from Wing et al. (2005) who showed that magnetosheath ions in the magnetosphere on the dawn side have significantly enhanced temperature, as displayed in Fig. 9d. As discussed in Sect. 3.2, the dawn side temperature in Fig. 9d actually underestimates the actual temperature. Thus, the dawn-dusk temperature asymmetry of the cold component is actually stronger than shown in Fig. 9d. The figure also shows that the dusk temperature at $r < 20\ \mathrm{R_E}$ is higher than at $r > 20\ \mathrm{R_E}$, which may be attributed to the dawn side hotter ions undergoing $\mathbf{E} \times \mathbf{B}$ earthward and curvature and gradient duskward drifts, resulting in higher dusk side temperature at the near Earth region (e.g., Spence and Kivelson 1993).

While at this stage we do not have simulation results verifying the transport of magnetosheath plasma across the magnetopause in KAWs, there have been recent advances in understanding the local generation processes of these waves. Lin et al. (2010) showed with hybrid simulations that a compressional wave driver naturally leads to the pile up of wave energy at the Alfvén resonance location with mode conversion efficiency consistent with

analytical estimates based on linear theory (Hasegawa and Chen 1976; Johnson and Cheng 1997, 2001), and the solutions exhibit gyro-radius scale across the boundary. Although the linear mode conversion process produces small-scale waves at the magnetopause, there are legitimate questions about whether those waves can provide adequate transport because the transport coefficients are controlled by the azimuthal wave vector, k_y rather than the radial component, k_x and the linear mode conversion provides waves with k_x only. However, the 3D simulations of Lin et al. (2012) have shown that following a stage dominated by linear physics, where waves of large amplitude grow near the resonant surface, there is a parametric decay through three-wave coupling between the KAWs and damped sound waves that leads to a broad spectrum of modes with azimuthal wavelength of the order of the gyro-radius consistent with analytical estimates (Chen and Zonca 2011). This nonlinear process can facilitate large transport across the boundary consistent with the observed transport coefficients. Recently, global hybrid simulations have shown, in detail, that mode conversion process takes place at the magnetopause boundary with wave characteristics consistent with KAWs (Shi et al. 2013).

The diffusion coefficient estimates, the distribution of waves on the magnetopause, and the corresponding plasma distributions and properties in the magnetosphere together provide a plausible argument that KAWs are important for facilitating the entry of magnetosheath ions into the magnetosphere. Before closing however, it is necessary to identify two unresolved issues in the case for KAW driven cross magnetopause transport. The first is alluded to above and relates to the requirement that a large component of $\boldsymbol{k}$ be azimuthal (k_y) to the magnetopause for the resonant transport mechanism of Johnson and Cheng (1997) to operate. Attempts have been made to infer the direction of $\boldsymbol{k}$ from the minimum variance direction of the magnetic field fluctuations (Rezeau et al. 2001). However, given the nearly linear polarization of KAWs and the turbulent nature of the fields analyzed, these measurements, as acknowledged by the authors are somewhat ambiguous. To robustly identify the k_y requires either the fortuitous alignment of the separation vector between two spacecraft along the magnetopause or preferably measurements from at least 3-points separated by distances of the order of ion gyro-radii so that the orientation and gradient scale of the magnetopause can be simultaneously determined. If we are seeking to account for the formation of the low latitude boundary layer these measurements should also be performed near the ecliptic plane. To our knowledge, a suitable spacecraft configuration has not yet been attained; however with the imminent launch of the Magnetospheric Multi-scale Mission we should be able to perform this needed measurement.

The second unresolved issue for KAW driven cross magnetopause transport is that to prevent suppression of the transport process by the occurrence of large ambipolar electric fields it is necessary that electrons be transported at the same rate as the ions. Hasegawa and Mima (1978) argue that equivalent transport rates for electrons and ions arise naturally from the energy balance between electrons and ions interacting in the wave. Whether or not this actually occurs at the magnetopause seems questionable since the energy in the waves presumably arises from an upstream source or mode conversion on the magnetopause from compressional waves (Hasegawa and Chen 1976; Johnson et al. 2001; Lin et al. 2010). Observations do however show quite clearly that KAWs locally interact with electrons (Chaston et al. 2007, 2008) along the magnetopause and flux enhancements of ionospheric electron populations are commonly observed in the boundary layers (Song et al. 1993). It is conceivable that these processes serve to neutralize the charge due to the high mobility of electrons along field lines and thereby allow cross-field transport to proceed. Nonetheless further consideration of this issue seems necessary and can perhaps be best addressed through simulations.

2.4 Impulsive Penetration

The concept of Impulsive Penetration (IP) of solar wind plasma elements across a planetary magnetopause is based on the evidence that the solar wind is gusty, that the magnetosheath plasma and magnetic field are generally varying over time scales smaller than the time required for the solar wind plasma to encompass the magnetosphere (e.g., Burlaga et al. 1969; Turner et al. 1977; Sibeck 1990; Turner et al. 2011; Hietala et al. 2012; Karlsson et al. 2012; Archer and Horbury 2013; Plaschke et al. 2013; Savin et al. 2014). The IP mechanism is also inspired by the classical behavior of laboratory plasmas injected across non-uniform magnetic fields (e.g., Schmidt 1960; Baker and Hammel 1965; Demidenko et al. 1969).

The evidence for small scale patchiness of the solar wind plasma led Lemaire (1977) to argue that localized dynamical pressure pulses along the bow shock propagate across the entire magnetosheath, and impact the magnetopause surface which they can traverse as shown in Fig. 5 (Lemaire 1977, 1985; Lemaire and Roth 1978). The higher resolution multi-point measurements of plasma and field properties in the solar wind, magnetosphere and magnetosheath performed in the late 1990s and during the last decade by INTERBALL, Cluster and THEMIS confirm that the plasma impacting on the magnetopause is not-uniform but turbulent and patchy, as considered in the original scenario of the IP. Case study events (e.g., Nemecek et al. 1998; Savin et al. 2008; Hietala et al. 2009; Amata et al. 2011), and recent statistical analysis over longer time intervals (Karlsson et al. 2012; Archer and Horbury 2013; Plaschke et al. 2013) reveal that the plasma flow in the magnetosheath is dominated by pulses of increased dynamic pressure, also called plasma jets or blobs/plasmoids.

Karlsson et al. (2012) showed from Cluster data that the probability to observe large amplitude density enhancements (50 % higher than the background) is about 45 % in the magnetosheath. The spatial scale of these structures on average is of the order of 1 R_E, and about 30 % of the density enhancements have also an excess of the plasma bulk velocity.

In a recent statistical study, Archer and Horbury (2013) revealed that the magnetosheath inhomogeneities (or jets or plasmoids or blobs) characterized by dynamic pressure enhancements (mainly velocity increases) are detected quite regularly in THEMIS data—the dynamic pressure may be enhanced by up to 15 times than the background magnetosheath flow. Plaschke et al. (2013) analyzed THEMIS data and found numerous cases of high speed jets moving towards the magnetopause in the subsolar magnetosheath. Their study reveals not only isolated jets/blobs but also series of jets/blobs or periods of quasi-continuous increasing of the dynamic pressure in the magnetosheath impacting on the magnetopause. Note also that rolled-up Kelvin-Helmholtz vortices identified by single spaceraft techniques may be signatures of flow anomalies related to the dynamic pressure pulses in the vicinity of the magnetopause (Plaschke et al. 2014).

The impulsive penetration mechanism is based on four main pre-requisites: (1) the existence of plasma irregularities and solar wind gusts in the magnetosheath with an excess density and/or velocity with respect to the background magnetosheath flow; (2) a non-vanishing component of the velocity normal to the magnetopause; (3) a spatial scale of the irregularity/jet/plasmoid/blob larger than δ, the minimum width of the space charge layer at the edges of the blob, as explained below; (4) a plasma dielectric constant, ε, much larger than one. When these conditions are satisfied the solar wind and/or magnetosheath plasmoids/jets can penetrate across the magnetopause due to a self-polarization electric field ($\mathbf{E_P}$) generated by polarization charges piling up along the edges/surface of the propagating irregularities. This polarization process has been described first by Schmidt (1960). The electric charges are carried sidewards by the Lorentz force, $q\mathbf{u} \times \mathbf{B}$, and by polarization drifts, in opposite

directions for the electrons and the ions. The polarization drifts drive "polarization currents" perpendicular to $\mathbf{B}$ and $\mathbf{u}$ determined by $\mathbf{j_P} = (\rho/B^2)\partial\mathbf{E}/\partial t$ as pointed out by Lemaire and Roth (1978), see also Lemaire (1985) and Roth (1992).

It is important to stress that ε, the dielectric constant (or permittivity) of the plasma, must be much larger than unity for the Schmidt's kinetic theory to be applicable:

$$\varepsilon = 1 + \frac{\rho c^2}{B^2 \mu_0} = 1 + \frac{\omega_p^2}{\Omega_c^2} \gg 1 \tag{1}$$

where ω_p is the plasma frequency and Ω_c is the proton Larmor frequency (Lemaire 1985). A large dielectric constant polarizes plasma irregularities and makes their motion to be dominated by collective effects in contrast to the motion of individual charged particles described by Alfvén's first order guiding center theory.

Within the magnetosphere the plasmoids/jets interact with the geomagnetic field through a coupling magnetic force similar to the interaction between two magnetic dipoles (Lemaire et al. 1979; Lemaire 1987 and Lemaire and Roth 1991). During northward IMF, the penetration of magnetosheath plasmoids/jets is favored in the magnetospheric tail regions as consequence of this magnetic dipole-dipole interaction. The penetration is, however, inhibited in the frontside and the nose of the magnetosphere. Conversely, for southward IMF: the impulsive penetration of plasma elements with an excess kinetic pressure is favored in the frontside magnetospheric regions. An illustration of the IMF control of the impulsive penetration due to the magnetic dipole-dipole interaction is shown in Fig. 11 (Roth 1995).

Inside the magnetosphere the irregularities are slowed down adiabatically as a consequence of the conservation of the magnetic moment $\mu = (\mathbf{v} - \mathbf{u})_\perp^2/B$ of the electrons and ions, a process demonstrated by laboratory experiments (Demidenko et al. 1969, 1972) and 3D electromagnetic Particle-in-Cell (PIC) simulations (Voitcu 2014).

The mechanism that decouples the plasmoid from the background plasma and field is based on the formation of a parallel electric field (Lemaire and Roth 1981; Lemaire 1985). This magnetic field aligned component is described by the self-consistent Vlasov equilibrium solutions obtained by Echim (2004) and Echim and Lemaire (2005). The parallel component of the electric field violates locally the "frozen-in" condition $E \cdot B = 0$ and is sustained by parallel gradients of the kinetic pressure (Lemaire and Scherer 1974, 1978), and/or a shear in the field-aligned direction of the perpendicular plasma bulk velocity (Echim 2004; Echim and Lemaire 2005). Note also that in the coarse grained MHD simulations the condition $E \cdot B = 0$ is not rigorously satisfied due to the numerical resistivity (Guo et al. 2010). Indeed, in general parallel electric fields have spatial scales of the order of the ion inertial length, much smaller than the macroscopic MHD grid scales. Nevertheless, in kinetic models, the parallel electric field is computed based on physical principles and the effects of the numerical resistivity are well understood and quantified.

A positive gradient of the plasma density is formed during the inward motion of plasma elements inside the geomagnetic field since the volume expands and the density decreases (Echim and Lemaire 2002). Such characteristic positive density gradients of magnetosheath like plasma have been observed in the "magnetopause boundary layer" by Sibeck et al. (2000).

In addition to the adiabatic breaking, the inward motion of the magnetosheath plasma elements is slowed down non-adiabatically through magnetosphere-ionosphere coupling via field-aligned currents along geomagnetic field lines connecting the plasma irregularity with the resistive ionosphere. A fraction of the excess energy of the magnetosheath plasma element is thus dissipated in the ionosphere where the electric conductivity is large enough

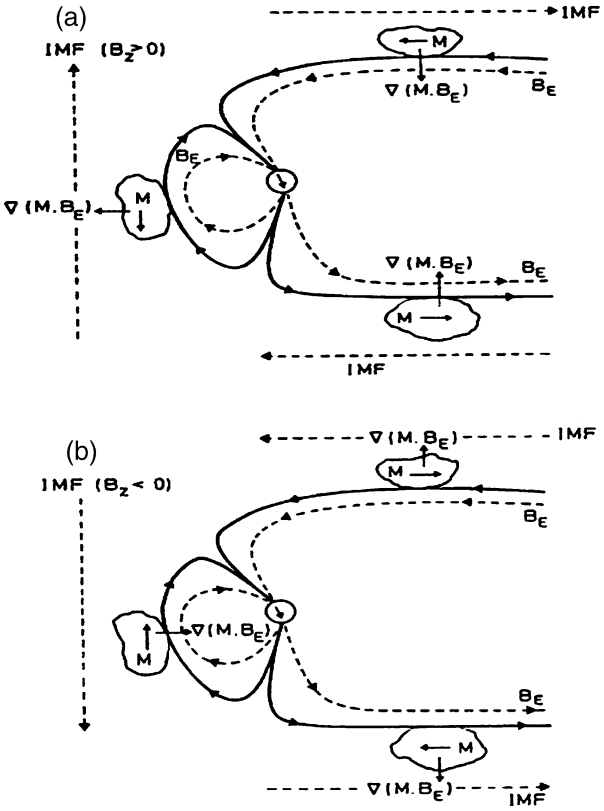

Fig. 11 Meridional section illustrating the dipole-dipole interaction between the intruding plasmoids/jets and the geomagnetic field, in various sectors and for various orientations of the IMF: (**a**) Northward IMF, when the impulsive penetration mechanism is favored in the tail; (**b**) Southward IMF when the impulsive penetration is favored through the frontside of the magnetosphere. $\mathbf{M}$ = the magnetic dipolar field of the solar wind irregularity and $\mathbf{B_E}$ = Earth's magnetic field. (From Roth 1995)

to produce significant Ohmic dissipation of the ionospheric Pedersen currents. By this irreversible process the intruding plasma blobs dissipate their kinetic energy into the polar ionosphere by Joule heating.

Observations of magnetosheath plasma elements engulfed in the magnetospheric boundary layer have been reported (Lundin and Aparicio 1982; Lundin and Dubinin 1984; Lundin 1988). Simultaneous magnetic field signatures from all four Cluster spacecraft give the opportunity to clearly separate MHD oscillatory wave motion of the magnetopause from magnetosheath plasmoids moving inwards inside the magnetosphere, and detached from the magnetopause (Stasiewicz and Gustafsson 2000; De Keyser et al. 2001). Sibeck et al. (2000) examined INTERBALL/Tail and MAGION-4 observations in the LLBL and found instances of magnetosheath-like plasma present inside the magnetosphere in 11 cases out of 57 magnetopause crossings. These were interpreted by Echim and Lemaire (2002) as effects of spreading along geomagnetic field lines of impulsively penetrating magnetosheath plasma elements. A review of laboratory and numerical simulations of IP can be found in the papers by Lemaire (1989), and Echim and Lemaire (2000).

All these observations, simulations and theoretical arguments support the IP model as a magnetospheric process relevant for plasma entry and transport during northward IMF. As emphasized above this model is based on the mechanism first introduced by Schmidt (1960) to explain the adiabatic motion of diamagnetic plasma elements across a non-uniform magnetic field, when the dielectric constant of the plasma is much larger than unity.

3 Constraints to Solar Wind Entry

3.1 Plasma Sheet Filling Rate

In the discussion of which entry mechanisms are significant in filling the plasma sheet with solar wind plasma, it is useful to establish first whether each entry mechanism is able to explain the observed plasma sheet filling rate. In other words, how much of the observed filling rate can be attributed to each entry mechanism.

In an attempt to do this, Wing et al. (2006) examined a northward IMF interval in which the plasma sheet ion filling rate is about 0.5 $cm^{-3}\,h^{-1}$ as observed locally by Geotail and remotely by DMSP satellites. They performed an order of magnitude calculation of the magnetosheath entry rate for (1) double cusp or double lobe reconnection (e.g., Song and Russell 1992), (2) KHI (e.g., Otto and Fairfield 2000), and (3) KAW (e.g., Johnson and Cheng 1997) and found that each of the three mechanisms is capable to fill the plasma sheet at the observed filling rate. This result is consistent with double cusp reconnection studies (e.g., Øieroset et al. 2005; Li et al. 2008) and KHI studies (e.g., Nykyri and Otto 2004; Nykyri et al. 2006), which showed that double cusp reconnection or KHI is sufficient to fill the plasma sheet with cold dense ions, respectively. The diffusive entry rate (either KHI or KAW) scales with solar wind density (n_{sw}) (Wing et al. 2006) while the double cusp reconnection entry rate depends weakly and non-monotonically with n_{sw} (Li et al. 2008). Some of the magnetospheric plasma is lost to the solar wind, inner magnetosphere, and ionosphere. Hence, the net plasma sheet filling rate would need to take into account not just the entry rate but also the loss rate.

The statistical studies by Plaschke et al. (2013) with THEMIS data and by Karlsson et al. (2012) with Cluster data give an estimate of the occurrence frequency, geometrical and dynamical properties of magnetosheath plasma elements directed towards the magnetopause; these magnetosheath plasma structures are good candidates for impulsive entry. The experimental characteristics give an estimate of the upper limit of plasma sheet filling rate by impulsively entering magnetosheath blobs/jets. Plaschke et al. (2013) and Karlsson et al. (2012) estimated the size of the plasmoids (or jets or blobs) to be of the order of 1 R_E. Both studies found a probability of jet/blob encounter of the order of $P \approx 40$ %, e.g. Plaschke et al. (2013) found 2859 jets for 6960 THEMIS magnetosheath crossings. The same authors indicate a median of the detection recurrence time (i.e. the time between two consecutive detection of plasmoids by the same spacecraft) of the order of $\Delta T = 140$ seconds for the dayside magnetosheath with a total range spanning from 6 to roughly 8000 seconds. Assuming a cylindrical shape of the plasma sheet as in Wing et al. (2006) with a volume $V_{ps} = 9.3 \times 10^{24}$ m^3, an upper limit of the plasma sheet filling rate by impulsively entering magnetosheath plasma blobs or jets is of the order of:

$$\frac{\partial n_{ps}}{\partial t} = \frac{N_{plasmo} V_{plasmo} n_{msh} f_{plasmo}}{V_{ps}} \tag{2}$$

where N_{plasmo} is an estimate of the number of plasmoids in the magnetosheath, V_{plasmo} is an estimate of the average volume of a plasmoid roughly equal to 1 R_E^3, n_{msh} is the magnetosheath density and f_{plasmo} is the plasmoid occurrence frequency. A rough estimate of N_{plasmo} is given by the plasmoid/jet detection rate, $P \approx 40$ % and by assuming that the volume of a plasmoid scales as $\sim$1 R_E^3 and the cross surface scales as $A_{plasmo} \sim 1$ R_E^2. Thus the upper limit of the total number of plasmoids is $N_{plasmo} = P \frac{A_{dayside}}{A_{plasmo}} = 0.4 \times \frac{2\pi 100 R_E^2}{R_E^2} = 80\pi$,

where $A_{dayside}$ is an estimate of the dayside magnetopause surface exposed to the magnetosheath (half of a sphere with 10 R_E radius). An estimate of the occurrence frequency is given by the median of the average plasmoid recurrence rate from the observations of Plaschke et al. (2013): $f_{plasmo} \approx (\frac{1}{140})\ s^{-1}$. Thus the plasma sheet filling rate by impulsively penetrating plasmoids/jets for a magnetosheath density of the order of 30 cm^{-3} (Wing et al. 2006) scales like 0.14 $cm^{-3}\,hr^{-1}$, comparable with the filling rate reported by Wing et al. (2006).

3.2 Dawn-Dusk Asymmetries

Global asymmetries in plasma sheet properties, particularly of the cold component, can provide significant constraints on plasma entry. Using ISEE-1 spacecraft potential as a proxy for the plasma density, Escoubet et al. (1997) showed that the density was slightly higher on the dawnside of the plasmasheet than on the duskside. Furthermore they showed that this asymmetry extended up to the dayside magnetosphere. Fujimoto et al. (1998) showed that in Geotail observations, during northward IMF, ions frequently have two distinct components (a hot and a cold component) on the dusk flanks, but only one component with a broad peak on the dawn flank, as shown in Fig. 12. Moreover, Hasegawa et al. (2003) reported that the ion hot component is generally nearly isotropic on both the dusk and dawn flanks. However, the cold component, which is similar to the magnetosheath ion population, is heated in the direction perpendicular to the magnetic field on the dawnside while it remains isotropic on the duskside, as shown in Figs. 9a and 9b (Hasegawa et al. 2003). In their follow-up study, Hasegawa et al. (2004a) performed a statistical study of the ion properties on both flanks. The results are shown in Fig. 13 (from Hasegawa et al. 2004a). When the ions have two clear components, one component with $T_h > 3$ keV and one with $T_c < 3$ keV, they are plotted as red and green dots respectively. However, when the ions have just one peak, then they are plotted as black dots. Figure 13 shows statistically that ions frequently have two components on the duskside, but only one component on the dawnside. Moreover, the cold component of the electron (temperature less than a few hundred eVs) has been heated in the direction parallel to the magnetic field line (Hasegawa et al. 2003; Fujimoto et al. 1998).

Wing et al. (2005) used DMSP satellites to infer plasma sheet temperatures and densities during periods of northward IMF. One advantage of using DMSP satellites is that these satellites have low altitude orbits with orbital periods of about 100 min. So, in about 2 hours, each DMSP satellite can cut through the footprint of the entire plasma sheet twice. Wing et al. (2005) fitted the ion spectra to one-component Maxwellian, two-component Maxwellian, and Kappa distributions and selected the best fits.

Their cold component (obtained from two-component Maxwellian fits) density and temperature profiles are displayed in Figs. 9c and 9d, respectively. The cold component density profile has peaks at dawn and dusk flanks, as shown in Fig. 9c. This suggests that the source of the cold component is magnetosheath or LLBL. In contrast, the hot component ion density profile does not have peaks at the flanks (see Fig. 8 in Wing et al. 2005), which would be expected if the direct source of the hot component is not the solar wind. Interestingly, the density of the cold component is higher on the dawnside than that on the duskside, suggesting perhaps there is more solar wind ion entry on the dawnside than on the duskside of the magnetopause (see also Guild et al. 2008 and Nagata et al. 2007). Figure 9d shows that the cold component temperatures are higher on the dawnside than the duskside, consistent with Hasegawa et al. (2003). This observation suggests that the magnetosheath ions have been heated in the entry process on the dawnside. The dawnside cold ion temperature is about 30–40 % higher than that on the duskside (see Fig. 7 in Wing et al. 2005). This estimate

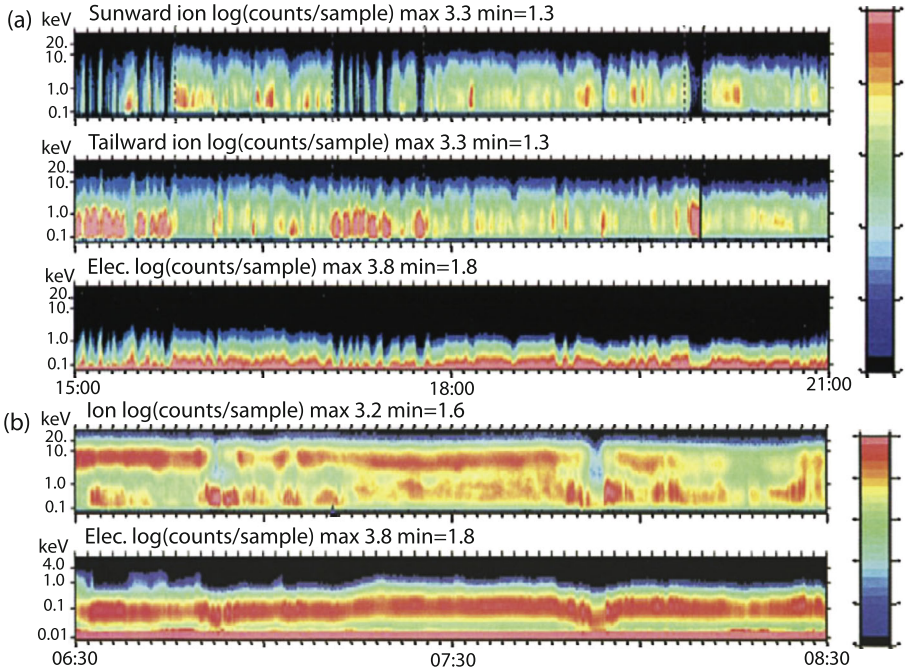

Fig. 12 Spectrograms showing Geotail observations during northward IMF in the magnetotail just inside the magnetopause on (**a**) the dawnside and (**b**) the duskside. On the dawnside (**a**) the ions appear as having one component with a broad peak, but on the duskside, the ions have two components: (1) hot and (2) cold components. (**a**) The three panels show sunward ions, tailward ions, and omnidirectional electrons. *Color codes* are assigned according to logarithms of counts per sample with maximum = *red* and minimum = *dark blue*. (**b**) *Top panel* shows omnidirectional ions depicting mixing of hot and cold components and *bottom panel* shows omnidirectional electrons. (From Fujimoto et al. 1998)

may actually understate the cold ion temperature dawn-dusk asymmetry. The reason is that on the dawnside, we can only obtain two components when the cold ion temperatures are sufficiently low or hot ion temperatures are sufficient high to give a two component distribution (e.g., Johnson and Wing 2009). Otherwise, the distribution would appear to have a single κ distribution and the cold and hot components are not discernable (e.g., Wing et al. 2005).

In agreement with Fujimoto et al. (1998) and Hasegawa et al. (2003, 2004a), Wing et al. (2005) found that two components are more frequently found on the dusk flank than on the dawn flank. The hot component has higher temperatures on the dusk flank than on the dawn flank, which can be attributed to the curvature and gradient drifts. The cold component, on the other hand, has higher temperatures on the dawn flank than the dusk flank. Hence, on the dusk flank, the cold and hot component temperatures frequently have distinct separations and the ions can be identified as having two components. In contrast, on the dawn flank, the cold and hot component temperatures frequently are closer to each other, frequently forming one component having a broad peak.

3.2.1 Possible Causes of the Temperature Asymmetry

It is not clear what causes the temperature asymmetry in the cold ion profile. For the solar wind Parker spiral, which is the dominant solar wind orientation, the magnetosheath mag-

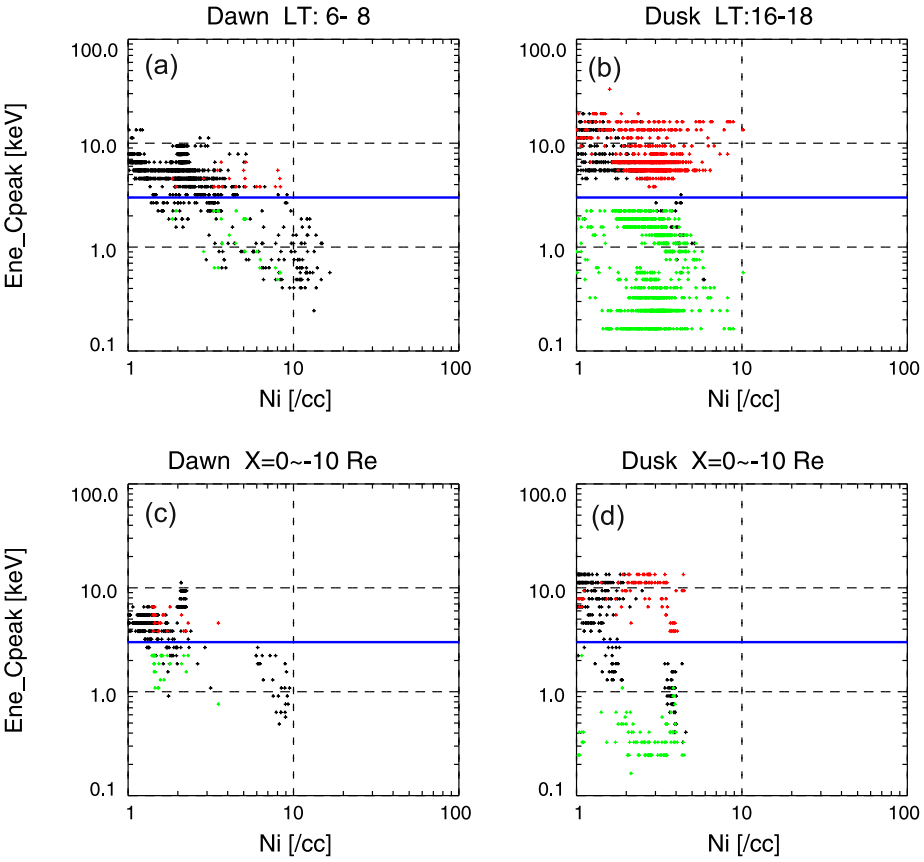

Fig. 13 Ion energy spectrum behavior in the mixed region during extended northward IMF periods in the [(**a**), (**c**)] dawn and [(**b**), (**d**)] dusk flanks. For each data sample, if the ion energy spectrum has a count rate (energy flux) peak both below and above 3 keV, the higher and lower peak energies are plotted as *red* and *green dots*, respectively. Otherwise, the energy at which the count rate reaches maximum is plotted as a *black dot*. There is a clear dawn-dusk asymmetry. There are more two-component ions on the duskside than on the dawnside. Conversely, there are more one-component ions on the dawnside than on the duskside. On the dawnside, the hot and cold components (*red* and *green dots*) are closer together in energy/temperature space. (From Hasegawa et al. 2004a)

netic field has been shown to be more turbulent down stream of the quasi-parallel shock (the dawnside magnetosheath) than down stream of the quasi-perpendicular shock (the duskside magnetosheath). An example of this for solar wind Parker spiral orientation can be seen in Fig. 14, which shows Geotail magnetic field observations in the magnetosheath (from Petrinec 2013). The fluctuations in the magnetic field could indicate the presence of the compressional waves. KAW can be generated when the compressional waves interact with the magnetospheric boundary, which can lead to diffusive transport of the solar wind/magnetosheath ions across the magnetopause boundary (Johnson and Cheng 1997). The waves have a parallel electric field, which can heat electrons in the direction of the magnetic field (Hasegawa and Chen 1975; Hasegawa and Mima 1978). When the waves have large amplitudes, they can also heat ions in the direction perpendicular to the magnetic field (Johnson and Cheng 2001). Because the source of compressions could be compres-

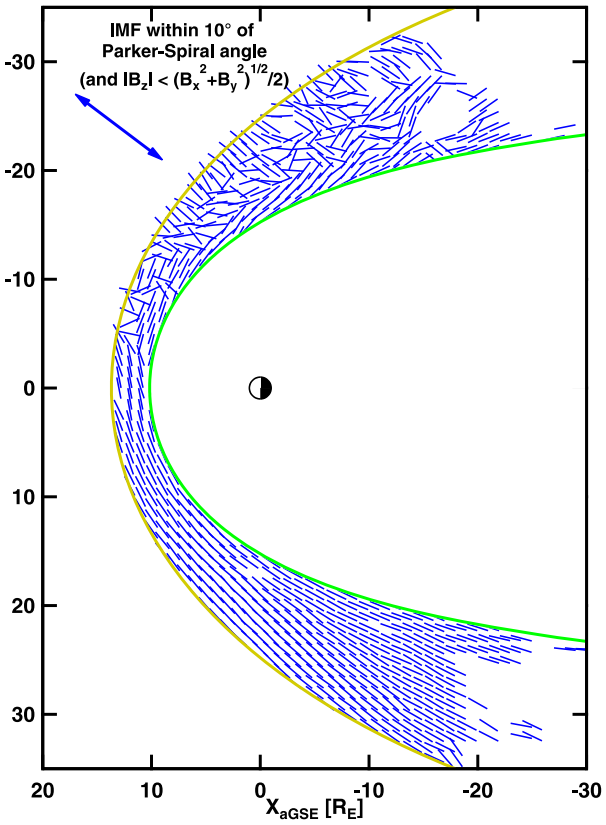

Fig. 14 Median magnetic field vector orientation in 1×1 R_E bins in the equatorial plane when IMF is within 10° of Parker spiral angle. (Adapted from Fig. 6 in Petrinec 2013)

sional instabilities generated in the magnetosheath or compressions driven directly by the solar wind, in a statistical sense, there can be a dawn-dusk asymmetry in the KAWs and ion heating during entry. A recent survey of wave power in the sheath and magnetopause suggests that the wave power associated with transverse KAWs is enhanced along the dawn flank (Yao et al. 2011; Chaston et al. 2013), which would provide enhanced transport. This is shown in Fig. 8 and discussed in Sect. 2.3. The study of Chaston et al. (2008, 2013) also provides observational evidence of stochastic heating of ions by KAWs as predicted by Johnson et al. (2001).

3.2.2 Possible Causes of the Density Asymmetry

Magnetosheath Density Asymmetry It is not clear what causes the dawn-dusk asymmetry in the cold ion density profile. The dawn-dusk density asymmetry may also be caused by the dawn-dusk asymmetry in the source, i.e., magnetosheath population itself. Several magnetosheath studies showed that the magnetosheath density (n) is higher on the dawnside than the duskside (e.g., Paularena et al. 2001; Nemecek et al. 2002). More interestingly, Walsh et al. (2012) found that in THEMIS observations close to magnetopause, near noon, the magnetosheath density is essentially dawn-dusk symmetrical, $n_{\mathrm{dawn}}/n_{\mathrm{dusk}} \sim 1$, but $n_{\mathrm{dawn}}/n_{\mathrm{dusk}}$ ratio grows larger away from noon, reaching $\sim$1.2 at 5 h away from noon. They also found similar patterns in BATS-R-US MHD, except that the asymmetry is even more pronounced, $\sim n_{\mathrm{dawn}}/n_{\mathrm{dusk}} \sim 1.5$, near the dawn and dusk flanks. This new result may put an additional

constraint on the entry location of the magnetosheath ions, in light of the observed dawn-dusk density asymmetry in the plasma sheet. On the other hand, a recent statistical study utilizing 5+ years of magnetosheath observations by THEMIS in aberrated Magnetosheath InterPlanetary Medium (MIPM) reference frame did not find a clear dawn-dusk density asymmetry (Dimmock and Nykyri 2013).

KHI The dawn-dusk asymmetry in the cold ion density may also be attributed to the dawn-dusk asymmetry in the entry rate or entry process, i.e., the entry rate at the dawn flank magnetopause is higher than that at the dusk flank. Hasegawa et al. (2006) examined the occurrence rate of the KHI on the dawn and dusk flanks during northward IMF in Geotail data 1995–2003 and found that the occurrence rate is roughly equal. However, a recent simulation study by Nykyri (2013) shows that for the Parker spiral IMF orientation and for a large range of upstream solar wind plasma and field parameters, the KHI always grows faster at the dawn flank magnetopause compared to dusk flank, even though the plasma velocity is higher at the dusk flank. This may partly help explain the observed dawn-dusk density and temperature asymmetry of the CDPS because the IMF is statistically more often in Parker Spiral orientation. The study showed that the KHI growth rate is faster at the dawn flank because the tangential magnetic field along the typical KH k-vector is smaller at the dawn than at the dusk flank for the Parker Spiral IMF orientation. The growth rates of the KHI at dawn and dusk flanks correlated well with the ratio of the velocity shear and Alfvén speed along the wave vector k. Also, the statistical study of THEMIS measurements in the magnetosheath showed that dusk flank has stronger tangential magnetic field and plasma velocity compared to dawn flank (Dimmock and Nykyri 2013). The enhanced KHI activity at dawn could both increase plasma transport and heating via reconnection in KH vortices (Nykyri and Otto 2001), and due to enhanced KAW activity associated with the KHI, e.g., (Johnson and Cheng 1997). The dawn-dusk asymmetrical distribution of heavy ions can also contribute to the asymmetry in the KHI activities and entry rate (Johnson et al. 2014).

Interestingly, Wang et al. (2007) reported that the magnetosheath ion entry from the dawn flank is more efficient with decreasing Vsw, but no significant Vsw effect is seen on the dusk flank.

KAW The asymmetric heating of the cold component/magnetosheath ions may suggest an asymmetry in the KAW led entry, i.e., more KAW led entry on the dawnside than the duskside magnetopause. The dawn-dusk asymmetry in KAW activities has been discussed in Sect. 3.2.1.

Reconnection The dawn-dusk asymmetry in the solar wind entry rate may also be attributed to the asymmetry in the magnetotail flank reconnection. Peroomian and El-Alaoui (2008) performed large-scale kinetic (LSK) simulations that show that most solar wind ions enter along the dawn flank primarily through reconnection. They also found that the entry locations can be modulated by IMF By. When IMF By is positive, the solar wind ion entrees along the dusk flank can increase. Similarly, using the same technique, Peroomian et al. (2011) showed that a large number of solar wind ions enter along the dawn flank through reconnection and get energized nonadiabatically before reaching the dawnside ring current.

Li et al. (2008) studied the double cusp reconnection entry mechanism with MHD simulations and found that ionospheric conductance affects the convection of the newly closed field lines and can introduce asymmetry in the entry rate. Hence, the asymmetries in MHD simulations may result from local time differences in ionospheric conductance (Zhang et al. 2012). However, this mechanism may not introduce dawn-dusk asymmetry in the cold component temperature.

Impulsive Penetration The impulsively penetrating magnetosheath irregularities that move inside the magnetosphere across the northward oriented magnetic field lines are deflected by the charge and energy dependent gradient-B and curvature drifts sustained by the nonuniform magnetospheric electric and geomagnetic field. Lemaire (1985) showed that for northward IMF the magnetosheath irregularities experience an asymmetric eastward deflection inside the magnetosphere by the gradient and curvature drifts leading to a dawn-dusk asymmetry. Indeed, the magnetosheath irregularities that penetrate the dawn flank during northward IMF are deflected towards East and gradually expand and therefore their density diminishes: the density is larger closer to the entry regions, i.e. closer to the magnetopause. At the dusk flank the deflection is towards East and therefore, the magnetosheath irregularities accumulates in the duskside LLBL, closer to the entry region. It was also suggested that magnetosheath jets are more often observed during radial IMF (Hietala et al. 2012), thus they would preferably be present downstream the quasi-parallel geometry of the bow shock, thus in the dawn flank of the magnetosheath.

Gradient Drift Entry (GDE) Olson and Pfitzer (1985) proposed that gradient drift entry (GDE) would allow magnetosheath ions to enter along the dawn flank and the electrons along the dusk flank. They argued that this entry mechanism can lead to the observed field-aligned current (FAC) polarity and the dawn-dusk current in the magnetotail, at least qualitatively. However, it is not clear if GDE alone can account for the observed filling rate or the cold dense state of the plasma sheet. Treumann and Baumjohann (1988) calculated that only 5 % of the magnetosheath particles that come in contact with the magnetopause can be trapped in the magnetosphere in their model. The difficulty here is that the number of particles that come in contact with the magnetopause is unknown in any realistic magnetopause model. Hence, the efficiency of GDE is unknown. Richard et al. (1994) traced thousands of ions in a fixed MHD electric and magnetic fields and found that most solar wind ions enter the magnetosphere through double cusp type reconnection (Song and Russell 1992) and found only a small fraction enters with GDE mechanism.

More recently, Zhou et al. (2007) used a simple model to calculate GDE efficiency and found that only electrons and ions having energies larger than several keV can gradient drift into the magnetosphere during southward IMF. However, during northward IMF, lower energy particles can enter, but their efficiency was not calculated. In any case, GDE cannot explain the ion and electron heating in the entry process.

3.2.3 Asymmetries During Southward IMF

During southward IMF, there is evidence that solar wind particles can still enter from the flank magnetopause albeit in smaller amounts. Figure 15 panels a–d show plasma sheet ion n and T profiles for northward and southward IMF obtained from DMSP observations (note here the hot and cold components are combined) (Wing and Newell 2002). Panels a and b show that during northward IMF, there are density maxima and temperature minima along both flanks, which can be taken as a signature for solar wind ion entry, as discussed above. Interestingly, during southward IMF, there is also evidence for solar wind ion entry along the flank, as suggested by the density maxima and temperature minima along both flanks in panels c and d, albeit the density maxima and the temperature minima are smaller compared to those for northward IMF. Panel c shows that during southward IMF, the density is higher along the dawn flank than the dusk flank, which suggests a dawn-dusk asymmetry in the solar wind entry along the flanks. These DMSP observations are corroborated by Geotail observations in panels e–h, which show that during southward IMF, there are density peaks

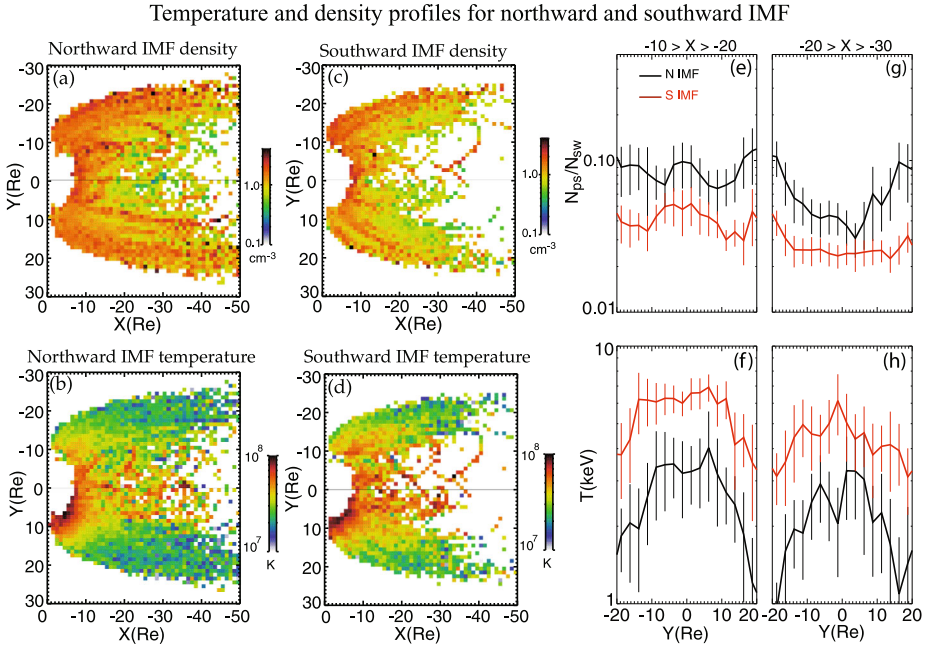

Fig. 15 The plasma sheet ion density 2D profiles inferred from DMSP observations for the northward and southward IMF are shown in (**a**) and (**c**) respectively and their corresponding temperature profiles are shown in (**b**) and (**d**) respectively (from Wing and Newell 2002). The density and temperature 1D profiles obtained from Geotail observations at $-10 > X > -20$ R_E are plotted in (**e**) and (**f**), respectively and at $-20 > X > -30$ RE in (**g**) and (**h**), respectively. (From Wang et al., PET09 Workshop, Fairbanks, Alaska, March 2009; the method is described in Wang et al. 2010)

and temperature minima on both flanks, but the flank source is weaker (Wang et al. 2006). Figure 15 panels e and g show that in Geotail observations for southward IMF, the density is higher on the dawn side than the dusk side, consistent with DMSP observations.

Presently, it is not firmly established what is/are the entry mechanism(s) for solar wind ions along the flanks during southward IMF, but KHI and KAW, in principle, can still operate under southward IMF, although KHI may be less favorable for southward IMF than northward IMF (Miura 1995). Recently, Hwang et al. (2011) observed KH waves under southward IMF on the dawnside, but the KH vortices can be irregular and intermittent. Under dawnward IMF, Hwang et al. (2012) reported KH waves near the northern exterior cusp that were propagating tailward perpendicular to the magnetosphere and magnetosheath magnetic field.

3.3 Entropy

For studies of plasma transport into and within the plasma sheet, it is often useful to consider what parameters are conserved and under what conditions. One fundamental quantity is the entropy, which is conserved both locally and globally when the plasma response is adiabatic (Birn et al. 2006b). Locally, the entropy per unit mass in an ideal, isotropic plasma is $\sigma = C \log(p^{1/\gamma}/\rho)$ where $p =$ the plasma pressure, $\rho =$ mass density, $\gamma =$ the polytropic index $= 5/3$ (Baumjohann 1993). For an entropy-conserving process, σ or equivalently, $s = p/\rho^{\gamma}$ (sometimes termed specific entropy or local entropy) is conserved.

In the ideal MHD description, the pressure response is typically prescribed by an adiabatic equation of state such that $ds/dt = 0$. In a multi-fluid description, specific entropies for each species are also conserved as long as pressures are basically isotropic and there is no heat exchange between species, heat fluxes, or other dissipative processes.

The total entropy of a flux tube of unit magnetic flux is obtained by integrating the entropy per unit mass over the flux tube volume $\Sigma = \int \rho s dl/B$ where dl = infinitesimal length along B and B is the magnetic field. Equivalently, the pressure equation implies an integral constraint on the total mass content of a flux tube, $M = \int \rho dl/B$, is proportional to $S = \int p^{1/\gamma} dl/B$. If the plasma in a flux tube is in quasi-equilibrium, the pressure is constant and $S = p^{1/\gamma} V$ is conserved (i.e. $pV^{\gamma} =$ constant) where V is the flux tube volume. While S is not exactly the entropy of the flux tube, it is entropy-like in nature (Birn et al. 2006b) and is sometimes referred to as the flux tube entropy parameter or flux tube entropy or total entropy or global entropy. The specific entropy is an intensive variable whereas the total entropy is an extensive variable.

More detailed discussion and application of entropy can be found in the 2009 JGR special section on "Entropy Properties and Constraints Related to Space Plasma Transport" (see Wing and Johnson 2010 and references therein).

Specific entropy, s, places significant constraints on plasma entry mechanisms. Figure 16a shows that statistically the magnetosheath ion specific entropy is 2–3 orders of magnitude lower than plasma sheet ion s. Hence, it would be expected that a signature of the solar wind entry is to lower s in the plasma sheet. This is indeed observed, as shown in Fig. 16b, which shows that s is lower in both flanks, where there is a higher concentration of cold (solar wind) ions (Wing et al. 2005), than that near the midnight meridian. Figure 16c suggests that there is a duskward heat flux in the hot ion entropy profile, as would be expected from the curvature and gradient drifts. Figure 16 illustrates two interesting and relevant points: (1) during entry, solar wind ion specific entropy increases by 2–3 orders of magnitude (Fig. 16a); and (2) upon entry, the transport process that moves cold ions of solar wind origin from the flanks to near midnight increases the specific entropy further by a factor of ~5 (Fig. 16d). Point (2) can be crucial in resolving another key issue: what process transports this cold plasma from the flanks to the midnight meridian. Figure 16d suggests that whatever the process may be it would need to increase the specific entropy by a factor of ~5. This is discussed further in Sect. 4.2.

Changes in specific entropy, s, may be associated with wave-particle interactions, heat fluxes of captured populations, and other dissipative mechanisms. Three-dimensional simulations of shear flow instabilities show that magnetic reconnection can mix magnetosheath and magnetosphere populations leading to reduced entropy on closed field line regions. Eddy diffusion and kinetic drifts can also affect the entropy profiles in the plasma sheet.

The total entropy, $S = p^{1/\gamma} V$, provides an important constraint on the source of plasma sheet material, because once material is captured on closed flux tubes it should satisfy the entropy constraint, if it is convected adiabatically into the plasma sheet. The value of this constraint, S, can be estimated from solar wind conditions and assumptions about the plasma capture process and compared with typical values in the plasma sheet. Total entropy does not increase significantly for double cusp reconnection (Johnson and Wing 2009), but it may increase significantly for reconnection in Kelvin-Helmholtz vortices. The total entropy, S, is an important parameter in the plasma transport within the plasma sheet and interchange instability, as discussed in Sect. 4.3.

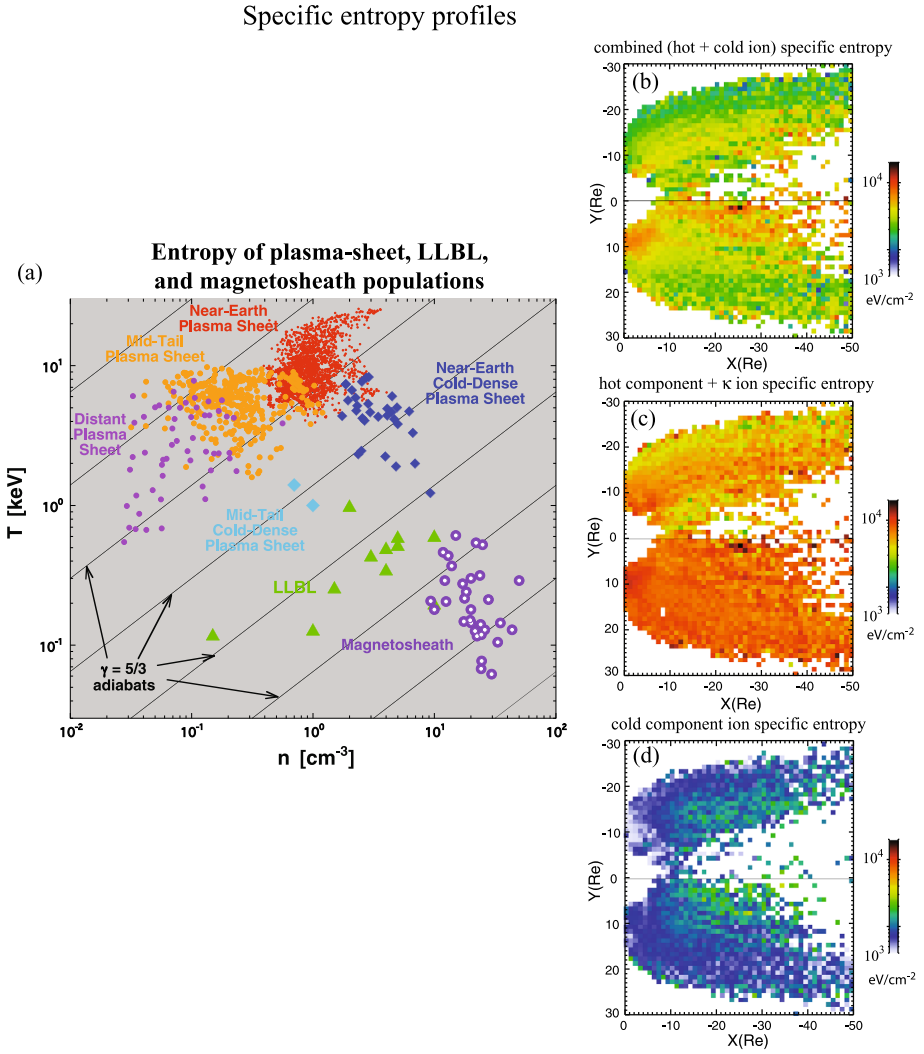

Fig. 16 (**a**) Entropy density of plasma sheet, LLBL, and magnetosheath ions in the n–T log–log space. The ions in the distant, mid-tail, and near-Earth plasma sheet tend to have the same adiabats, indicated by the diagonal lines with slope $\gamma = 5/3$, although the scatter is large. The magnetosheath entropy is lower than that of the LLBL, which is lower than that of the cold, dense plasma sheet. The data source and treatment for this figure is described in Borovsky et al. (1998b) (figure courtesy of *Joe Borovsky*). Plasma sheet specific entropy profiles for (**b**) combined hot and cold components, (**c**) hot component, and (**d**) cold component. Here the specific entropy, $s = p/\rho^{\gamma}$ is calculated as T/n^{γ}, assuming single species. The hot component profiles shows a dawn–dusk gradient, while the cold component profile shows s approximately conserved in the x direction and a gradient toward the midnight meridian. (From Johnson and Wing 2009)

3.4 Ion to Electron Temperature Ratio (T_i/T_e)

Another important observational "constraint" on solar wind plasma entry and transport processes in the plasma sheet is the rough, not exact, preservation of the temperature ratio of ions and electrons, T_i/T_e. For example, Baumjohann et al. (1989) reported that

$5.5 < T_i/T_e < 11$ in the plasma sheet. T_i/T_e has been shown to have a dependence on solar wind Alfvén Mach number (M_A). For example, Lavraud et al. (2009) examined an event during which the solar wind M_A is low, ~3, and found that T_i/T_e is also unusually low ~3 in both the magnetosheath and magnetopause boundary layers (i.e., inside the magnetopause). Wang et al. (2012) found a similar dependence on solar wind velocity.

The ratio of T_i/T_e changes significantly at the bow shock and is determined by solar wind parameters and shock physics. However, it is particularly interesting that the solar wind entry process appears to roughly conserve the T_i/T_e of the magnetosheath particles during the transport across the magnetopause (Lavraud et al. 2009; Wang et al. 2012). This property can be seen in Fig. 17a, which shows that $5 < T_i/T_e < 10$ in the magnetosheath and plasma sheet. Within the magnetosheath, T_i/T_e remains the same as the particles flow downstream and cool adiabatically, as would be expected. Figures 17b and 17c show two events in which THEMIS crossed from the magnetosheath to the plasma sheet. Both figures show that T_i/T_e of the magnetosheath (green line in the third panel from the top) appears to be similar to the T_i/T_e of the cool plasma (blue line in the third panel from the top). Figures 17d and 17e show statistically T_i/T_e of the magnetosheath and the cool plasma (not necessarily cold component, although it should be dominated by cold component) on both sides of the dusk and dawn magnetopause, respectively, at $X < -40$ R_E. Figures 17d and 17e suggest that when ions and electrons cross the magnetopause boundary from the magnetosheath to the magnetosphere, T_i and T_e increase by a factor of ~6 to 10 and specific entropies, s_i and s_e increase by a factor of ~20. Wang et al. (2012) interpreted these changes as the signature of a non-adiabatic heating process at the boundary that heats the ions and electrons by the same proportion. The case analyzed in Lavraud et al. (2009) further shows that T_i/T_e can be preserved even for unusual parameter regimes, i.e., in that case for a low value of the ratio as set at the bow shock during low solar wind M_A.

In the kinetic theory of the impulsive penetration the magnetic moments of each individual electron and ion forming the intruding plasmoids are conserved. Since the average magnetic moment of all particles species is proportional to their perpendicular kinetic energy, $\langle \mu_j \rangle \frac{W_j}{B} = \frac{kT_j}{B}$, the ratio of their perpendicular temperatures must necessarily be conserved during entry and transport, as shown by the observations of Lavraud et al. (2009).

Within the plasma sheet, there is a strong dawn-dusk asymmetry in T_i/T_e in the near-Earth region which can be attributed to the curvature and gradient drifts with high-energy ions (electrons) drifting toward dusk (dawn). As a result, T_i/T_e is higher at dusk than at dawn (e.g., Wang et al. 2012). Hence, T_i/T_e depends on the locations. Kaufmann et al. (2005) found that T_i/T_e decreases earthward near the midnight meridian. They offered several possible explanations: (1) electrons proportionally gain more energy than ions; (2) the ions lose energy through parallel heat flux to the ionosphere by radiating Alfvén waves; and (3) magnetic reconnection can heat ions and electrons differently. Fast flows can reduce ion density, but increase ion temperature. Because of these, Kaufmann et al. (2005) suggested that the factors influencing T_i/T_e variability can be more complicated than just curvature and gradient drifts. The nearly constant T_i/T_e suggests that ions absorb 5–10 times as much heat as the electrons in the plasma sheet (e.g., Kaufmann and Paterson 2009).

In one of a few theoretical and modeling studies that try to explain T_i/T_e, Schriver et al. (1998) modeled ion and electron acceleration in the magnetotail by following trajectories of thousands of particles in T89 magnetic field model (Tsyganenko 1989) and a constant dawn-dusk electric field of 0.25 mV/m in the magnetotail. They obtained $T_i/T_e = 4$–6. To explain this ratio, they derived an expression of $T_i/T_e = (m_i/m_e)^{1/3}(B'_e/B'_i)^{2/3}$ where $B' =$ the magnetic field gradient where electron or ion first cross the neutral sheet. Hence, to obtain the observed T_i/T_e, they would require ions to cross the neutral sheet closer to Earth than electrons.

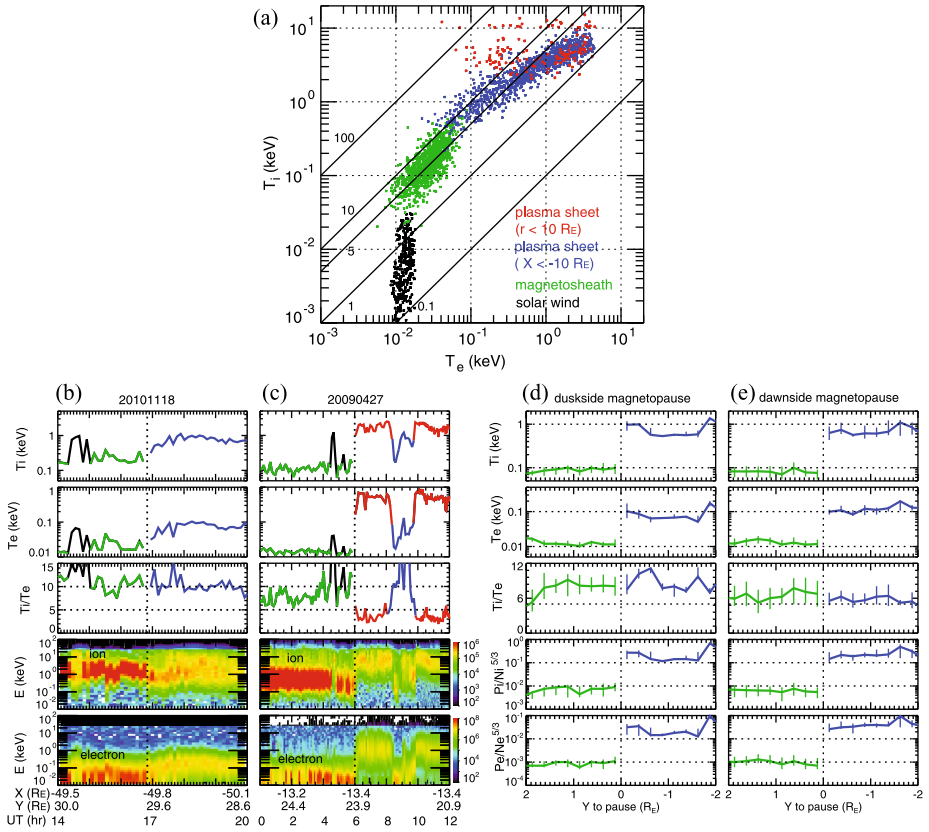

Fig. 17 (**a**) Scatter diagram of ion temperature (T_i) versue electron temperature (T_e) in the solar wind, magnetosheath, and plasma sheet. $T_i/T_e = 0.1, 1, 5, 10$, and 100 are indicated by the *black lines*. T_i, T_e, T_i/T_e, and energy spectrums of ion and electron energy fluxes (eV/(s-sr-cm^2-eV)) observed by THEMIS-b as it crossed the magnetopause (indicated by the *dotted vertical lines*) on (**b**) 20090423 and (**c**) 20090427. The *green curves* indicate magnetosheath plasma while the *black curves* indicate the hot plasma leaking out from the magnetosphere. The cool (warm) plasma sheet plasma are indicated by the *blue* (*red*) *curves*. T_i, T_e, T_i/T_e, ion specific entropy $P_i/N_i^{5/3}$ (nPa-cm^5) and electron specific entropy $P_e/N_e^{5/3}$ (nPa-cm^5) versus the Y-distance to the magnetopause (positive Y for the magnetosheath and negative Y for the plasma sheet) at (**d**) the duskside magnetopause and (**e**) the dawnside magnetopause. (From Wang et al. 2012)

4 Plasma Transport Within the Plasma Sheet

4.1 $E \times B$ and Curvature and Gradient Drifts

Three transport mechanisms that play significant roles in the plasma sheet and that have successfully explained large-scale features in the plasma sheet are (1) $\mathbf{E} \times \mathbf{B}$ (electric) and (2) curvature and gradient drifts (magnetic). For example, panels a–d in Fig. 15 show that the quiet time or northward IMF ion T and n profiles have the following large scale features: (1) density peaks along both flanks and the inner edge of the plasma sheet; (2) temperature peaks at the dusk-midnight sectors at the inner edge of the plasma sheet ($r = 8$–10 R_E); and (3) temperature minima along both flanks (Wing and Newell 1998, 2002; Wing et al. 2005; Johnson and Wing 2009). These large scale features have also been found with in situ ob-

servations (Wang et al. 2001, 2006). These features can be attributed to two plasma sources: (cold ions from the LLBL, and hot ions from distant tail) and three transport mechanisms: ($\mathbf{E} \times \mathbf{B}$ and curvature and gradient drifts) (e.g., Spence and Kivelson 1993; Wing and Newell, 1998, 2002; Wang et al. 2001, 2006, 2011, Wing et al. 2005). Cold ions that enter the plasma sheet from the flanks undergo $\mathbf{E} \times \mathbf{B}$ drift without significant cross-tail drift, resulting in temperature minima and density maxima along both flanks. In contrast, the hot plasma sheet ions $\mathbf{E} \times \mathbf{B}$ drift primarily sunward while curvature and gradient drifting westward, especially in the near-Earth region where the magnetic field is stronger ($r < 10\ R_E$), leading to the temperature peak at the dusk-midnight sector at the inner edge of the plasma sheet. The importance of the magnetic drift increases whereas the importance of $\mathbf{E} \times \mathbf{B}$ drift decreases with decreasing distance from Earth. Once the plasma sheet particles reach the inner magnetosphere, having been somewhat energized in the process, curvature and gradient drifts become dominant over $\mathbf{E} \times \mathbf{B}$ drift. As a result, the ions and electrons mainly move azimuthally, with the ions moving westward while the electrons eastward. As they circle around the Earth, some of these particles are lost by exiting through the magnetopause and by precipitating into the ionosphere (Gkioulidou et al. 2012; Wing et al. 2013). These particle precipitations provide a way to infer plasma sheet population (e.g., Wing and Newell 1998; Wing et al. 2005).

As shown in Fig. 15, relative to northward IMF, during southward IMF: (1) fewer solar wind ions enter along the flanks and (2) the stronger convection and dawn-dusk electric field leads to larger $\mathbf{E} \times \mathbf{B}$ drift. The differences mentioned so far in terms of transport processes and plasma sheet properties between northward and southward IMF give rise to the question: what happens when the IMF turns southward after a prolonged northward IMF and the plasma sheet has been loaded with cold and dense plasma? Thomsen et al. (2003) investigated this phenomenon and found that a strong ring current can ensue when prolonged northward IMF is followed by strong convection due to southward IMF or a sudden increase in solar wind dynamic pressure. Basically, when IMF turns southward, the preloaded cold-dense material in the plasma sheet is delivered to the inner magnetosphere, resulting in enhanced ring current (Denton et al. 2005; Lavraud et al. 2006a; Lavraud and Jordanova 2007). This has been referred to as "the calm before the storm" for the special case of corotating interaction regions (Borovsky and Steinberg 2006). Lavraud et al. (2006b) also studied the effect of prolonged northward IMF followed by southward IMF on inner magnetosphere plasma properties. They found two cold dense ion populations at the geosynchronous orbit: (1) at midnight and (2) near dawnside. The dawnside cold dense ions at the near-Earth plasma sheet during active times or substorm growth phase have been previously observed (Wing and Johnson 2009; Wing and Newell 1998, 2002; Korth et al. 1999; Denton et al. 2005) and modeled (Wang et al. 2004). It has been attributed to the stagnation point where $\mathbf{E} \times \mathbf{B}$ drift and corotation is nearly balanced by the curvature and gradient drifts (Friedel et al. 2001) and solar wind entry from the dawn flank. The midnight cold dense ions can be attributed to the earthward injections, e.g., fast flows, of the plasma sheet ions.

Interestingly, Ashour-Abdalla et al. (2010) found that during northward IMF, the plasma sheet can temporarily split into dawn and dusk halves in LSK simulation. They attributed this division to the presence of flux ropes in the center of the tail possibly due to the localized near-Earth reconnection.

Ion outflows during active times can significantly increase plasma sheet O^+ population, which can at times carry much of the energy (e.g. storm-time ring current) (e.g., Kistler et al. 2006; Keika et al. 2013; Maggiolo and Kistler 2014). Ion outflow rates have been found to increase dramatically after onset (e.g., Tung et al. 2001; Wilson et al. 2004). Escaping O^+ has higher fluxes in the 00–12 MLT (midnight-dawn-noon) sector than 12–24 MLT (noon-dusk-midnight) sector (Redmon et al. 2012; Collin et al. 1988). More recently, Maggiolo

and Kistler (2014) found that O^+ density increases with decreasing distance from the Earth and for magnetically active times and in the near Earth region, O^+ density is higher at postmidnight than premidnight. This may be related to the presence of cold dense ions in the plasma sheet post-midnight sector after substorm onset (Wing et al. 2007; Wing and Johnson 2009). Peterson et al. (2009) argued the importance of in-transit populations for ionospheric outflows for the quicker than expected arrival time of the outflows in the plasma sheet.

These outflows (combined with associated energization processes) could significantly modify the background plasma and magnetospheric $\mathbf{E} \times \mathbf{B}$ convection (e.g., Winglee et al. 2002). Several important physical effects might be expected. The study of Karimabadi et al. (2011) suggests that heavy ions only affect the reconnection rate when they are the primary current carrier, but in the nonlinear stage, a proton-dominated current sheet can be replaced by heavy ions in the surrounding plasma leading to reduced reconnection efficiency, reduction in the production of secondary islands, and broadening of the reconnection structures. MHD simulations show that dayside O^+ outflows would convect to the nightside and may move the magnetotail X-line closer to Earth in order to maintain the same reconnection rate on the dayside (e.g., Brambles et al. 2010; Wiltberger et al. 2010). On the other hand, nightside O^+ outflows may have the opposite effect, moving the magnetotail X-line further from the Earth due to the increased plasma pressure (e.g., Garcia et al. 2010).

4.2 Turbulence

Plasma of solar wind origin is observed as distributed throughout the plasma sheet. Observations show that the cold dense ions can be found throughout the entire plasma sheet during northward IMF (e.g., Terasawa et al. 1997; Øieroset et al. 2005; Wing and Newell 2002; Thomsen et al. 2003; Wing et al. 2005, 2006; Lavraud et al. 2006b; Johnson and Wing 2009). However, the mechanism for transporting cold dense plasma from the flanks to the midnight meridian (center of the plasma sheet) has not been clearly established or uniformly accepted.

The plasma sheet has been observed to be turbulent, which can play some roles in the plasma transport (Borovsky et al. 1997; Borovsky and Funsten 2003; Weygand et al. 2005). One source of the turbulence may be velocity shear instabilities (Borovsky et al. 1997). Entry of cold particles from the flanks establishes a spatial density gradient pointed from midnight toward the flanks. Turbulent flows in this spatial gradient thus result in diffusive particle transport from the flanks toward midnight. Wang et al. (2010) estimated diffusion coefficients associated with turbulent flows from Geotail observations. They performed a simulation that shows that diffusive transport due to turbulence can move cold particles from the flank to the midnight meridian to form a CDPS with density increase rates consistent with the statistical Geotail results. As such, turbulence is an important process that is intrinsic to the quasi-stable state of the tail and boundary layer (Antonova 2005), as well as its stability (Stepanova et al. 2011).

Ionospheric velocity measurements inferred from SuperDARN also suggest that even under steadily driven conditions, there are significant ionospheric velocity fluctuations (Bristow 2008). They occur for all local times, though are largest in the afternoon sector at auroral latitudes, and the prenoon polar cap. The level of fluctuation seems to be independent of substorm/nonsubstorm conditions. The average time for a significant fluctuation is on the order of ten minutes for all latitudes and local times, and they obey a power law distribution for at least part of its range. The ionospheric fluctuations could be a remote indicator of plasma sheet turbulence, and useful for studies of plasma sheet transport. The convection velocity fluctuations are also observed in the lobes by Cluster (Förster et al. 2007).

4.3 Entropy and Interchange Instability

Section 3.3 discusses the concept of total entropy, S, and specific entropy, s, and their importance to the solar wind plasma entry problem. These two entropy parameters are also relevant for the study of plasma transport within the plasma sheet. S is an important parameter for identifying when and where the magnetospheric plasma is interchange unstable. In particular, flux tubes with reduced S relative to the surrounding plasma may be interchange unstable, which can lead to earthward plasma transport at high speed, commonly known as fast flows (e.g., Pontius and Wolf 1990) that redistribute plasma into a more stable magnetospheric configuration (Gold 1959; Sonnerup and Laird 1963; Hill 1976; Chen and Wolf 1999).

Statistical studies have shown fairly definitively that, in the magnetotail, S is not conserved along a typical Earthward convective path—-S decreases with decreasing distance from Earth (Erickson and Wolf 1980; Garner et al. 2003; Kaufmann and Paterson 2009; Wing and Johnson 2009; Wang et al. 2009). Nonconservation of S can occur in nonadiabatic processes such as wave-particle interactions, heat flux, gradient/curvature drifts (Tsyganenko 1982; Kivelson and Spence 1988; Wang et al. 2001, 2004; Wolf et al. 2009; Wing and Johnson 2009; Kaufmann and Paterson 2008) and deviation from Earthward-directed $\mathbf{E} \times \mathbf{B}$ drift (Kaufmann et al. 2004). However, while these processes may explain the tailward gradient of S during relatively quiet times, they are probably not sufficient to explain the tailward gradient inferred from observations during periods of enhanced convection. For example, simulations of Lemon et al. (2004) that include electric shielding and gradient/curvature drifts show that strong adiabatic Earthward convection of plasma from the mid-tail region leads to intense stretching of the magnetic field that is almost certainly unstable physically.

If the localized process leads to field-line reconfiguration (reconnection), then the change of S is likely more related to the change of flux tube volume than to changes in s within that volume. Erickson and Wolf (1980) and others have pointed out that reconnection, substorms, and other processes that reduce the plasma content of flux tubes will reduce S (e.g., Pontius and Wolf 1990; Borovsky et al. 1998b; Chen and Wolf 1993; Kaufmann and Paterson 2006; Wing and Johnson 2009), which could explain the statistically observed tailward gradient in S. S and s can also change when plasma is added to the flux tube, e.g., through solar wind plasma entry or ionospheric outflow (e.g., Johnson and Wing 2009).

Birn et al. (2006a, 2009), Kaufmann and Paterson (2006), and Wing and Johnson (2009) discussed S changes in flux-tube reconfiguration in magnetic field reconnection process in which the closed field line splits into two parts: (1) a newly closed field line albeit with reduced length and (2) a tailward convecting plasmoid. The newly closed field line has much lower S and V compared to those in the original flux tube, while the remainder resides in the newly formed plasmoid.

An earthward fast flow can attain velocity greater than 400 km/s and has been associated with a bubble, which is a magnetotail flux tube having lower density, pressure, and S than surrounding flux tubes (e.g., Angelopoulos et al. 1994; Sergeev et al. 1996; Nakamura et al. 2005). Herein, the term fast flow includes bubbles, bursty bulk flows (BBF) and flow burst (shorter duration than BBF). Fast earthward flows are more frequently observed during magnetically active times, have been associated with substorm onsets, and their occurrence frequency reaches a peak at the start of the recovery phase (e.g., Nakamura et al. 2002; Angelopoulos et al. 1994; Baumjohann et al. 1990; McPherron et al. 2011; Sergeev et al. 2008; Slavin et al. 2002). Fast flow observations and simulations often show two parts: (1) the head where Bz is large (the dipolarization front) and (2) the tail. The

pressure inside the bubble is smaller than that outside the bubble. This pressure gradient leads to the field-aligned current with region-1 polarity, whose particle precipitation signature in optical images often appears as an auroral streamer. Thus, many studies pair auroral streamers with fast flows (e.g., Sergeev et al. 2004; Nakamura et al. 2001; Lyons et al. 1999; Sanchez et al. 2012).

There is no clear picture of the earthward fast flows at distances $r < 10$–12 R_E. It appears that many fast flows slow down at $r < 10$–12 R_E (e.g., McPherron et al. 2011; Panov et al. 2010a) and many do not reach the inner magnetosphere or geosynchronous orbit (e.g., Ohtani et al. 2006; Sergeev et al. 2012; Kim et al. 2012). Observations and theory suggest that in the final stage of the bubble earthward motion, the filamentary bubble executes a damped oscillation about an equilibrium (interchange oscillation) as the bubble slows down and eventually comes to a stop (interchange oscillation) (Chen and Wolf 1999; Panov et al. 2010b, 2013; Wolf et al. 2012). In Rice Convection Model-Equilibrium (RCM-E) simulations, flux tubes do not generally reach the inner magnetosphere, unless their total entropies have been reduced (Lemon et al. 2004; Zhang et al. 2008), and their depth of penetration is determined by the severity of the entropy reduction (Yang et al. 2012).

In Birn et al. (2009) simulations, after the reconnection, the newly closed field line, which has smaller total entropy and flux tube volume than the surrounding flux tubes, can initiate the unstable growth of ballooning and interchange instability, resulting in the earthward propagation of the flux tube. These bubbles would move earthward until their S equals that of their neighbors (Wolf et al. 2009). The more depleted the flux tube, the closer to Earth it can penetrate. This view has been supported in some recent observational studies (e.g., Dubyagin et al. 2011).

Recently, Birn et al. (2011) showed that as bubbles move earthward, vortices of return flow develop and the bubbles also fragment, developing cross-tail structuring in the later stages. This process is displayed in Fig. 18. Initially, reconnection at $X = -8$ (simulation scale; $X = -10$ corresponds to $X_{GSM} = -23$ Re) leads to fast earthward flows through interchange instability generated by buoyancy forces. In Figs. 18a and 18d, the blue patch that is aligned with the X axis near midnight corresponds to fast earthward flow of flux tube with depleted S (BBF), which brakes in the inner magnetosphere at about $X = -2$ (simulation scale). Some time later, the earthward flow near midnight is reversed as shown in Figs. 18b and 18e. Additionally, two secondary earthward fast flow channels develop eastward and westward of the initial fast flow. Small scale structuring develops. Finally, the flow subsides and the entire region in the inner magnetosphere has overwhelmingly low entropy plasma (blue), as shown in Fig. 18c. This final configuration suggests that the BBFs have successfully carried the low-entropy plasma from the magnetotail into a large region in the inner magnetosphere.

5 Summary and Conclusion

This paper reviews our current understanding of the plasma transport from the solar wind to the magnetotail and transport within the magnetotail. Four solar entry mechanisms are examined for northward IMF solar wind entrees: (1) double cusp reconnection (e.g., Song and Russell 1992), (2) KHI (e.g., Otto and Fairfield 2000), (3) KAW (Lee et al. 1994; Johnson and Cheng 1997), and (4) IP (Lemaire 1977; Lemaire and Roth 1978). In order to determine which of these mechanisms plays the most significant roles and under what conditions, we examined four observational constraints: (1) plasma sheet filling rate; (2) dawn-

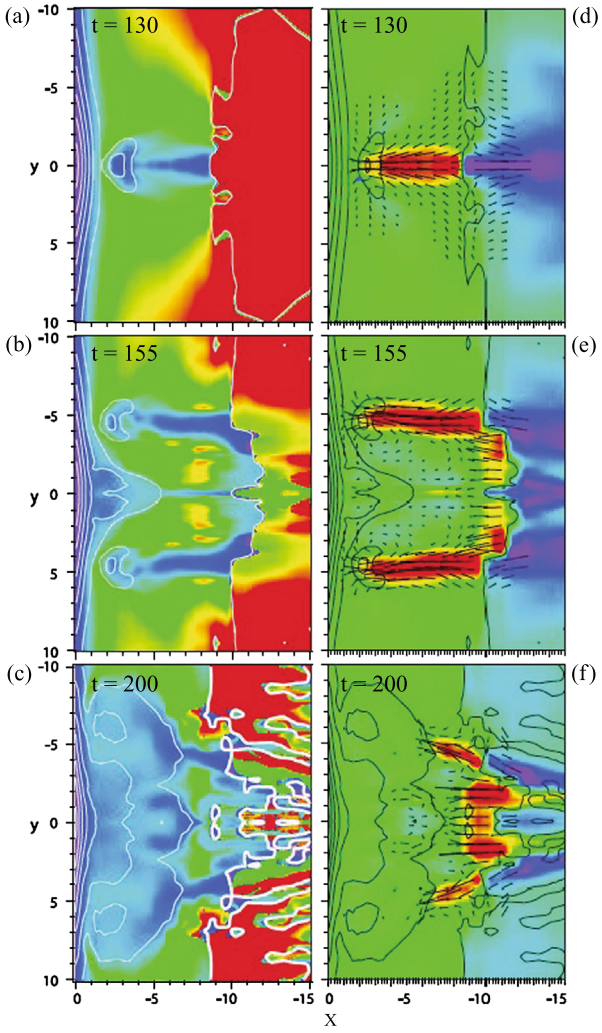

Fig. 18 Total entropy, S, (**a**), (**b**), (**c**), and flow in the X–Y plane (**d**), (**e**), and (**f**) at three different times in Birn et al. (2011) MHD simulation. (From Birn et al. 2011)

dusk asymmetries; (3) specific and total entropies; and (4) ion-to-electron temperature ratio (T_i / T_e).

It turns out that all four mechanisms are capable of filling the plasma sheet with cold dense plasma. The entry rate from each mechanism is quite similar and consistent with the observed filling rate. The observed plasma sheet densities, temperatures, velocities, and magnetic fields during northward IMF seem to agree well with those found in OpenGGCM MHD simulations of double cusp (or lobe) reconnection.

In situ and remote observations of the cold component (magnetosheath/solar wind origin) ions at the plasma sheet flanks near the magnetopause reveal that the cold component density and temperature are higher on dawn flank than on the dusk flank. In situ observations show that while on the duskside, the ion hot (magnetospheric origin) and cold component temperatures are isotropic, on the dawnside, the ion cold component appears to have been heated in the direction perpendicular to the magnetic field and the electrons have been heated in the direction parallel to the magnetic field. These observations are consistent with the expected

signature of KAW interaction with particles. A recent survey of Alfvén waves in the magnetosheath and magnetopause found that the Alfvén wave spectral energy density is higher at dawn–morning sector than at dusk–afternoon sector. Inside the magnetosphere, along the flanks, on the duskside, the ions are frequently observed to have two components whereas on the dawnside, the ions are frequently observed to have one component. The hot component has higher temperature on the duskside than the dawnside because of the curvature and gradient drifts. In contrast, the cold component has higher temperature on the dawnside than the duskside. As a result, on the duskside, the hot and cold components are often easily identified. In contrast, on the dawnside, the hot and cold component temperatures are often so close to each other that the ions often appear to have one component with a broad peak.

The higher density of the cold component on the dawnside magnetotail may result from the dawn-dusk asymmetry of the magnetosheath ion density. The magnetosheath ion density has been observed to be higher on the dawnside than the duskside and the asymmetry appears to increase away from noon. The higher density of the cold component of the dawnside magnetotail may also result from a dawn-dusk asymmetry of the entry rate. An MHD simulation shows that KH growth rate is higher on the dawn flank than the dusk flank for a Parker spiral solar wind orientation, which is the prevalent solar wind orientation. An expected signature of the impulsive penetration mechanism is a dawn-dusk asymmetry due to first order drift of the plasmoids/jest inside the magnetosphere and to a possible preference of the blobs/jets to form in the dawn magnetosheath, during radial IMF.

The entry of solar wind/magnetosheath plasma reduces the specific entropy, s, of the plasma sheet ions. The cold component s increases by a factor of 5 from the flanks to the midnight meridian. So, whatever mechanism that transports the cold ions from the flanks to the midnight meridian has to explain this increase in s.

T_i/T_e appears to be roughly conserved when the magnetosheath particles are transported across the magnetopause into plasma sheet even though T_i, T_e, s_i and s_e all increase significantly. If the adiabatic equation is $TV^{(\gamma-1)}$, then T_i and T_e would increase according to the flux tube volume, V, and T_i/T_e can be conserved. However, the increases of s_i and s_e suggest non-adiabatic heating during entry. The fluctuation in T_i/T_e also indicates non-adiabatic processes.

Within the magnetotail, $\mathbf{E} \times \mathbf{B}$ and curvature and gradient drifts play important roles in the plasma transport and can explain the large-scale observed features of the n, T, p profiles. Turbulence can also play a significant role, particularly in transporting cold plasma from the flanks to the midnight meridian. Total entropy, S, and fast flows can play significant roles in the sunward transport. Many fast flows do not reach the inner magnetosphere, but simulations show that fast flows would only travel inward until its total entropy matches that of the ambient plasma.

Acknowledgements International Space Science Institute (ISSI), Bern, Switzerland funded and hosted our International Team "Plasma entry and transport in the plasma sheet" that led to the publication of this paper. We are especially grateful for the ISSI facility that allows for in-depth, informal, and inspiring discussions. We acknowledge the contribution of Prof. Joseph Lemaire to the mechanism of impulsive penetration in this paper. Simon Wing gratefully acknowledges supports from NSF Grants ATM-0802715, and AGS-1058456 and NASA Grant NNX13AE12G. Jay Johnson was funded by NASA grants (NNH09AM53I, NNH09AK63I, and NNH11AR07I), NSF Grants ATM0902730 and AGS-1203299, and DOE contract DE-AC02-09CH11466. Joachim Raeder acknowledges support from the NASA THEMIS mission (UCB subcontract SA405826326) and NSF grants ATM-0902907 and AGS-1303579. Chris Chaston was supported by NASA grant NNX09AF49G and Australian Research Council FT110100316. Katariina Nykyri was supported by NSF grant 0847120. Marius Echim acknowledges support from the European Community's Seventh Framework Programme (FP7/2007-2013) under grant agreement no 313038/STORM, from the Romanian Ministry of National Education, CNCS, UEFISCDI, project number PN-II-ID PCE-2012-4-0418, and from the Interuniversity Attraction Poles Programme initiated by the Belgian Science Policy Office (IAP P7/08

CHARM). Colby Lemon was supported by NSF grant AGS-1003874. We also thank NSF GEM for supporting Plasma entry and transport into and within the magnetotail (PET) Focus Group, which provided a forum for fruitful discussions of the topics covered in this paper.

References

E. Amata, S.P. Savin, D. Ambrosino, Y.V. Bogdanova, M.F. Marcucci, S. Romanov, A. Skalsky, High kinetic energy density jets in the Earth's magnetosheath: a case study. Planet. Space Sci. **59**(7), 482–494 (2011)

B.J. Anderson, S.A. Fuselier, Response of thermal ions to electromagnetic ion cyclotron waves. J. Geophys. Res. **99**, 19413–19425 (1994)

V. Angelopoulos, W. Baumjohann, C.F. Kennel, F.V. Coroniti, M.G. Kivelson, R. Pellat, R.J. Walker, H. Lühr, G. Paschmann, Bursty bulk flows in the inner central plasma sheet. J. Geophys. Res. **97**(A4), 4027–4039 (1992). doi:10.1029/91JA02701

V. Angelopoulos et al., Statistical characteristics of bursty bulk flow events. J. Geophys. Res. **99**, 21257–21280 (1994)

E.E. Antonova, The structure of the magnetospheric boundary layers and the magnetospheric turbulence. Planet. Space Sci. **53**, 161–168 (2005). doi:10.1016/j.pss.2004.09.041

M.O. Archer, T.S. Horbury, Magnetosheath dynamic pressure enhancements: occurrence and typical properties. Ann. Geophys. **31**(2), 319–331 (2013)

M. Ashour-Abdalla, J.M. Bosqued, M. El-Alaoui, V. Peroomian, R. Walker, Observations and simulations of a highly structured plasma sheet during northward IMF. J. Geophys. Res. **115**, A10227 (2010). doi:10.1029/2009JA015135

D.A. Baker, J.E. Hammel, Experimental studies of the penetration of a plasma stream into a transverse magnetic field. Phys. Fluids **8**, 713–722 (1965)

W. Baumjohann, The near-Earth plasma sheet: an AMPTE/IRM perspective. Space Sci. Rev. **64**, 141–163 (1993)

W. Baumjohann, G. Paschmann, C.A. Cattell, Average plasma properties in the central plasma sheet. J. Geophys. Res. **94**, 6597 (1989)

W. Baumjohann, G. Paschmann, H. Luhr, Pressure balance between lobe and plasma sheet. Geophys. Res. Lett. **17**, 45–48 (1990)

J. Berchem, C.T. Russell, The thickness of the magnetopause current layer: ISEE 1 and 2 observations. J. Geophys. Res. **87**(A4), 2108–2114 (1982). doi:10.1029/JA087iA04p02108

J. Birn, M. Hesse, K. Schindler, On the role of entropy conservation and entropy loss governing substorm phases, in *Proceedings of the Eighth International Conference of Substorms*, ed. by M. Syrjäsuo, E. Donovan (Univ. of Calgary, Calgary, 2006a), pp. 19–24

J. Birn, M. Hesse, K. Schindler, Entropy conservation in simulations of magnetic reconnection. Phys. Plasmas **13**, 092117 (2006b). doi:10.1063/1.2349440

J. Birn, M. Hesse, K. Schindler, S. Zaharia, Role of entropy in magnetotail dynamics. J. Geophys. Res. **114**, A00D03 (2009). doi:10.1029/2008JA014015

J. Birn, R. Nakamura, E.V. Panov, M. Hesse, Bursty bulk flows and dipolarization in MHD simulations of magnetotail reconnection. J. Geophys. Res. **116**, A01210 (2011). doi:10.1029/2010JA016083

J.E. Borovsky, H.O. Funsten, MHD turbulence in the Earth's plasma sheet: dynamics, dissipation, and driving. J. Geophys. Res. **108**, 1284 (2003). doi:10.1029/2002JA009625

J.E. Borovsky, J.T. Steinberg, The "calm before the storm" in CIR/magnetosphere interactions: occurrence statistics, solar wind statistics, and magnetospheric preconditioning. J. Geophys. Res. **111**, A07S10 (2006). doi:10.1029/2005JA011397

J.E. Borovsky, R.C. Elphic, H.O. Funsten, M.F. Thomsen, The Earth's plasma sheet as a laboratory for turbulence in high-beta MHD. J. Plasma Phys. **57**, 1–34 (1997)

J.E. Borovsky, M.F. Thomsen, R.C. Elphic, The driving of the plasma sheet by the solar wind. J. Geophys. Res. **103**, 17617–17639 (1998a)

J.E. Borovsky, M.F. Thomsen, R.C. Elphic, T.E. Cayton, D.J. McComas, The transport of plasma sheet material from the distant tail to geosynchronous orbit. J. Geophys. Res. **103**(A9), 20297–20331 (1998b)

O.J. Brambles, W. Lotko, P.A. Damiano, B. Zhang, M. Wiltberger, J. Lyon, Effects of causally driven cusp O^+ outflow on the storm time magnetosphere-ionosphere system using a multifluid global simulation. J. Geophys. Res. **115**, A00J04 (2010). doi:10.1029/2010JA015469

W. Bristow, Statistics of velocity fluctuations observed by SuperDARN under steady interplanetary magnetic field conditions. J. Geophys. Res. **113**, A11202 (2008). doi:10.1029/2008JA013203

J.L. Burch, P.H. Reiff, R.W. Spiro, R.A. Heelis, S.A. Fields, Cusp region particle precipitation and ion convection for northward interplanetary magnetic field. Geophys. Res. Lett. **7**, 393–396 (1980). doi:10.1029/GL007i005p00393

W.J. Burke, M.C. Kelley, R.C. Sagalyn, M. Smiddy, S.T. Lai, Polar cap electric field structures with a northward interplanetary magnetic field. Geophys. Res. Lett. **6**(1), 21–24 (1979). doi:10.1029/GL006i001p00021
L.F. Burlaga, K.W. Ogilvie, D.H. Fairfield, Microscale fluctuations in the interplanetary magnetic field. Astrophys. J. **155**, L171 (1969)
M.B.B. Cattaneo et al., Ion kinetic features around a lobe reconnection site, in *Proceedings of the Cluster and Double Star Symposium, 5th Anniversary of Cluster in Space* (2006), p. 369. ESA SP-598
B.D.G. Chandran, B. Li, B.N. Rogers, E. Quataert, K. Germaschewski, Perpendicular ion heating by low-frequency Alfvén-wave turbulence in the solar wind. Astrophys. J. **720**, 503–515 (2010). doi:10.1088/0004-637X/720/1/503
S. Chandrasekhar, *Hydrodynamic and Hydromagnetioc Stability* (Clarendon, Oxford, 1961)
C.R. Chappell, T.E. Moore, J.H. Waite Jr., The ionosphere as a fully adequate source of plasma for the Earth's magnetosphere. J. Geophys. Res. **92**(A6), 5896–5910 (1987). doi:10.1029/JA092iA06p05896
C.C. Chaston, T.D. Phan, J.W. Bonnell, F.S. Mozer, M. Acun, M.L. Goldstein, A. Balogh, M. Andre, H. Reme, A. Fazakerley, Drift-kinetic Alfvén waves observed near a reconnection x line in the Earth's magnetopause. Phys. Rev. Lett. **95**(6), 065002 (2005)
C.C. Chaston, M. Wilber, F.S. Mozer, M. Fujimoto, M.L. Goldstein, M. Acuna, M.H. Reme, A. Fazakerley, Mode conversion and anomalous transport in Kelvin-Helmholtz vortices and kinetic Alfvén waves at the Earth's magnetopause. Phys. Rev. Lett. **99**, 175004 (2007)
C.C. Chaston et al., Turbulent heating and cross-field transport near the magnetopause from THEMIS. Geophys. Res. Lett. **35**, L17S08 (2008). doi:10.1029/2008GL033601
C.C. Chaston, J.R. Johnson, M. Wilber, M. Acuna, M.L. Goldstein, H. Reme, Kinetic Alfvén wave turbulence and transport through a reconnection diffusion region. Phys. Rev. Lett. **102**, 015001 (2009)
C.C. Chaston, Y. Yao, N. Lin, C. Salem, G. Ueno, Ion heating by broadband electromagnetic waves in the magnetosheath and across the magnetopause. J. Geophys. Res. (Space Phys.) **118**, 5579–5591 (2013). doi:10.1002/jgra.50506
L. Chen, Theory of plasma transport induced by low-frequency hydromagnetic waves. J. Geophys. Res. **104**(A2), 2421–2427 (1999). doi:10.1029/1998JA900051
C.X. Chen, R.A. Wolf, Interpretation of high-speed flows in the plasma sheet. J. Geophys. Res. **98**, 21409–21419 (1993)
C.X. Chen, R.A. Wolf, Theory of thin-filament motion in Earth's magnetotail and its application to bursty bulk flows. J. Geophys. Res. **104**(A7), 14613–14626 (1999). doi:10.1029/1999A900005
L. Chen, Z. Lin, R. White, On resonant heating below the cyclotron frequency. Phys. Plas. **8**, 4713 (2001)
L. Chen, F. Zonca, Gyrokinetic theory of parametric decays of kinetic Alfvén waves. EPL (Europhys. Lett.) **96**, 35001 (2011). doi:10.1209/0295-5075/96/35001
G.F. Chew, M.L. Goldberger, F.E. Low, The Boltzmann equation and the one-fluid hydrodynamic equations in the absence of particle collisions. Proc. Roy. Soc. London **236A**, 112–118 (1956)
S.G. Claudepierre, S.R. Elkington, M. Wiltberger, Solar wind driving of magnetospheric ULF waves: pulsations driven by velocity shear at the magnetopause. J. Geophys. Res. **113**, A05218 (2008). doi:10.1029/2007JA012890
H.L. Collin, W.K. Peterson, J.F. Drake, A.W. Yau, The helium components of energetic terrestrial ion upflows: their occurrence, morphology, and intensity. J. Geophys. Res. **93**, 7558–7564 (1988). doi:10.1029/JA093iA07p07558
F.V. Coroniti, C.F. Kennel, Changes in magnetospheric configuration during the substorm growth phase. J. Geophys. Res. **77**, 3361 (1972)
M.M. Cowee, D. Winske, S.P. Gary, Two-dimensional hybrid simulations of superdiffusion at the magnetopause driven by Kelvin-Helmholtz instability. J. Geophys. Res. (Space Phys.) **114**, 10209 (2009). doi:10.1029/2009JA014222
M.M. Cowee, D. Winske, S.P. Gary, Hybrid simulations of plasma transport by Kelvin-Helmholtz instability at the magnetopause: density variations and magnetic shear. J. Geophys. Res. (Space Phys.) **115**, 6214 (2010). doi:10.1029/2009JA015011
S.W.H. Cowley, Plasma populations in a simple open model magnetosphere. Space Sci. Rev. **26**, 217 (1980)
S.W.H. Cowley, Magnetospheric and ionospheric flow and the interplanetary magnetic field, in *AGARD The Phys, Basis of the Ionosphere in the Solar-Terrest. System*, 14 pp., see N81–23507 14–42 (1981)
S.W.H. Cowley, D.J. Southwood, Some properties of a steady-state geomagnetic tail. Geophys. Res. Lett. **7**, 833 (1980)
N.U. Crooker, Dayside merging and cusp geometry. J. Geophys. Res. **84**(A3), 951–959 (1979). doi:10.1029/JA084iA03p00951
N.U. Crooker, Global geometry of merging at the dayside magnetopause, in *Solar Wind—Magnetosphere Coupling*, ed. by Y. Kamide, J.A. Slavin (1986), p. 287. Terra Scientific Publishing Company
N.U. Crooker, Reverse convection. J. Geophys. Res. **97**(A12), 19363–19372 (1992). doi:10.1029/92JA01532

J. De Keyser, F. Darrouzet, M. Roth, O.L. Vaisberg, N. Rybjeva, V. Smirnov, L. Avanov, Z. Nemecek, J. Safrankova, Transients at the dusk side magnetospheric boundary: surface waves or isolated plasma blobs? J. Geophys. Res. **106**(A11), 25503–25516 (2001)
P.A. Delamere, Hybrid code simulations of the solar wind interaction with Pluto. J. Geophys. Res. (Space Phys.) **114**, 3220 (2009). doi:10.1029/2008JA013756
P.A. Delamere, R.J. Wilson, A. Masters, Kelvin-Helmholtz instability at Saturn's magnetopause: hybrid simulations. J. Geophys. Res. (Space Phys.) **116**, 10222 (2011). doi:10.1029/2011JA016724
P.A. Delamere, R.J. Wilson, S. Eriksson, F. Bagenal, Magnetic signatures of Kelvin-Helmholtz vortices on Saturn's magnetopause: global survey. J. Geophys. Res. (Space Phys.) **118**, 393–404 (2013). doi:10.1029/2012JA018197
I.I. Demidenko, N.S. Lomino, V.G. Padalka, B.N. Rutkevich, K.D. Sinel'Nikov, Plasma stream in an inhomogeneous transverse magnetic field. Sov. Phys. Tech. Phys. **14**, 16 (1969)
I.I. Demidenko, N.S. Lomino, V.G. Padalka, Plasma flow in a strong transverse magnetic field. Sov. Phys. Tech. Phys. **16**, 1096 (1972)
M.H. Denton, M.F. Thomsen, H. Korth, S. Lynch, J.C. Zhang, M.W. Liemohn, Bulk plasma properties at geosynchronous orbit. J. Geophys. Res. **110**, A07223 (2005). doi:10.1029/2004JA010861
A.P. Dimmock, K. Nykyri, The statistical mapping of magnetosheath plasma properties based on THEMIS measurements in the magnetosheath interplanetary medium reference frame. J. Geophys. Res. Space Phys. **118**, 4963–4976 (2013). doi:10.1002/jgra.50465
S. Dubyagin, V. Sergeev, S. Apatenkov, V. Angelopoulos, A. Runov, R. Nakamura, W. Baumjohann, J. McFadden, D. Larson, Can flow bursts penetrate into the inner magnetosphere? Geophys. Res. Lett. **38**, L08102 (2011). doi:10.1029/2011GL047016
J.W. Dungey, Interplanetary magnetic field and the auroral zone. Phys. Res. Lett. **6**, 47 (1961)
J.W. Dungey, The structure of the exosphere, or adventures in velocity space, in Geophysics, in *The Earth's Environment*, ed. by C. DeWitt, J. Hieblot, A. Lebeau (Gordon and Breach, New York, 1963), p. 505
M. Echim, Kinetic investigation of the impulsive penetration mechanism of 2D plasma elements into the Earth's magnetosphere, Ph.D. thesis (2004), http://dial.academielouvain.be
M. Echim, J. Lemaire, Laboratory and numerical simulations of the impulsive penetration mechanism. Space Sci. Rev. **92**(3/4), 565–601 (2000)
M. Echim, J. Lemaire, Positive density gradients at the magnetopause: interpretation in the framework of the impulsive penetration mechanism. J. Atmos. Sol.-Terr. Phys. **64**(18), 2019–2028 (2002)
M. Echim, J. Lemaire, Two-dimensional Vlasov solution for a collisionless plasma jet across transverse magnetic field lines with a sheared bulk velocity. Phys. Rev. E **72**, 036405 (2005)
G.M. Erickson, R.A. Wolf, Is steady convection possible in the Earth's magnetotail? Geophys. Res. Lett. **7**, 897–900 (1980). doi:10.1029/GL007i011p00897
S. Eriksson, H. Hasegawa, W.-L. Teh, B.U.Ö. Sonnerup, J.P. McFadden, K.-H. Glassmeier, O. Le Contel, V. Angelopoulos, C.M. Cully, D.E. Larson, R.E. Ergun, A. Roux, C.W. Carlson, Magnetic island formation between large-scale flow vortices at an undulating postnoon magnetopause for northward interplanetary magnetic field. J. Geophys. Res. (Space Phys.) **114** (2009). doi:10.1029/2008JA013505
C.P. Escoubet, A. Pedersen, R. Schmidt, P.A. Lindqvist, Density in the magnetosphere inferred from ISEE 1 spacecraft potential. J. Geophys. Res. **102**(A8), 17595–17609 (1997). doi:10.1029/97JA00290
C.P. Escoubet et al., Effect of a northward turning of the interplanetary magnetic field on cusp precipitation as observed by Cluster. J. Geophys. Res. **113**, A07S13 (2008). doi:10.1029/2007JA012771
M. Faganello, F. Califano, F. Pegoraro, T. Andreussi, S. Benkadda, Magnetic reconnection and Kelvin-Helmholtz instabilities at the Earth's magnetopause. Plasma Phys. Control. Fusion **54**(12), 124037 (2012). doi:10.1088/0741-3335/54/12/124037
D.H. Fairfield, A. Otto, T. Mukai, S. Kokubun, R.P. Lepping, J.T. Steinberg, A.J. Lazarus, T. Yamamoto, Geotail observations of the Kelvin-Helmholtz instability at the equatorial magnetotail boundary for parallel northward fields. J. Geophys. Res. **105**, 21159–21173 (2000)
J.A. Fedder, J.G. Lyon, The Earth's magnetosphere is 165 *RE* long: self-consistent currents, convection, magnetospheric structure, and processes for northward interplanetary magnetic field. J. Geophys. Res. **100**, 3623 (1995)
M. Förster, G. Paschmann, S.E. Haaland, J.M. Quinn, R.B. Torbert, H. Vaith, C.A. Kletzing, High-latitude plasma convection from Cluster EDI: variances and solar wind correlations. Ann. Geophys. **25**, 1691–1707 (2007). doi:10.5194/angeo-25-1691-2007
H.U. Frey, T.D. Phan, S.A. Fuselier, S.B. Mende, Continuous magnetic reconnection at Earth's magnetopause. Nature **426**, 533 (2003)
R.H.W. Friedel, H. Korth, M.G. Henderson, M.F. Thomsen, J.D. Scudder, Plasma sheet access to the inner magnetosphere. J. Geophys. Res. **106**(A4), 5845–5858 (2001). doi:10.1029/2000JA003011
M. Fujimoto, T. Terasawa, Anomalous ion mixing within an MHD scale Kelvin-Helmholtz vortex. J. Geophys. Res. **99**, 8601–8614 (1994)

M. Fujimoto, T. Terasawa, Anomalous ion mixing within an MHD scale Kelvin-Helmholtz vortex, 2, Effects of inhomogeneity. J. Geophys. Res. **100**, 12025–12034 (1995)
M. Fujimoto, T. Terasawa, T. Mukai, Y. Saito, T. Yamamoto, S. Kokubun, Plasma entry from the flanks of the near-Earth magnetotail: geotail observations. J. Geophys. Res. **103**(A3), 4391–4408 (1998). doi:10.1029/97JA03340
M. Fujimoto, T. Tonooka, T. Mukai, Vortex-like fluctuations in the magnetotail flanks and their possible roles in plasma transport, in *Earth's Low-Latitude Boundary Layer*, ed. by P. Newell, T. Onsager. Geophysical Monograph (AGU, Washington, 2003), pp. 241–251. AGU
S.A. Fuselier, J. Berchem, K.J. Trattner, R. Friedel, Tracing ions in the cusp and low-latitude boundary layer using multispacecraft observations and a global MHD simulation. J. Geophys. Res. **107**(A9), 1226 (2002a). doi:10.1029/2001JA000130
S.A. Fuselier, J.H. Waite, L.A. Avanov, V.M. Smirnov, O.L. Vaisberg, G. Siscoe, C.T. Russell, Characteristics of magnetosheath plasma in the vicinity of the high-altitude cusp. Planet. Space Sci. **50**, 559–566 (2002b)
K.S. Garcia, V.G. Merkin, W. Hughes, Effects of nightside O^+ outflow on magnetospheric dynamics: results of multifluid MHD modeling. J. Geophys. Res. **115**, A00J09 (2010). doi:10.1029/2010JA015730
T.W. Garner, R.A. Wolf, R.W. Spiro, M.F. Thomsen, H. Korth, Pressure balance inconsistency exhibited in a statistical model of magnetospheric plasma. J. Geophys. Res. **108**, 1331 (2003). doi:10.1029/2003JA009877
M. Gkioulidou, C.-P. Wang, S. Wing, L.R. Lyons, R.A. Wolf, T.-S. Hsu, Effect of an MLT dependent electron loss rate on the magnetosphere-ionosphere coupling. J. Geophys. Res. **117**, A11218 (2012). doi:10.1029/2012JA018032
T. Gold, Motions in the magnetosphere of the earth. J. Geophys. Res. **64**, 1219 (1959)
J.T. Gosling, D.N. Baker, J.J. Bame, W.C. Feldman, R.D. Zwickl, E.J. Smith, North-South and dawn-dusk asymmetries in the distant tail lobes: ISEE 3. J. Geophys. Res. **90**, 6354 (1985)
J.T. Gosling, M.F. Thomsen, S.J. Bame, R.C. Elphic, Observations of reconnection of interplanetary and lobe magnetic field lines at the high-latitude magnetopause. J. Geophys. Res. **96**, 14097 (1991)
T.B. Guild, H.E. Spence, E.L. Kepko, V. Merkin, J.G. Lyon, M. Wiltberger, C.C. Goodrich, Geotail and LFM comparisons of plasma sheet climatology: 1. Average values. J. Geophys. Res. **113**, A04216 (2008). doi:10.1029/2007JA012611
H. Gunell, H. Nilsson, G. Stenberg, M. Hamrin, T. Karlsson, R. Maggiolo, M. André, R. Lundin, I. Dandouras, Plasma penetration of the dayside magnetopause. Phys. Plasmas **19**(7), 072906 (2012)
J.-N. Guo, J. Büchner, A. Otto, J. Santos, E. Marsch, W.-Q. Gan, Is the 3-D magnetic null point with a convective electric field an efficient particle accelerator? Astron. Astrophys. **513**, A73 (2010). 13 pp.
X.C. Guo, C. Wang, Y.Q. Hu, Global MHD simulation of the Kelvin-Helmholtz instability at the magnetopause for northward interplanetary magnetic field. J. Geophys. Res. **115**, A10218 (2010). doi:10.1029/2009JA015193
A. Hasegawa, L. Chen, Kinetic process of the plasma heating by Alfvén wave. Phys. Rev. Lett. **35**, 370 (1975)
A. Hasegawa, L. Chen, Kinetic processes in plasma heating by resonant mode conversion of Alfven wave. Phys. Fluids **19**, 1925–1934 (1976)
A. Hasegawa, K. Mima, Anomalous transport produced by kinetic Alfvén wave turbulence. J. Geophys. Res. **83**(A3), 1117–1123 (1978). doi:10.1029/JA083iA03p01117
H. Hasegawa, B.U.Ö. Sonnerup, B. Klecker, G. Paschmann, M.W. Dunlop, H. Rème, Optimal reconstruction of magnetopause structures from Cluster data. Ann. Geophys. **23**, 973–982 (2005). doi:10.5194/angeo-23-973-2005
H. Hasegawa, M. Fujimoto, K. Maezawa, Y. Saito, T. Mukai, Geotail observations of the dayside outer boundary region: interplanetary magnetic field control and dawn-dusk asymmetry. J. Geophys. Res. **108**(A4), 1163 (2003). doi:10.1029/2002JA009667
H. Hasegawa, M. Fujimoto, T.-D. Phan, H. Rème, A. Balogh, M.W. Dunlop, C. Hashimoto, R. TanDokoro, Transport of solar wind into Earth's magnetosphere through rolled-up Kelvin-Helmholtz vortices. Nature **430**, 755–758 (2004b)
H. Hasegawa, M. Fujimoto, Y. Saito, T. Mukai, Dense and stagnant ions in the low-latitude boundary region under northward interplanetary magnetic field. Geophys. Res. Lett. **31**, L06802 (2004a). doi:10.1029/2003GL19120
H. Hasegawa, M. Fujimoto, K. Takagi, Y. Saito, T. Mukai, H. Rème, Single-spacecraft detection of rolled-up Kelvin-Helmholtz vortices at the flank magnetopause. J. Geophys. Res. **111**, A09203 (2006). doi:10.1029/2006JA011728
H. Hasegawa, A. Retinò, A. Vaivads, Y. Khotyaintsev, M. André, T.K.M. Nakamura, W.-L. Teh, B.U.Ö. Sonnerup, S.J. Schwartz, Y. Seki, M. Fujimoto, Y. Saito, H. Rème, P. Canu, Kelvin-Helmholtz waves at the Earth's magnetopause: multiscale development and associated reconnection. J. Geophys. Res. (Space Phys.) **114**, 12207 (2009). doi:10.1029/2009JA014042

H. Hietala, T.V. Laitinen, K. Andréeová, R. Vainio, A. Vaivads, M. Palmroth, T.I. Pulkkinen, H.E.J. Koskinen, E.A. Lucek, H. Rème, Supermagnetosonic jets behind a collisionless quasiparallel shock. Phys. Rev. Lett. **103**(24), 245001 (2009)

H. Hietala, N. Partamies, T.V. Laitinen, L.B.N. Clausen, G. Facskó, A. Vaivads, H.E.J. Koskinen, I. Dandouras, H. Rème, E.A. Lucek, Supermagnetosonic subsolar magnetosheath jets and their effects: from the solar wind to the ionospheric convection. Ann. Geophys. **30**(1), 33–48 (2012)

T.W. Hill, Origin of the plasma sheet. J. Geophys. Res. **79**, 379 (1974)

T.W. Hill, Interchange stability of a rapidly rotating magnetosphere. Planet. Space Sci. **24**, 1151 (1976)

E.W. Hones, Transient phenomena in the magnetotail and their relation to substorms. Space Sci. Rev. **23**, 393 (1979)

E.W. Hones, J.R. Asbridge, S.J. Bame, S. Singer, Magnetotail plasma flow measured by Vela 4A. J. Geophys. Res. **78**, 5463 (1973)

K.-J. Hwang, M.M. Kuznetsova, F. Sahraoui, M.L. Goldstein, E. Lee, G.K. Parks, Kelvin-Helmholtz waves under southward interplanetary magnetic field. J. Geophys. Res. **116**, A08210 (2011). doi:10.1029/2011JA016596

K.-J. Hwang, M.L. Goldstein, M.M. Kuznetsova, Y. Wang, A.F. Viñas, D.G. Sibeck, The first in situ observation of Kelvin-Helmholtz waves at high-latitude magnetopause during strongly dawnward interplanetary magnetic field conditions. J. Geophys. Res. **117**, A08233 (2012). doi:10.1029/2011JA017256

S.M. Imber, S.E. Milan, B. Hubert, The auroral and ionospheric flow signatures of dual lobe reconnection. Ann. Geophys. **24**, 3115–3129 (2006). doi:10.5194/angeo-24-3115-2006

T. Izutsu, H. Hasegawa, T.K.M. Nakamura, M. Fujimoto, Plasma transport induced by kinetic Alfvén wave turbulence. Phys. Plasmas **19**, 102305 (2012). doi:10.1063/1.4759167

J.R. Johnson, C.Z. Cheng, Kinetic Alfvén waves and plasma transport at the magnetopause. Geophys. Res. Lett. **24**, 1423–1426 (1997)

J.R. Johnson, C.Z. Cheng, Stochastic ion heating at the magnetopause due to kinetic Alfvén waves. Geophys. Res. Lett. **28**, 4421–4424 (2001)

J.R. Johnson, S. Wing, Northward interplanetary magnetic field plasma sheet entropies. J. Geophys. Res. **114**, A00D08 (2009). doi:10.1029/2008JA014017

J.R. Johnson, C.Z. Cheng, P. Song, Signatures of mode conversion and kinetic Alfvén waves at the magnetopause. Geophys. Res. Lett. **28**(2), 227–230 (2001)

J.R. Johnson, S. Wing, P.A. Delamere, Kelvin Helmholtz instability in planetary magnetospheres. Space Sci. Rev. 1–31 (2014). doi:10.1007/s11214-014-0085-z

H. Karimabadi, V. Roytershteyn, C.G. Mouikis, L.M. Kistler, W. Daughton, Flushing effect in reconnection: effects of minority species of oxygen ions. Planet. Space Sci. **59**, 526–536 (2011). doi:10.1016/j.pss.2010.07.014

T. Karlsson, N. Brenning, H. Nilsson, J.-G. Trotignon, X. Vallières, G. Facsko, Localized density enhancements in the magnetosheath: three-dimensional morphology and possible importance for impulsive penetration. J. Geophys. Res. **117**(A3), A03227 (2012)

R.L. Kaufmann, W.R. Paterson, Magnetic flux and particle transport in the plasma sheet. J. Geophys. Res. **111**, A10214 (2006). doi:10.1029/2006JA011734

R.L. Kaufmann, W.R. Paterson, Ion heat flux and energy transport near the magnetotail neutral sheet. J. Geophys. Res. **113**, A05207 (2008). doi:10.1029/2007JA012929

R.L. Kaufmann, W.R. Paterson, Boltzmann H function and entropy in the plasma sheet. J. Geophys. Res. **114**, A00D04 (2009). doi:10.1029/2008JA014030

R.L. Kaufmann, W.R. Paterson, L.A. Frank, Pressure, volume, density relationships in the plasma sheet. J. Geophys. Res. **109**, A08204 (2004). doi:10.1029/2003JA010317

R.L. Kaufmann, W.R. Paterson, L.A. Frank, Relationships between the ion flow speed, magnetic flux transport rate, and other plasma sheet parameters. J. Geophys. Res. **110**, A09216 (2005). doi:10.1029/2005JA011068

K. Keika, L.M. Kistler, P.C. Brandt, Energization of O^+ ions in the Earth's inner magnetosphere and the effects on ring current buildup: a review of previous observations and possible mechanisms. J. Geophys. Res. Space Phys. **118**, 4441–4464 (2013). doi:10.1002/jgra.50371

A. Keiling et al., New properties of energy-dispersed ions in the plasma sheet boundary layer observed by Cluster. J. Geophys. Res. **109**, A05215 (2004). doi:10.1029/2003JA010277

R.L. Kessel, S.-H. Chen, J.L. Green, S.F. Fung, S.A. Boardsen, L.C. Tan, T.E. Eastman, J.D. Craven, L.A. Frank, Evidence of high-latitude reconnection during northward IMF: Hawkeye observations. Geophys. Res. Lett. **23**, 583 (1996)

S.A. Kiehas, V. Angelopoulos, A. Runov, M.B. Moldwin, C. Möstl, On the formation of tilted flux ropes in the Earth's magnetotail observed with ARTEMIS. J. Geophys. Res. **117**, A05231 (2012). doi:10.1029/2011JA017377

H.-S. Kim, D.-Y. Lee, S. Ohtani, M.-Y. Park, B.-H. Ahn, On near-tail bubble penetration into geosynchronous altitude. J. Geophys. Res. **117**, A07205 (2012). doi:10.1029/2012JA017749

L.M. Kistler et al., Ion composition and pressure changes in storm time and nonstorm substorms in the vicinity of the near-Earth neutral line. J. Geophys. Res. **111**, A11222 (2006). doi:10.1029/2006JA011939

L.M. Kistler, C.G. Mouikis, B. Klecker, I. Dandouras, Cusp as a source for oxygen in the plasma sheet during geomagnetic storms. J. Geophys. Res. **115**, A03209 (2010). doi:10.1029/2009JA014838

M.G. Kivelson, H.E. Spence, On the possibility of quasistatic convection in the quiet magnetotail. Geophys. Res. Lett. **15**, 1541–1544 (1988)

H. Korth, M.F. Thomsen, J.E. Borovsky, D.J. McComas, Plasma sheet access to geosynchronous orbit. J. Geophys. Res. **104**(A11), 25047–25061 (1999). doi:10.1029/1999JA900292

J. LaBelle, R.A. Treumann, Plasma waves at the dayside magnetopause. Space Sci. Rev. **47**, 175 (1988)

B. Lavraud, V.K. Jordanova, Modeling the effects of cold-dense and hot-tenuous plasma sheet on proton ring current energy and peak location. Geophys. Res. Lett. **34**, L02102 (2007). doi:10.1029/2006GL027566

B. Lavraud et al., Cluster observations of the exterior cusp and its surrounding boundaries under northward IMF. Geophys. Res. Lett. **29**(20), 1995 (2002). doi:10.1029/2002GL015464

B. Lavraud, A. Fedorov, E. Budnik, M.F. Thomsen, A. Grigoriev, P.J. Cargill, M.W. Dunlop, H. Rème, I. Dandouras, A. Balogh, High-altitude cusp flow dependence on IMF orientation: a 3-year Cluster statistical study. J. Geophys. Res. **110**, A02209 (2005b). doi:10.1029/2004JA010804

B. Lavraud, M.F. Thomsen, M.G.G.T. Taylor, Y.L. Wang, T.D. Phan, S.J. Schwartz, R.C. Elphic, A. Fazakerley, H. Réme, A. Balogh, Characteristics of the magnetosheath electron boundary layer under northward interplanetary magnetic field: implications for high-latitude reconnection. J. Geophys. Res. **110**, A06209 (2005a). doi:10.1029/2004JA010808

B. Lavraud, M.F. Thomsen, J.E. Borovsky, M.H. Denton, T.I. Pulkkinen, Magnetosphere preconditioning under northward IMF: evidence from the study of coronal mass ejection and corotating interaction region geoeffectiveness. J. Geophys. Res. **111**, A09208 (2006a). doi:10.1029/2005JA011566

B. Lavraud, M.F. Thomsen, B. Lefebvre, E. Budnik, P.J. Cargill, A. Fedorov, M.G.G.T. Taylor, S.J. Schwartz, H. Rème, A.N. Fazakerley, A. Balogh, Formation of the cusp and dayside boundary layers as a function of IMF orientation: Cluster results, in *Proceedings of the Cluster–Double Star Symposium, ESA SP-598* (2006c), pp. 221–228

B. Lavraud, M.F. Thomsen, B. Lefebvre, S.J. Schwartz, K. Seki, T.D. Phan, Y.L. Wang, A. Fazakerley, H. Rème, A. Balogh, Evidence for newly closed magnetosheath field lines at the dayside magnetopause under northward IMF. J. Geophys. Res. **111**(A5), A05211 (2006d). doi:10.1029/2005JA011266

B. Lavraud, M.F. Thomsen, S. Wing, M. Fujimoto, M.H. Denton, J.E. Borovsky, A. Aasnes, K. Seki, J. Weygand, Observations of two distinct cold, dense ion populations at geosynchronous orbit: local time asymmetry, solar wind dependence and origin. Ann. Geophys. **24**(12), 3451–3465 (2006b)

B. Lavraud et al., Tracing solar wind plasma entry into the magnetosphere using ion-to-electron temperature ratio. Geophys. Res. Lett. **36**, L18109 (2009). doi:10.1029/2009GL039442

G. Le, C.T. Russell, J.T. Gosling, M.F. Thomsen, ISEE observations of low-latitude boundary layer for northward interplanetary magnetic field: implications for cusp reconnection. J. Geophys. Res. **101**, 27239 (1996)

L.C. Lee, J.R. Johnson, Z.W. Ma, Kinetic Alfvén waves as a source of plasma transport at the dayside magnetopause. J. Geophys. Res. **99**, 17405–17411 (1994)

J. Lemaire, Impulsive penetration of filamentary plasma elements into the magnetospheres of the Earth and Jupiter. Planet. Space Sci. **25**, 887–890 (1977)

J. Lemaire, Plasmoid motion across a tangential discontinuity—with application to the magnetopause. J. Plasma Phys. **33**, 425–436 (1985)

J. Lemaire, Interpretation of the Northward Bz (NBZ) Birkeland current system and polar cap convection patterns in terms of the impulsive penetration model, in *Magnetotail Physics*, ed. by A.T.Y. Lui (Johns Hopkins University Press, Baltimore, 1987), pp. 83–90

J. Lemaire, Impulsive penetration of solar wind plasma irregularities into the magnetosphere: relevant laboratory experiments, in *Electromagnetic Coupling in the Polar Clefts and Caps*, ed. by P.E. Sandholt, A. Egeland (Kluwer Academic, Dordrecht, 1989), pp. 27–42

J. Lemaire, M. Roth, Penetration of solar wind plasma elements into the magnetosphere. J. Atmos. Terr. Phys. **40**, 331–335 (1978)

J. Lemaire, M. Roth, Differences between solar wind plasmoids and ideal magnetohydrodynamic filaments. Planet. Space Sci. **29**, 843–849 (1981)

J. Lemaire, M. Roth, Non-steady-state solar wind-magnetosphere interaction. Space Sci. Rev. **57**, 59–108 (1991). ISSN 0038-6308

J. Lemaire, M. Scherer, Ionosphere-plasmasheet field-aligned currents and parallel electric fields. Planet. Space Sci. **22**, 1485–1490 (1974)

J. Lemaire, M. Scherer, Field aligned distribution of plasma mantle and ionospheric plasmas. J. Atmos. Terr. Phys. **40**, 337–342 (1978)
J. Lemaire, M.J. Rycroft, M. Roth, Control of impulsive penetration of solar wind irregularities into the magnetosphere by the interplanetary magnetic field direction. Planet. Space Sci. **27**, 47–57 (1979)
C. Lemon, R.A. Wolf, T.W. Hill, S. Sazykin, R.W. Spiro, F.R. Toffoletto, J. Birn, M. Hesse, Magnetic storm ring current injection modeled with the Rice Convection Model and a self-consistent magnetic field. Geophys. Res. Lett. **31**, L21801 (2004). doi:10.1029/2004GL020914
W. Li, J. Raeder, J. Dorelli, M. Øieroset, T.D. Phan, Plasma sheet formation during long period of northward IMF. Geophys. Res. Lett. **32**, L12S08 (2005). doi:10.1029/2004GL021524
W. Li, J. Raeder, M.F. Thomsen, B. Lavraud, Solar wind plasma entry into the magnetosphere under northward IMF conditions. J. Geophys. Res. **113**, A04204 (2008). doi:10.1029/2007JA012604
W. Li, J. Raeder, M. Øieroset, T.D. Phan, Cold dense magnetopause boundary layer under northward IMF: results from THEMIS and MHD simulations. J. Geophys. Res. **114**, A00C15 (2009). doi:10.1029/2008JA013497
W. Li, C. Wang, B. Tang, X. Guo, D. Lin, Global features of Kelvin-Helmholtz waves at the magnetopause for northward interplanetary magnetic field. J. Geophys. Res. (Space Phys.) **118**, 5118–5126 (2013). doi:10.1002/jgra.50498
Y. Lin, J.R. Johnson, X.Y. Wang, Hybrid simulation of mode conversion at the magnetopause. J. Geophys. Res. **115**, A04208 (2010). doi:10.1029/2009JA014524
Y. Lin, J.R. Johnson, X. Wang, Three-dimensional mode conversion associated with kinetic Alfvén waves. Phys. Rev. Lett. **109**, 125003 (2012). doi:10.1103/PhysRevLett.109.125003
G. Lu, P.H. Reiff, M.R. Hairston, R.A. Heelis, J.L. Karty, Distribution of convection potential around the polar cap boundary as a function of the interplanetary magnetic field. J. Geophys. Res. **94**, 13447 (1989)
G. Lu et al., Reversed two-cell convection in the northern and southern hemispheres during northward interplanetary magnetic field. J. Geophys. Res. **116**, A12237 (2011)
E.A. Lucek, D. Constantinescu, M.L. Goldstein, J. Pickett, J.L. Pinçon, F. Sahraoui, R.A. Treumann, S.N. Walker, The magnetosheath. Space Sci. Rev. **118**, 95–152 (2005). doi:10.1007/s11214-005-3825-2
J.G. Luhmann, C.T. Russell, R.C. Elphic, Spatial distributions of magnetic field fluctuations in the dayside magnetosheath. J. Geophys. Res. **91**, 1711–1715 (1986). doi:10.1029/JA091iA02p01711
R. Lundin, On the magnetospheric boundary layer and solar wind energy transfer into the magnetosphere. Space Sci. Rev. **48**(3–4), 263–320 (1988). ISSN 0038-6308
R. Lundin, B. Aparicio, Observations of penetrated solar wind plasma elements in the plasma mantle. Planet. Space Sci. **30**, 81–91 (1982)
R. Lundin, E. Dubinin, Solar wind energy transfer regions inside the dayside magnetopause. I—Evidence for magnetosheath plasma penetration. Planet. Space Sci. **32**, 745–755 (1984)
L.R. Lyons et al., Association between geotail plasma flows and auroral poleward boundary intensifications observed by Canopus photometer. J. Geophys. Res. **104**(A3), 4484–4500 (1999). doi:10.1029/1998JA900140
X. Ma, A. Otto, P.A. Delamere, Interaction of magnetic reconnection and Kelvin-Helmholtz modes for large magnetic shear: 2. Reconnection trigger. J. Geophys. Res. Space Phys. **119**, 808–820 (2014a). doi:10.1002/2013JA019225
X. Ma, A. Otto, P.A. Delamere, Interaction of magnetic reconnection and Kelvin-Helmholtz modes for large magnetic shear: 1. Kelvin-Helmholtz trigger. J. Geophys. Res. Space Phys. **119**, 781–797 (2014b). doi:10.1002/2013JA019224
K. Maezawa, Magnetospheric convection induced by the positive and negative Z components of the interplanetary magnetic field: quantitative analysis using polar cap magnetic records. J. Geophys. Res. **81**(13), 2289–2303 (1976). doi:10.1029/JA081i013p02289
R. Maggiolo, L.M. Kistler, Spatial variation in the plasma sheet composition: dependence on geomagnetic and solar activity. J. Geophys. Res. Space Phys. **119**, 2836–2857 (2014). doi:10.1002/2013JA019517
Y. Matsumoto, M. Hoshino, Onset of turbulence induced by a Kelvin-Helmholtz vortex. Geophys. Res. Lett. **31**, L02807 (2004). doi:10.1029/2003GL018195=
Y. Matsumoto, M. Hoshino, Turbulent mixing and transport of collisionless plasmas across a stratified velocity shear layer. J. Geophys. Res. **111**, A05213 (2006). doi:10.1029/2004JA010988
Y. Matsumoto, K. Seki, Formation of a broad plasma turbulent layer by forward and inverse energy cascades of the Kelvin–Helmholtz instability. J. Geophys. Res. **115**, A10231 (2010). doi:10.1029/2009JA014637
R.L. McPherron, in *Physical Processes Producing Magnetospheric Substorms and Magnetic Storms*, ed. by J. Jacobs. Geomagnetism, vol. 4 (Academic Press, San Diego, 1991), p. 593
R.L. McPherron, T.-S. Hsu, J. Kissinger, X. Chu, V. Angelopoulos, Characteristics of plasma flows at the inner edge of the plasma sheet. J. Geophys. Res. **116**, A00133 (2011). doi:10.1029/2010JA015923
V.G. Merkin, J.G. Lyon, S.G. Claudepierre, Kelvin-Helmholtz instability of the magnetospheric boundary in a three-dimensional global MHD simulation during northward IMF conditions. J. Geophys. Res. Space Phys. **118**, 5478–5496 (2013). doi:10.1002/jgra.50520

A. Miura, Simulation of Kelvin-Helmholtz instability at the magnetospheric boundary. J. Geophys. Res. **92**, 3195–3206 (1987). doi:10.1029/JA092iA04p03195

A. Miura, Dependence of the magnetopause Kelvin-Helmholtz instability on the orientation of the magnetosheath magnetic field. Geophys. Res. Lett. **22**, 2993–2996 (1995)

A. Miura, Compressible magnetohydrodynamic Kelvin-Helmholtz instability with vortex pairing in the two-dimensional transverse configuration. Phys. Plasmas **4**, 2871–2885 (1997). doi:10.1063/1.872419

C.G. Mouikis, L.M. Kistler, Y.H. Liu, B. Klecker, A. Korth, I. Dandouras, H^+ and O^+ content of the plasma sheet at 15–19 Re as a function of geomagnetic and solar activity. J. Geophys. Res. **115**, A00J16 (2010). doi:10.1029/2010JA015978

D. Nagata, S. Machida, S. Ohtani, Y. Saito, T. Mukai, Solar wind control of plasma number density in the near-Earth plasma sheet. J. Geophys. Res. **112**, A09204 (2007). doi:10.1029/2007JA012284

D. Nagata, S. Machida, S. Ohtani, Y. Saito, T. Mukai, Solar wind control of plasma number density in the near-Earth plasma sheet: Three-dimensional structure. Ann. Geophys. **26**, 4031–4049 (2008)

T.K.M. Nakamura, M. Fujimoto, Magnetic reconnection within rolled-up MHD-scale Kelvin-Helmholtz vortices: two-fluid simulations including finite electron inertial effects. Geophys. Res. Lett. **32**, L21102 (2005). doi:10.1029/2005GL023362

T.K.M. Nakamura, M. Fujimoto, Magnetic effects on the coalescence of Kelvin-Helmholtz Vortices. Phys. Rev. Lett. **101**, 165002 (2008)

R. Nakamura, W. Baumjohann, M. Brittmacher, V.A. Sergeev, M. Kubyshkina, T. Mukai, K. Liou, Flow bursts and auroral activations. J. Geophys. Res. **106**(A6), 10777–10789 (2001)

Nakamura et al., Fast flow during current sheet thinning. Geophys. Res. Lett. **29**(23), 2140 (2002). doi:10.1029/2002GL016200

R. Nakamura et al., Localized fast flow disturbance observed in the plasma sheet and in the ionosphere. Ann. Geophys. **23**(2), 553–566 (2005)

T.K.M. Nakamura, M. Fujimoto, A. Otto, Magnetic reconnection induced by weak Kelvin-Helmholtz instability and the formation of the low-latitude boundary layer. Geophys. Res. Lett. **33**, 14106 (2006). doi:10.1029/2006GL026318

T.K.M. Nakamura, H. Hasegawa, I. Shinohara, M. Fujimoto, Evolution of an MHD-scale Kelvin-Helmholtz vortex accompanied by magnetic reconnection: two-dimensional particle simulations. J. Geophys. Res. (Space Phys.) **116**, 3227 (2011). doi:10.1029/2010JA016046

T.K.M. Nakamura, W. Daughton, H. Karimabadi, S. Eriksson, Three-dimensional dynamics of vortex-induced reconnection and comparison with THEMIS observations. J. Geophys. Res. (Space Phys.) **118**, 5742–5757 (2013). doi:10.1002/jgra.50547

Z. Němeček, J. Šafránková, L. Přech, D.G. Sibeck, S. Kokubun, T. Mukai, Transient flux enhancements in the magnetosheath. Geophys. Res. Lett. **25**(8), 1273–1276 (1998)

Z. Nemecek, J. Safrankova, G.N. Zastenkar, P. Pisoft, K.I. Paularena, Spatial distribution of the magnetosheath ion flux. Adv. Space. Res. **30**, 2751–2756 (2002). doi:10.1016/S0273-1177(02)80402-1

P.T. Newell, T. Sotirelis, K. Liou, C.-I. Meng, F.J. Rich, A nearly universal solar wind-magnetosphere coupling function inferred from 10 magnetospheric state variables. J. Geophys. Res. **112**, A01206 (2007). doi:10.1029/2006JA012015

A. Nishida, E.W. Hones, Association of plasma sheet thinning with neutral line formation in the magnetotail. J. Geophys. Res. **79**, 535 (1974)

M.N. Nishino, M. Fujimoto, T. Terasawa, G. Ueno, K. Maezawa, T. Mukai, Y. Saito, Geotail observations of temperature anisotropy of the two-component protons in the dusk plasma sheet. Ann. Geophys. **25**, 769–777 (2007)

K. Nykyri, Impact of MHD shock physics on magnetosheath asymmetry and Kelvin-Helmholtz instability. J. Geophys. Res. Space Phys. **118**, 5068–5081 (2013). doi:10.1002/jgra.50499

K. Nykyri, A. Otto, Plasma transport at the magnetospheric boundary due to reconnection in Kelvin-Helmholtz vortices. Geophys. Res. Lett. **28**, 3565–3568 (2001)

K. Nykyri, A. Otto, Influence of the Hall term on KH instability and reconnection inside KH vortices. Ann. Geophys. **22**, 935–949 (2004)

K. Nykyri, A. Otto, B. Lavraud, C. Mouikis, L.M. Kistler, A. Balogh, H. Reme, Cluster observations of reconnection due to the Kelvin-Helmholtz instability at the downside magnetospheric flank. Ann. Geophys. **24**, 2619–2643 (2006)

T. Ogino, R.J. Walker, M. Ashour-Abdalla, A global magnetohydrodynamic simulation of the response of the magnetosphere to a northward turning of the interplanetary magnetic field. J. Geophys. Res. **99**, 11027 (1994)

S. Ohtani, H.J. Singer, T. Mukai, Effects of the fast plasma sheet flow on the geosynchronous magnetic configuration: geotail and GOES coordinated study. J. Geophys. Res. **111**, A01204 (2006). doi:10.1029/2005JA011383

M. Øieroset, J. Raeder, T.D. Phan, S. Wing, J.P. McFadden, W. Li, M. Fujimoto, H. Rème, A. Balogh, Global cooling and densification of the plasma sheet during an extended period of purely northward IMF on October 22–24. Geophys. Res. Lett. **32**, L12S07 (2005). doi:10.1029/2004GL021523

M. Øieroset, T.D. Phan, V. Angelopoulos, J.P. Eastwood, J. McFadden, D. Larson, C.W. Carlson, K.-H. Glassmeier, M. Fujimoto, J. Raeder, THEMIS multi-spacecraft observations of magnetosheath plasma penetration deep into the dayside low-latitude magnetosphere for northward and strong B_y IMF. Geophys. Res. Lett. **35**, L17S11 (2008). doi:10.1029/2008GL033661

W.P. Olson, K.A. Pfitzer, Magnetospheric responses to the gradient drift entry of solar wind plasma. J. Geophys. Res. **90**, 10823–10833 (1985). doi:10.1029/JA090iA11p10823

T.G. Onsager, C.A. Kletzing, J.B. Austin, H. MacKiernan, Model of magnetosheath plasma in the magnetosphere: cusp and mantle particles at low-altitudes. Geophys. Res. Lett. **20**, 479 (1993)

T.G. Onsager, J.D. Scudder, M. Lockwood, C.T. Russell, Reconnection at the high-latitude magnetopause during northward interplanetary magnetic field conditions. J. Geophys. Res. **106**(A11), 25467–25488 (2001)

A. Otto, Mass transport at the magnetospheric flanks associated with three-dimensional Kelvin–Helmholtz modes, abstract #SM33B-0365, in *AGU Fall Meeting Abstracts* (2006)

A. Otto, D.H. Fairfield, Kelvin-Helmholtz instability at the magnetotail boundary: MHD simulation and comparison with geotail observations. J. Geophys. Res. **105**, 21175–21190 (2000)

E.V. Panov et al., Plasma sheet thickness during a bursty bulk flow reversal. J. Geophys. Res. **115**, A05213 (2010a). doi:10.1029/2009JA014743

E.V. Panov et al., Multiple overshoot and rebound of a bursty bulk flow. Geophys. Res. Lett. **37**, L08103 (2010b). doi:10.1029/2009GL041971

E.V. Panov, W. Baumjohann, R. Nakamura, O. Amm, M.V. Kubyshkina, K.-H. Glassmeier, J.M. Weygand, V. Angelopoulos, A.A. Petrukovich, V.A. Sergeev, Ionospheric response to oscillatory flow braking in the magnetotail. J. Geophys. Res. Space Phys. **118**, 1529–1544 (2013). doi:10.1002/jgra.50190

J. Paral, R. Rankin, Dawn-dusk asymmetry in the Kelvin-Helmholtz instability at Mercury. Nat. Commun. **4**, 1645 (2013). doi:10.1038/ncomms2676

G. Paschmann, B.U.O. Sonnerup, I. Papamastorakis, N. Sckopke, G. Haerendel, S.J. Bame, J.R. Asbridge, J.T. Gosling, C.T. Russell, R.C. Elphic, Plasma acceleration at the Earth's magnetopause: evidence for reconnection. Nature **282**, 243 (1979)

K.I. Paularena, J.D. Richardson, M.A. Kolpak, C.R. Jackson, G.L. Siscoe, A dawn-dusk density asymmetry in Earth's magnetosheath. J. Geophys. Res. **106**(A11), 25377–25394 (2001). doi:10.1029/2000JA000177

V. Peroomian, M. El-Alaoui, The storm-time access of solar wind ions to the nightside ring current and plasma sheet. J. Geophys. Res. **113**, A06215 (2008). doi:10.1029/2007JA012872

V. Peroomian, M. El-Alaoui, P.C. Brandt, The ion population of the magnetotail during the 17 April 2002 magnetic storm: large-scale kinetic simulations and IMAGE/HENA observations. J. Geophys. Res. **116**, A05214 (2011). doi:10.1029/2010JA016253

W.K. Perreault, S.-I. Akasofu, A study of geomagnetic storms. Geophys. J. R. Astron. Soc. **54**, 547 (1978)

W.K. Peterson, L. Andersson, B. Callahan, S.R. Elkington, R.W. Winglee, J.D. Scudder, H.L. Collin, Geomagnetic activity dependence of O^+ in transit from the ionosphere. J. Atmos. Sol.-Terr. Phys. **71**, 1623–1629 (2009). doi:10.1016/j.jastp.2008.11.003

S.M. Petrinec, On the magnetic field configuration of the magnetosheath. Terr. Atmos. Ocean. Sci. **24**, 265–272 (2013). doi:10.3319/TAO.2012.10.17.02(SEC)

T. Phan et al., Simultaneous Cluster and IMAGE observations of cusp reconnection and auroral proton spot for northward IMF. Geophys. Res. Lett. **30**(10), 1509 (2003). doi:10.1029/2003GL016885

W.G. Pilipp, G. Morfill, Formation of plasma sheet resulting from plasma mantle dynamics. J. Geophys. Res. **83**, 5670 (1978)

F. Pitout, C.P. Escoubet, M.G.G.T. Taylor, J. Berchem, A.P. Walsh, Overlapping ion structures in the mid-altitude cusp under northward IMF: signature of dual lobe reconnection? Ann. Geophys. **30**, 489–501 (2012). doi:10.5194/angeo-30-489-2012

F. Plaschke, H. Hietala, V. Angelopoulos, Anti-sunward high-speed jets in the subsolar magnetosheath. Ann. Geophys. **31**(10), 1877–1889 (2013)

F. Plaschke, M.G.G.T. Taylor, R. Nakamura, Alternative interpretation of results from Kelvin-Helmholtz vortex identification criteria. Geophys. Res. Lett. **41**(2), 244–250 (2014)

D.H. Pontius, R.A. Wolf, Transient flux tubes in the terrestrial magnetoshere. Geophys. Res. Lett. **17**(1), 49–52 (1990)

J. Raeder, Global geospace modeling: tutorial and review, in *Space Plasma Simulation*, ed. by J. Büchner, C.T. Dum, M. Scholer (Springer, New York, 2003)

J. Raeder, R.J. Walker, M. Ashour-Abdalla, The structure of the distant geomagnetic tail during long periods of northward IMF. Geophys. Res. Lett. **22**, 349 (1995)

J. Raeder et al., Boundary layer formation in the magnetotail: geotail observations and comparisons with a global MHD simulation. Geophys. Res. Lett. **24**, 951–954 (1997). doi:10.1029/97GL00218
R.J. Redmon, W.K. Peterson, L. Andersson, P. Richards, Dawnward shift of the dayside O^+ outflow distribution: the importance of field line history in O^+ escape from the ionosphere. J. Geophys. Res. **117**, A12222 (2012). doi:10.1029/2012JA018145
P.H. Reiff, Sunward convection on both polar caps. J. Geophys. Res. **87**, 5976 (1982)
P.H. Reiff, J.L. Burch, R.W. Spiro, Cusp proton signatures and the interplanetary magnetic field. J. Geophys. Res. **85**, 5997–6005 (1980). doi:10.1029/JA085iA11p05997
L. Rezeau, A. Morane, S. Perraut, A. Roux, R. Schmidt, Characterization of Alfvénic fluctuations in the magnetopause boundary layer. J. Geophys. Res. **94**, 101–110 (1989). doi:10.1029/JA094iA01p00101
L. Rezeau, F. Sahraoui, E. d'Humieres, G. Belmont, T. Chust, N. Cornilleau-Wehrlin, L. Mellul, O. Alexandrova, E. Lucek, P. Robert, P. Décréau, P. Canu, I. Dandouras, A case study of lowfrequency waves at the magnetopause. Ann. Geophys. **19**, 1463–1470 (2001)
R.L. Richard, R.J. Walker, M. Ashour-Abdalla, The population of the magnetosphere by solar winds ions when the interplanetary magnetic field is northward. Geophys. Res. Lett. **21**, 2455–2458 (1994). doi:10.1029/94GL01427
H. Rosenbauer, H. Grunwaldt, M.D. Montgomery, G. Paschmann, N. Sckopke, HEOS 2 plasma observations in the distant polar magnetosphere: the plasma mantle. J. Geophys. Res. **80**, 2723 (1975)
M. Roth, On impulsive penetration of solar wind plasmoids into the geomagnetic field. Planet. Space Sci. **40**, 193–201 (1992)
M. Roth, Impulsive transport of solar wind into the magnetosphere physics of the magnetopause, in *Geophysical Monograph 90*, ed. by P. Song, B.U.Ö. Sonnerup, M.F. Thomsen (American Geophysical Union, Washington, DC, 1995), p. 343
A. Runov, V. Angelopoulos, M.I. Sitnov, V.A. Sergeev, J. Bonnell, J.P. McFadden, D. Larson, K.H. Glassmeier, U. Auster, THEMIS observations of an earthward-propagating dipolarization front. Geophys. Res. Lett. **36**, L14106 (2009). doi:10.1029/2009GL038980
A. Runov et al., Dipolarization fronts in the magnetotail plasma sheet. Planet. Space Sci. **59**(7), 517–525 (2011b). doi:10.1016/j.pss.2010.06.006
A. Runov, V. Angelopoulos, X.-Z. Zhou, X.-J. Zhang, S. Li, F. Plaschke, J. Bonnell, A THEMIS multicase study of dipolarization fronts in the magnetotail plasma sheet. J. Geophys. Res. **116**, A05216 (2011a). doi:10.1029/2010JA016316
J. Safrankova, Z. Nemecek, D.G. Sibeck, L. Prech, J. Merka, O. Santolik, Two point observation of high-latitude reconnection. Geophys. Res. Lett. **25**, 4301 (1998)
E.R. Sanchez, D. Summers, G.L. Siscoe, Downstream evolution of an open MHD magnetotail boundary. J. Geophys. Res. **95**(20), 743–758 (1990)
E.R. Sanchez, S. Wing, E. Spanswick, E. Donovan, Entropy conservation and rate of propagation of bubbles in the Earth's magnetotail: a case study. J. Geophys. Res. **117**, A05226 (2012). doi:10.1029/2011JA017287
P.E. Sandholt, C.J. Farrugia, S.W.H. Cowley, W.F. Denig, M. Lester, J. Moen, B. Lybekk, Capture of magnetosheath plasma by the magnetosphere during northward IMF. Geophys. Res. Lett. **26**, 2833–2836 (1999)
S. Savin, E. Amata, L. Zelenyi et al., A high energy jets in the Earth's magnetosheath: implications for plasma dynamics and anomalous transport. JETP Lett. **87**(11), 593–599 (2008)
S. Savin, E. Amata, V. Budaev, L. Zelenyi, E.A. Kronberg, J. Buechner, J. Safrankov, Z. Nemecek, J. Blecki, L. Kozak, S. Klimov, A. Skalsky, L. Lezhen, On nonlinear cascades and resonances in the outer magnetosphere. JETP Lett. **99**, 16–21 (2014). doi:10.1134/S002136401401010X
G. Schmidt, Plasma motion across magnetic fields. Phys. Fluids **3**, 961–965 (1960)
D. Schriver, M. Ashour-Abdalla, R.L. Richard, On the origin of the ion-electron temperature difference in the plasma sheet. J. Geophys. Res. **103**(A7), 14879–14895 (1998). doi:10.1029/98JA00017
V.A. Sergeev, V. Angelopoulos, J.T. Gosling, C.A. Cattell, C.T. Russell, Detection of localized plasma-depleted flux tubes or bubbles in the midtail plasma sheet. J. Geophys. Res. **101**, 10817–10826 (1996). doi:10.1029/96JA00460
V.A. Sergeev, K. Liou, P.T. Newell, S.-I. Ohtani, M.R. Hairston, F. Rich, Auroral streamers: characteristics of associated precipitation, convection and field-aligned currents. Ann. Geophys. **22**, 537–548 (2004)
V.A. Sergeev, S.V. Apatenkov, V. Angelopoulos, J.P. McFadden, D. Larson, J.W. Bonnell, M. Kuznetsova, N. Partamies, F. Honary, Simultaneous THEMIS observations in the near-tail portion of the inner and outer plasma sheet flux tubes at substorm onset. J. Geophys. Res. **113**, A00C02 (2008). doi:10.1029/2008JA013527
V.A. Sergeev, I.A. Chernyaev, S.V. Dubyagin, Y. Miyashita, V. Angelopoulos, P.D. Boakes, R. Nakamura, M.G. Henderson, Energetic particle injections to geostationary orbit: relationship to flow bursts and magnetospheric state. J. Geophys. Res. **117**, A10207 (2012). doi:10.1029/2012JA017773

F. Shi, Y. Lin, X. Wang, Global hybrid simulation of mode conversion at the dayside magnetopause. J. Geophys. Res. Space Phys. **118**, 6176–6187 (2013). doi:10.1002/jgra.50587
D. Sibeck, A model for the transient magnetospheric response to sudden solar wind dynamic pressure variations. J. Geophys. Res. **95**(1), 3755–3771 (1990)
D.G. Sibeck et al., Comprehensive study of the magnetospheric response to a hot flow anomaly. J. Geophys. Res. **104**(A3), 4577–4593 (1999). doi:10.1029/1998JA900021
D.G. Sibeck, L. Prech, J. Safrankova, Z. Nemecek, Two-point measurements of the magnetopause: interball observations. J. Geophys. Res. **105**(A1), 237–244 (2000)
G.L. Siscoe, E. Sanchez, An MHD model for the complete open magnetotail boundary. J. Geophys. Res. **92**, 7405–7412 (1987)
J.A. Slavin et al., Simultaneous observations of earthward flow bursts and plasmoid ejection during magnetospheric substorms. J. Geophys. Res. **107**(A7), 1106 (2002). doi:10.1029/2000JA003501
P. Song, C.T. Russell, Model of the formation of the low-latitude boundary layer for strongly northward interplanetary magnetic field. J. Geophys. Res. **97**, 1411–1420 (1992)
P. Song, C.T. Russell, R.J. Fitzenreiter, J.T. Gosling, M.F. Thomsen, D.G. Mitchell, S.A. Fuselier, G.K. Parks, R.R. Anderson, D. Hubert, Structure and properties of the subsolar magnetopause for northward interplanetary magnetic field: multiple-instrument particle observations. J. Geophys. Res. **98**(A7), 11319–11337 (1993). doi:10.1029/93JA00606
B.U.O. Sonnerup, Theory of the low-latitude boundary layer. J. Geophys. Res. **85**, 2017–2026 (1980). doi:10.1029/JA085iA05p02017
B.U.Ö. Sonnerup, M.J. Laird, On magnetospheric interchange instability. J. Geophys. Res. **68**(1), 131–139 (1963). doi:10.1029/JZ068i001p00131
B.U.Ö. Sonnerup, G. Paschmann, I. Papamastorakis, N. Sckopke, G. Haerendel, S.J. Bame, J.R. Asbridge, J.T. Gosling, C.T. Russell, Evidence for magnetic field reconnection at the Earth's magnetopause. J. Geophys. Res. **86**, 10049 (1981)
T.W. Speiser, Particle trajectories in model current sheets. J. Geophys. Res. **70**, 1717 (1965)
T.W. Speiser, Particle trajectories in model current sheets, 2. Applications to auroras using a geomagnetic tail model. J. Geophys. Res. **72**, 3919 (1967)
H.E. Spence, M.G. Kivelson, Contributions of the low-latitude boundary layer to the finite width magnetotail convection model. J. Geophys. Res. **98**(A9), 15487–15496 (1993). doi:10.1029/93JA01531
K. Stasiewicz, G. Gustafsson, *Alfvén Waves and Structures: What Can We Learn with Multipoint Measurements on Cluster-II, Cluster-II Workshop: Multiscale/Multipoint Plasma Measurements, Proceedings of the Workshop Held at Imperial College, London, UK, 22–24 September 1999*, ESA-SP, vol. 449 (European Space Agency, Paris, 2000), p. 177. ISBN: 9290927968
K. Stasiewicz, C.E. Seyler, F.S. Mozer, G. Gustafsson, J. Pickett, B. Popielawska, Magnetic bubbles and kinetic Alfvén waves in the high-latitude magnetopause boundary. J. Geophys. Res. **106**, 29503–29514 (2001). doi:10.1029/2001JA900055
H. Stenuit, M. Fujimoto, S.A. Fuselier, J.-A. Sauvaud, S. Wing, A. Fedorov, E. Budnik, S.P. Savin, K.J. Trattner, V. Angelopoulos, J. Bonnel, T.D. Phan, T. Mukai, A. Pedersen, Multi-spacecraft study ion the dynamics of the dusk-flank magnetosphere under northward IMF: January 10–11, 1997. J. Geophys. Res. **107**(A10), 1333 (2002). doi:10.1029/2002JA9009246
M. Stepanova, V. Pinto, J.A. Valdivia, E.E. Antonova, Spatial distribution of the eddy diffusion coefficients in the plasma sheet during quiet time and substorms from THEMIS satellite data. J. Geophys. Res. **116**, A00I24 (2011). doi:10.1029/2010JA015887
M.G.G.T. Taylor, B. Lavraud, Observation of three distinct ion populations at the Kelvin-Helmholtz-unstable magnetopause. Ann. Geophys. **26**, 1559–1566 (2008)
M.G.G.T. Taylor et al., The plasma sheet and boundary layers under northward IMF: a multi-point and multi-instrument 65 perspective. Adv. Space Res. **41**, 1619–1629 (2008). doi:10.1016/j.asr.2007.6610.013
M.G.G.T. Taylor, H. Hasegawa, B. Lavraud, T. Phan, C.P. Escoubet, M.W. Dunlop, Y.V. Bogdanova, A.L. Borg, M. Volwerk, J. Berchem, O.D. Constantinescu, J.P. Eastwood, A. Masson, H. Laakso, J. Soucek, A.N. Fazakerley, H.U. Frey, E.V. Panov, C. Shen, J.K. Shi, D.G. Sibeck, Z.Y. Pu, J. Wang, J.A. Wild, Spatial distribution of rolled up Kelvin-Helmholtz vortices at Earth's dayside and flank magnetopause. Ann. Geophys. **30**, 1025–1035 (2012). doi:10.5194/angeo-30-1025-2012
T. Terasawa et al., Solar wind control of density and temperature in the near-Earth plasma sheet: WIND/GEOTAIL collaboration. Geophys. Res. Lett. **24**, 935–938 (1997)
V.A. Thomas, D. Winske, Kinetic simulation of the Kelvin-Helmholtz instability at the Venus ionopause. Geophys. Res. Lett. **18**, 1943–1946 (1991)
V.A. Thomas, D. Winske, Kinetic simulations of the Kelvin-Helmholtz instability at the magnetopause. J. Geophys. Res. **98**, 11425–11438 (1993)
M.F. Thomsen, J.E. Borovsky, R.M. Skoug, C.W. Smith, Delivery of cold, dense plasma sheet material into the near-Earth region. J. Geophys. Res. **108**, 1151 (2003). doi:10.1029/2002JA009544

R.A. Treumann, W. Baumjohann, Particle trapping at a tangential discontinuity: multiple incidence. Planet. Space Sci. **36**, 1477–1484 (1988)
R.A. Treumann, J. Labelle, T.M. Bauer, *Diffusion Processes: An Observational Perspective*. Washington DC American Geophysical Union Geophysical Monograph Series, vol. 90 (1995), p. 331
B.T. Tsurutani, E.J. Smith, R.R. Anderson, K.W. Ogilvie, J.D. Scudder, D.N. Baker, S.J. Bame, Lion roars and nonoscillatory drift mirror waves in the magnetosheath. J. Geophys. Res. **87**, 6060–6072 (1982)
N.A. Tsyganenko, On the convective mechanism for formation of the plasma sheet in the magnetospheric tail. Planet. Space Sci. **30**, 1007–1012 (1982)
N.A. Tsyganenko, A magnetospheric magnetic field model with a warped tail current sheet. Planet. Space Sci. **37**, 5–20 (1989)
Y.-K. Tung, C.W. Carlson, J.P. McFadden, D.M. Klumpar, G.K. Parks, W.J. Peria, K. Liou, Auroral polar cap boundary ion conic outflow observed on FAST. J. Geophys. Res. **106**(A3), 3603–3614 (2001). doi:10.1029/2000JA900115
J.M. Turner, L.F. Burlaga, N.F. Ness, J.F. Lemaire, Magnetic holes in the solar wind. J. Geophys. Res. **82**, 1921–1924 (1977)
D.L. Turner, S. Eriksson, T.D. Phan, V. Angelopoulos, W. Tu, W. Liu, X. Li, W.-L. Teh, J.P. McFadden, K.-H. Glassmeier, Multispacecraft observations of a foreshock-induced magnetopause disturbance exhibiting distinct plasma flows and an intense density compression. J. Geophys. Res. **116**(A4), A04230 (2011)
G. Voitcu, Kinetic simulations of plasma dynamics across magnetic fields and applications to the physics of planetary magnetospheres, Ph.D. Thesis, University of Bucharest (2014)
B.M. Walsh, D.G. Sibeck, Y. Wang, D.H. Fairfield, Dawn-dusk asymmetries in the Earth's magnetosheath. J. Geophys. Res. **117**, A12211 (2012). doi:10.1029/2012JA018240
C.-P. Wang, L.R. Lyons, M.W. Chen, R.A. Wolf, Modeling the quiet time inner plasma sheet protons. J. Geophys. Res. **106**(A4), 6161–6178 (2001). doi:10.1029/2000JA000377
C.-P. Wang, L.R. Lyons, M.W. Chen, F.R. Toffoletto, Modeling the transition of the inner plasma sheet from weak to enhanced convection. J. Geophys. Res. **109**, A12202 (2004). doi:10.1029/2004JA010591
C.-P. Wang, L.R. Lyons, J.M. Weygand, T. Nagai, R. McEntire, Equatorial distributions of the plasma sheet ions, their electric and magnetic drifts, and magnetic fields under different interplanetary magnetic field B_z conditions. J. Geophys. Res. **111**, A04215 (2006). doi:10.1029/2005JA011545
C.-P. Wang, L.R. Lyons, T. Nagai, J.M. Weygand, R. McEntire, Sources, transport, and distributions of plasma sheet ions and electrons and dependences on interplanetary parameters under northward interplanetary magnetic field. J. Geophys. Res. **112**, A10224 (2007). doi:10.1029/2007JA012522
C.-P. Wang, L.R. Lyons, R.A. Wolf, T. Nagai, J.M. Weygand, A.T.Y. Lui, Plasma sheet $PV^{5/3}$ and nV and associated plasma and energy transport for different convection strengths and AE levels. J. Geophys. Res. **114**, A00D02 (2009). doi:10.1029/2008JA013849
C.-P. Wang, L.R. Lyons, T. Nagai, J.M. Weygand, A.T.Y. Lui, Evolution of plasma sheet particle content under different interplanetary magnetic field conditions. J. Geophys. Res. **115**, A06210 (2010). doi:10.1029/2009JA015028
C.-P. Wang, M. Gkioulidou, L.R. Lyons, R.A. Wolf, V. Angelopoulos, T. Nagai, J.M. Weygand, A.T.Y. Lui, Spatial distributions of ions and electrons from the plasma sheet to the inner magnetosphere: comparisons between THEMIS-Geotail statistical results and the Rice convection model. J. Geophys. Res. **116**, A11216 (2011). doi:10.1029/2011JA016809
C.-P. Wang, M. Gkioulidou, L.R. Lyons, V. Angelopoulos, Spatial distributions of the ion to electron temperature ratio in the magnetosheath and plasma sheet. J. Geophys. Res. **117**, A08215 (2012). doi:10.1029/2012JA017658
J.M. Weygand et al., Plasma sheet turbulence observed by Cluster II. J. Geophys. Res. **110**, A01205 (2005). doi:10.1029/2004JA010581
M. Wilber, R.M. Winglee, Dawn-dusk asymmetries in the low-latitude boundary layer arising from the Kelvin-Helmholtz instability: a particle simulation. J. Geophys. Res. **100**, 1883–1898 (1995)
D.J. Williams, Considerations of source, transport, acceleration/heating and loss processes responsible for geomagnetic tail particle populations. Space Sci. Rev. **80**, 369–389 (1997)
G.R. Wilson, D.M. Ober, G.A. Germany, E.J. Lund, The relationship between suprathermal heavy ion outflow and auroral electron energy deposition: polar/ultraviolet imager and fast auroral snapshot/time-of-flight energy angle mass spectrometer observations. J. Geophys. Res. **106**(A6), 18981–18993 (2004). doi:10.1029/2000JA000434
M. Wiltberger, W. Lotko, J.G. Lyon, P. Damiano, V. Merkin, Influence of cusp O^+ outflow on magnetotail dynamics in a multifluid MHD model of the magnetosphere. J. Geophys. Res. **115**, A00J05 (2010). doi:10.1029/2010JA015579
C.D. Winant, F.K. Browand, Vortex pairing: the mechanism of turbulent mixing-layer growth at moderate Reynolds number. J. Fluid Mech. **63**, 237–255 (1974). doi:10.1017/S0022112074001121

S. Wing, J.R. Johnson, Substorm entropies. J. Geophys. Res. **114**, A00D07 (2009). doi:10.1029/2008JA013989
S. Wing, J.R. Johnson, Introduction to special section on entropy properties and constraints related to space plasma transport. J. Geophys. Res. **115**, A00D00 (2010). doi:10.1029/2009JA014911
S. Wing, P.T. Newell, Central plasma sheet ion properties as inferred from ionospheric observations. J. Geophys. Res. **103**, 6785–6800 (1998)
S. Wing, P.T. Newell, 2D plasma sheet ion density and temperature profiles for northward and southward IMF. Geophys. Res. Lett. **29**, 21-1–21-4 (2002). doi:10.1029/2001GL013950
S. Wing, J.R. Johnson, P.T. Newell, C.-I. Meng, Dawn-dusk asymmetries, ion spectra, and sources in the northward interplanetary magnetic field plasma sheet. J. Geophys. Res. **110**, A08205 (2005). doi:10.1029/2005JA011086
S. Wing, J.R. Johnson, M. Fujimoto, Timescale for the formation of the cold-dense plasma sheet: a case study. Geophys. Res. Lett. **33**, L23106 (2006). doi:10.1029/2006GL027110
S. Wing, J.W. Gjerloev, J.R. Johnson, R.A. Hoffman, Substorm plasma sheet ion pressure profiles. Geophys. Res. Lett. **34**, L16110 (2007). doi:10.1029/2007GL030453
S. Wing, M. Gkioulidou, J.R. Johnson, P.T. Newell, C.-P. Wang, Auroral particle precipitation characterized by the substorm cycle. J. Geophys. Res. Space Phys. **118**, 1022–1039 (2013). doi:10.1002/jgra.50160
R.M. Winglee, D. Chua, M. Brittnacher, G.K. Parks, G. Lu, Global impact of ionospheric outflows on the dynamics of the magnetosphere and cross-polar cap potential. J. Geophys. Res. **107**(A9), 1237 (2002). doi:10.1029/2001JA000214
R.A. Wolf, Y. Wan, X. Xing, J. Zhang, S. Sazykin, Entropy and plasma sheet transport. J. Geophys. Res. **114**, A00D05 (2009). doi:10.1029/2009JA014044
R.A. Wolf, C.X. Chen, F.R. Toffoletto, Thin filament simulations for Earth's plasma sheet: interchange oscillations. J. Geophys. Res. **117**, A02215 (2012). doi:10.1029/2011JA016971
J. Yang, F.R. Toffoletto, X. Xing, V. Angelopoulos, RCM-E simulation of the 13 March 2009 steady magnetospheric convection event. J. Geophys. Res. **117**, A03224 (2012). doi:10.1029/2011JA017245
Y. Yao, C.C. Chaston, K.-H. Glassmeier, V. Angelopoulos, Electromagnetic waves on ion gyro-radii scales across the magnetopause. Geophys. Res. Lett. **38**, L09102 (2011). doi:10.1029/2011GL047328
J.-C. Zhang, R.A. Wolf, S. Sazykin, F.R. Toffoletto, Injection of a bubble into the inner magnetosphere. Geophys. Res. Lett. **35**, L02110 (2008). doi:10.1029/2007GL032048
B. Zhang, W. Lotko, O. Brambles, P. Damiano, M. Wiltberger, J. Lyon, Magnetotail origins of auroral Alfvénic power. J. Geophys. Res. **117**, A09205 (2012). doi:10.1029/2012JA017680
X.-Z. Zhou, Z.Y. Pu, Q.-G. Zong, L. Xie, Energy filter effect for solar wind particle entry to the plasma sheet via flank regions during southward interplanetary magnetic field. J. Geophys. Res. **112**, A06233 (2007). doi:10.1029/2006JA012180